Gas Explosions in, and Propagating from, Low Strength Enclosures

Jason Peter Gill

Submitted in accordance with the requirements for the degree of
Doctor of Philosophy

The University of Leeds
School of Chemical and Process Engineering

May 2024

Intellectual Property, Publications and Award

The candidate confirms that the work submitted is his own, except where work which has formed part of jointly-authored publications has been included. The contribution of the candidate and the other authors to this work has been explicitly indicated below. The candidate confirms that appropriate credit has been given within the thesis where reference has been made to the work of others.

Publications

Chapter 4

Part of the work in this chapter has appeared in the following publication:

Gill, J., G. Atkinson, E. Cowpe, and D. Painter, (2016), Vapour cloud explosions in steel clad structures. *Symposium Series No 161, HAZARDS 26 Conference, Edinburgh*.

Contributions of Authors

J. Gill—Designed and built experimental rigs, designed the experimental program, carried out all experiments, analysed the results, and wrote a paper. Designed and presented a poster for a conference.

G. Atkinson – Supervisor of experimental work providing technical advice and mentoring, technically reviewed publication.
E. Cowpe and D. Painter, the research's end-users, provided funding sponsorship and technical comments for the publication.

Chapter 5

Part of the work in this chapter has appeared in the following publication:

Gill, J., G. Atkinson, H. Phylaktou, G.E. Andrews, and E. Cowpe (2019), Explosions in Electrical Control Boxes as a Potential "Nested Bang-Box" Mechanism for Severe Vapour Cloud Explosions, *in Ninth International Seminar on Fire and Explosion Hazards, St Petersburg*.

Contributions of Authors

J. Gill – Designed and built experimental rigs, designed experimental program, carried out all experiments, analysed results, and wrote the paper. Wrote the presentation for a conference.

G. Atkinson – Supervisor of experimental work providing technical advice and mentoring, technically reviewed publication.

H. Phylaktou - Gave supervision and advice, presented at a conference in St Petersburg.

G.E. Andrews – Gave supervision and advice.

E. Cowpe – The end-user of research, provided sponsorship for funding and technical comments to the publication.

Chapter 5 and 6

Parts of these chapters have appeared in the following publications:

Gill, J., G. Atkinson, E. Cowpe, H. Phylaktou, and G. Andrews, (2019) Experimental investigation of potential confined ignition sources for vapour cloud explosions (Conference Paper) *Institution of Chemical Engineers Symposium Series, Volume 2019-May, Issue 166, 2019 29th Institution of Chemical Engineers Symposium on Hazards 2019, Hazards 2019; Birmingham International Convention Centre.*

Gill, J., G. Atkinson, E. Cowpe, H. Phylaktou, and G. Andrews, (2020), Experimental investigation of potential confined ignition sources for vapour cloud explosions*. Process Safety and Environmental Protection*. **135**: p. 187-206.

Contributions of Authors

J. Gill - Designed and built experimental rigs, designed the experimental program, carried out all experiments, analysed results, and wrote papers. Wrote the presentation for the conference and presented it in Birmingham.

G. Atkinson - Contributed to the development of the model presented in Chapter 5, was a supervisor of experimental work, providing technical advice and mentoring, and technically reviewed publications.

H. Phylaktou and G.E. Andrews - Gave supervision and advice.

E. Cowpe – The end-user of research, provided sponsorship for funding and technical comments to the publications.

Award

Poster for 'Gill, J., G. Atkinson, E. Cowpe, and D. Painter, (2016), Vapour cloud explosions in steel clad structures won the 'Best Poster Prize' award at HAZARDS 26 Conference in Edinburgh, 2016.

Acknowledgements

Abstract

This research aimed to investigate the escalating effects of explosion propagation from electrical control boxes within lightweight steel-constructed buildings, focusing on elucidating the flame propagation mechanisms responsible for intensifying Vapour Cloud Explosion (VCE) severity, as observed in the Buncefield incident of 2005. The research aimed to determine if any escalating effects could be caused by the explosion propagating from the control box and the building into a larger cloud.

A series of controlled explosion experiments were conducted using a 47 m^3 vessel designed to mimic the structural properties of buildings like the Buncefield pumphouse, where it is believed the cloud was first ignited. Initially, experiments utilising 4.2% propane-air mixtures were carried out to understand baseline venting mechanisms and pressure development, with the vessel vent covered with steel panels and, for comparison, plastic sheeting. Findings indicate that lightweight steel panels hinging open during the initial stages of an explosion significantly enhance explosion severity due to their function as congestion elements.

Subsequent experiments employed commercially available electrical control boxes to investigate the explosion propagation dynamics, resultant pressures, and flame speeds. Experiments were conducted without and with a flammable cloud of 8 m^3 external to the control box contained in a tent. High-speed venting from the control box demonstrated a localised increase in flame speeds and overpressures, albeit the flame speeds attenuated considerably with a 0.35 m travel. However, congestion placed 0.5 m away from the vent without confinement didn't result in increased flame speeds.

The observed escalated explosion severity in lightweight steel buildings on high VCE hazard sites reveals a pressing concern regarding their structural failure mechanisms. Explosions originating from electrical control boxes showed an amplification of explosion severity, which only affected the immediate volume close to the box, suggesting that an obstruction-free zone of approximately 0.5 m from the control box could prevent an escalating explosion event. However, further studies are needed to thoroughly map the roles of confinement, immediate congestion, and high reactivity gases in such scenarios. Overall, this research significantly contributes to a better understanding of explosion propagation dynamics within

industrially relevant and standard settings, thereby aiding in developing more robust safety measures and structural designs to mitigate the severity of VCEs.

Table of Contents

List of Tables

List of Figures

Nomenclature

Symbols

t	time after ignition
M	mass of unburned gas in the box
V	volume occupied by unburned gas in the box
H	height of the box
W	width of the box
ρ	density (of the unburned gas)
ρ_0	initial density (of the unburned gas)
P	pressure (of the unburned gas)
P_0	initial pressure
P_1	first pressure peak
P_2	second pressure peak
P_3	external explosion pressure peak
A_{door}	area of door opening
A_{vent}	effective area of vent (at the vena contracta)
C_d	discharge coefficient
I	moment of inertia of door and catch about hinges
θ	angle of the door to the closed position
E	expansion ratio
V_b	burning velocity
R	flame radius
C	speed of sound
a	linear acceleration of a detached panel
Δv	change in speed of a detached panel
L	height of a building
D	Diameter
k	thermal conductivity
L_{cpeak}	absolute highest noise level

Abbreviations

HSE   UK Health and Safety Executive

NFPA National Fire Protection Agency

BSI   British Standards Institute

MFC   mass flow controller

PT   pressure transducer

TC   thermocouple

VCE   vapour cloud explosion

LPG   liquid petroleum gas

Chapter 1
Introduction

Fire and explosions cause fatalities and financial losses to society [1]. A 2022 report by Allianz [2] shows fire and explosions are the most significant single identified cause of corporate insurance losses, accounting for 21% of the value of all claims in the five years from 2017 to 2021. This equates to €18 billion of insurance losses, despite all the research and improvements in prevention and risk management.

1.1 Vapour Cloud Explosions at Petrochemical Plants

A vapour cloud explosion (VCE) occurs when a combustible gas or vapour is formed as a flammable mixture with air and ignited. This can be in a confined or unconfined environment. Flammable vapour clouds in open areas are associated with losses of containment of gases (e.g., methane), flashing pressure-liquefied gases (e.g., LPG) and volatile liquids (e.g., petrol). Vapour cloud explosions constitute an essential part of the risk profile of various industrial sites, including refineries, liquid and gas fuel storage, pipelines, chemical manufacturers, and more.

Loss of containment can occur as a sudden massive loss of inventory due to catastrophic failure. At Flixborough in 1974 and Port Neches, Texas in 2019, large quantities of very reactive chemicals were released and ignited within seconds, resulting in severe explosions [3 & 4].

The most recent severe VCE in the United Kingdom was the Buncefield incident in 2005 [5], which, due to good fortune, did not result in any fatalities but caused damage exceeding £1 billion. A spillage caused the vapour cloud due to overfilling a tank lasting around 23 minutes. This incident was thoroughly investigated and has triggered a large quantity of peer-reviewed work, making it an obvious choice for research focus.

1.2 Previous Incidents

Since Flixborough, and despite all the research that stemmed from it, increased regulation, and improvements to risk management, explosion incidents still occur. There have been several recent VCE incidents that have similarities in cloud formation and severity [6]. Information about recent incidents tends to be more extensive and widely shared than in the past. New sources such as CCTV and mobile phone footage can be particularly valuable.

1.2.1 Buncefield 2005

The Buncefield incident occurred on December 11th, 2005, in Hertfordshire, UK, while importing winter-grade petrol from a long-distance pipeline [7]. The failure of a tank process level indicator and automatic high-level shut-off system led to a tank being overfilled for 23 minutes. The loss rate was 550 m^3/h, rising to around 900 m^3/h for the last 8 minutes. There was no wind, and the method of spillage resulted in a large un, unconfined, gravity-driven pancake vapour cloud that spread in all directions to cover most of the site and a substantial part of an off-site industrial estate. The maximum extent of the cloud was approximately 500 x 350 m [8-11].

A tanker driver reported it when the vapour cloud reached the tanker loading gantry. The site emergency system was activated, which involved starting the fire pump. The pump was in a steel frame building clad with lightweight steel panels. This pumphouse (Figure 1) was located close to the vapour source, in a depression forming the site's firewater lagoon. CCTV showed that the pumphouse was fully submerged in the vapour cloud for at least 15 minutes before ignition. A contactor inside an electrical control box was part of the pump's electrical controls within the building. Unlike numerous other steel enclosures around the Buncefield site, damage to this contactor box showed it had suffered violent internal pressurisation. CCTV records and other evidence clearly showed ignition occurred somewhere in the pumphouse, so it is reasonable to assume that a spark within the contactor box ignited the vapour cloud when the pump was activated. A severe VCE caused damage across the entire area covered by the vapour cloud. Severe explosion effects were confined to an area within a few tens of metres

beyond the edge of the cloud, but minor damage (e.g., windows breaking) extended to a range of more than 1 km. There were no fatalities, but this was down to the fact that the event happened in the early hours of the morning when the buildings in the area were unoccupied. Damage to the site and surrounding businesses was estimated to exceed more than £1 billion.

Figure 1 - Buncefield Emergency pump house before and after the explosion [12]

1.2.2 Jaipur 2009

The Jaipur incident occurred on the evening of October 29th, 2009, at the Indian Oil Corporation's POL (Petroleum Oil Lubricants) Terminal at Sanganer in Jaipur, India [13]. In a routine operation to prepare a tank to pump petrol to a neighbouring terminal, a massive leak of the product took place in the form of a jet of liquid in the air, driven by the head of the tank from the "Hammer Blind Valve" on the delivery line of the tank leading to the pump. The release continued for 75 minutes, and a vapour cloud spread in all directions to cover the site, approximately 700 m x 700 m. A boundary wall (height 2.5 m) prevented spillage of vapour from the site into the neighbourhood. The explosion caused 12 fatalities.

Like the Buncefield incident, this occurred in zero wind and blast damage data showed that overpressures generated must have been at least 200 kPa across the entire site. The ignition source has yet to be unambiguously identified. Still, there are strong indications of a transition to a severe explosion as the flame front passed through an emergency pump house [12]. This pump house was also a steel frame building (Figure 2), but unlike Buncefield, the cladding sheets used were cement and fragmented (Figure 3) as they were detached.

Figure 2 - Remains of the pump house at Jaipur [12]

Figure 3 - Fragments of cement cladding panels around the pump house at Jaipur [12]

1.2.3 San Juan 2009

The San Juan incident occurred on October 23rd, 2009, at the Caribbean Petroleum Corporation (CAPECO) facility in Bayamón, Puerto Rico, during the offloading of petrol from a tanker ship, the Cape Bruny, to the CAPECO

tank farm onshore [14]. The method of vapour dispersal was similar to that at Buncefield, with an overflow lasting 26 minutes that cascaded from the top of the tank in zero wind. The cloud had a radius of around 400 m (Figure 4).

Figure 4 - Extent of the vapour cloud at San Juan [12]

Excellent CCTV records of the flame's progress for this accident exist. Two views allow triangulation to determine the location of significant events. The initial ignition occurred right at the edge of the cloud, where the depth would have been very shallow. The ignition caused a flash fire that spread relatively slowly (around 30 m/s) for 8 seconds. The flame then approached the deeper parts of the cloud, and there was a transition to severe VCE in an area containing some pipework (Figure 5).

Crushed and bent objects and tanks suggest overpressures similar to those at Buncefield. CCTV records of the flame after transition showed the rate of progress was subsonic. The videos also indicated that the explosion might have an episodic character, with a succession of separate shock waves generated by separate phases of rapid combustion [12].
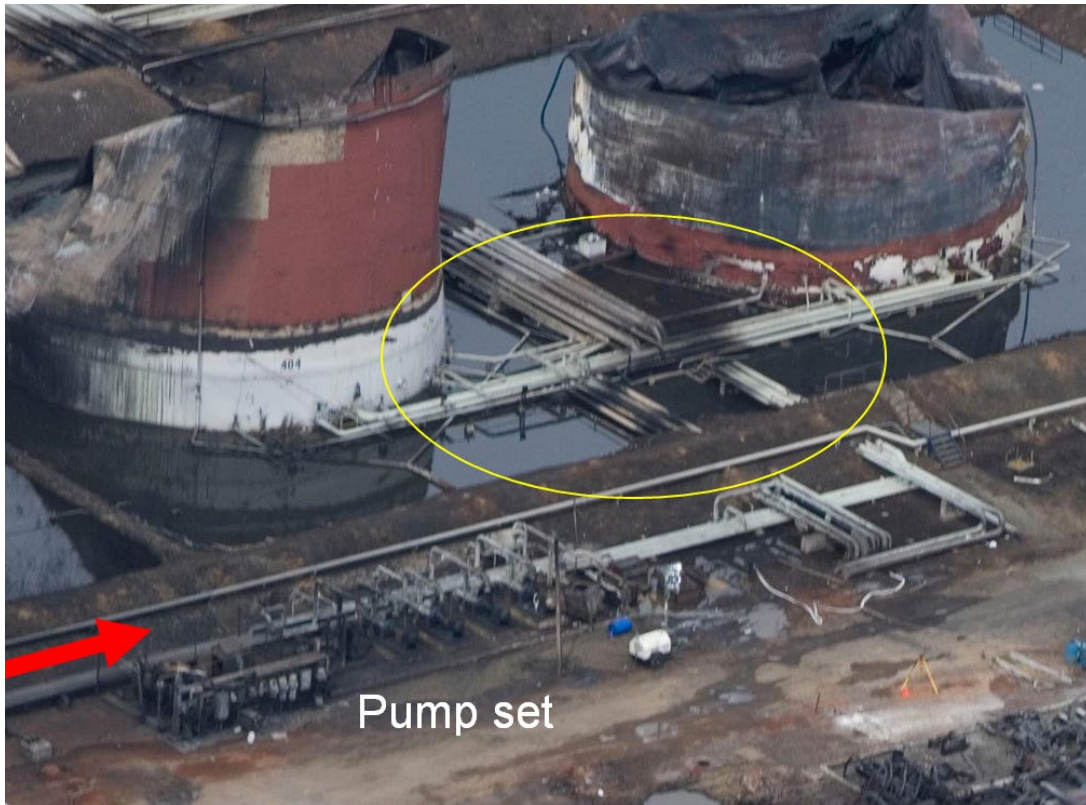
Figure 5 – Area (yellow circle) where the transition to a severe explosion occurred [12]

1.2.4 Amuay 2012

The Amuay incident occurred on August 25th, 2012, at the Paraguana Refinery Complex in Venezuela. Information on the incident is limited because of its political sensitivity. However, two available reports have been identified [12]. These were produced by RMG (Risk Management Group) and PDVSA (Petróleos de Venezuela, S.A., the plant operators). These reports concur about the leak's location and the vapour cloud's extent but not on the events leading up to the VCE. The plant produced liquefied natural gas (LNG) and liquefied petroleum gas (LPG).

According to the PDVSA report, a severe seal failure occurred in a canned pump at 00:00 am on August 25th. Inventory information for the associated C3/C4 olefin tank suggested a large leak of 67 kg/s lasting for 68 minutes until the explosion (273 tonnes total loss). The wind was near zero, and a cloud formed in at least 600 m range. The overpressure was at least

200 kPa, and the damage was consistent with that seen at Buncefield [15]. The incident caused over 50 fatalities, all but one off-site.

1.3 Investigation of Incidents

A crucial part of mainstream forensic science when investigating accidents and crimes is using reconstruction to test hypotheses; discovering the 'how' of the five WH (what, who, why, where, when, and how) is a crucial part of future prevention [16 & 17]. Severe VCE events are so massive that full-scale reconstruction is impossible. Therefore, using research, learning from past events, and small-scale reconstruction during an investigation is essential.

Severe VCEs are thankfully rare events; this, however, means that there is little opportunity to study real-life events. When events occur, they usually invoke a multiagency response to the investigation with regulators, government departments, emergency services, and insurers involved in the investigation into the event. Each stakeholder will have their agenda, but all will have the aim of helping prevent such events from happening again. Only a limited number of experts in the field are available to the stakeholders to undertake such an investigation, and good research is crucial to aiding them.

The conventional method of VCE severity analysis, the Multi Energy Method (MEM) [18], for example, assumes that high flame speeds and pressure are exclusively associated with highly congested areas and does not account for severe unconfined VCEs. But since Buncefield, there have been several very similar significant VCE incidents around the world, as discussed above, and these have led to fatalities. This shows that despite all the research after the Buncefield incident, the problem of large, severe VCEs has yet to be solved. Despite predictions to the contrary, devastating explosions resulting from large, unconfined pancake clouds are not only a possibility but also probable. A review of large VCEs by Atkinson et al. uncovered no records of flashfire-type explosions of large (R>200m) clouds [12].

There has been a lot of discussion regarding the actual explosion mechanisms at play in the Buncefield event; the official report concluded that the explosion might have been a deflagration to detonation transition (DDT),

likely in an area of trees which acted as congestion [5]. As conventional thinking assumes that a primary method of achieving DDT is through congestion, much of the research that contributed to the report and later research concentrated on the effect of congestion on flame speed. One such study investigated the effectiveness of objects such as trees to act as congestion [19]. However, Jaipur, San Juan, and Amuay did not have thick patches of trees or brushwood in the areas where the transition occurred [12].

1.4 Prevention and Mitigation of Incidents

Not losing containment of flammable inventory is the most effective means of preventing severe explosions. However, many losses result from a domino effect [20-22]. Therefore, loss prevention requires a multi-layered approach: first, preventing loss of containment, then preventing ignition, and if that is not possible, mitigating against the worst effects of possible ignition scenarios.

There are regulations to control ignition sources in hazardous areas. In the UK, they are covered by the Dangerous Substances and Explosive Atmosphere Regulation 2002 (DSEAR) [23] and in the European Union (EU) by Directive 99/92/EC - risks from explosive atmospheres 1999 [24]. The EU directive, along with Directive 2014/34/EU - equipment and protective systems intended for use in potentially explosive atmospheres 2014 [25], are known as the ATEX regulations.

Equipment installed in areas likely to have an explosive atmosphere, even in the event of a foreseeable loss of containment, must be intrinsically safe so as not to constitute an ignition source risk. Equipment that is ATEX-rated fits this requirement. To decide which areas this applies to, sites must be zoned with hazardous area classifications. This is undertaken with a risk assessment methodology using tools to calculate the likely extent of an explosive atmosphere in given scenarios.

Many studies and models have been used to determine the probability of ignition of losses for specific situations [26 & 27] and general accidents [28-32]. The issue with many VCE events is that the clouds are so massive that

they encroach on areas outside the hazardous classified areas to locations where ignition sources are not controlled. The clouds also often persist for long periods, increasing the probability of ignition [6].

1.5 Knowledge Gaps in Understanding

There is ample research generated in response to the Buncefield incident into the effects of congestion, confinement and turbulence on explosion severity once the explosion is established. There is also plenty of research on the propagation of an explosion from a chamber to another volume. A detailed literature review will be presented in the next Chapter. Still, in terms of this general introduction and primary motivation for this work, the following areas of uncertainty are identified:

More research is needed into the actual ignition mechanism at Buncefield and its effect on the explosion severity despite a call in 2012 by Bradley et al. for further study [33]. The Buncefield ignition is believed to have occurred due to a spark by an enclosed electrical contactor inside a congested building, a pumphouse [12].

The contactor enclosure was a steel electrical control box with five strong sides and a hinged door with a lock or catch. More needs to be understood about how these boxes fail during an explosion within them. There is also no information on how explosion propagation from such an enclosure affects the overall explosion severity. These types of control boxes are prolific on plants.

The pumphouse building was constructed of lightweight steel cladding panels attached to purlins. The panels are only designed to withstand wind loading. Buildings of this construction are commonly used to enclose processes on plants. It is assumed that due to the low failure pressure of these panels, the effect on explosion severity will be limited. However, little is known about how the failure mechanisms of the steel panels affect the severity of an explosion propagating from within.

The whole building was immersed in the larger, unconfined vapour cloud. This means that the external cloud was ignited by a venting explosion from the building, which in turn was ignited by a vented explosion from the control box, i.e., a nested, confined explosion ignition event.

1.6 Aim and Objectives of Research

The aim of this PhD research was to investigate how an explosion initiated in a confined and congested space and then propagated into a larger external flammable cloud affects the overall severity of the explosion. The understanding gained from this project will be used to improve the reliability of fire and explosion risk assessments for high-risk plants by industrial duty holders and inform the UK Health and Safety Executive (HSE) His Majesty's Inspectors, facilitating more focussed and informed site inspections, and help provide practical guidance on the design and layout of these confined ignition initiation spaces for less severe vapour cloud explosions.

The research objectives were:

1. Carry out explosions in a large vessel with a large vent area. Investigate any effects on explosion severity by adding lightweight steel cladding panels covering the vent area and comparing the results to plastic sheets as a membrane cover and steel cladding.
2. Investigate the box failure and flame propagation mechanisms from commercially available electrical control cabinets with a hinged door. This will be achieved by carrying out explosions inside a single type and size of cabinet with the door on and various vent coverings in place of the door. Experiments will also be carried out with and without internal congestion. Overpressures and flame speeds will be measured, and flame shapes will be recorded.
3. Investigate the effects on explosion severity in an 'unconfined' volume of pre-mixed gas when ignited by an explosion propagating from an electrical control box. The overpressures and flame speeds from such an event will be compared to when the ignition source is unconfined within the larger volume.

A further objective was to investigate the effect of nesting of an explosion propagating from a box into a building constructed from lightweight steel panels, combining the experiments from objectives 1 and 3. However, this objective was abandoned due to the severity of the explosions in the Objective 1 experimental programme, requiring a new test site and the

impact of the pandemic. This work will need to be the focus of future research.

1.7 Thesis Outline

The thesis is arranged into seven chapters, including this chapter, being the introduction. A brief outline and description of each chapter is as follows:

- Chapter 2 is the Literature Review, which gives a background of the science behind explosion mechanisms, the Buncefield Vapour Cloud Explosion incident, and details of any research relevant to the thesis.
- Chapter 3 provides an overview of the experimental equipment, rigs, and methodology used in all experiments.
- Chapter 4 presents the results and discusses the experiments with steel cladding panels related to Objective 1.
- Chapter 5 details and discusses the results of the experiments with steel control boxes, different vent coverings, and different levels of internal congestion, which relate to Objective 2.
- Chapter 6 presents and discusses the results of the experiments investigating the propagation of an explosion from a steel control box, relating to Objective 3,
- Chapter 7 summarises the research findings and provides recommendations for further research.

.

Chapter 2
Literature Review

2.1 Introduction

Published research is abundant on explosion mechanisms. Some of this research concerns the fundamentals of combustion science and engineering. However, there has also been a mass of published work in response to vapour cloud explosion incidents through the years. Some comprise reports related to the investigations, and some are published research undertaken to address questions raised during investigations. Most of this research was in response to the Buncefield incident.

This chapter aims to overview the combustion mechanisms relevant to this study, examine the cloud development, ignition, and investigation of the Buncefield incident, and discuss the issues and difficulty of forensic analysis of VCE incidents. It will also examine the developments and research since Buncefield.

2.2 Experimental and Analytical Studies of Explosions

The fundamentals of combustion mechanics provide a valuable foundation for this study.

2.2.1 Quiescent Gas – Small Scale

In the earliest stage, the first 100 mm of flame spread away from a spark; the flame is laminar and spherical in a homogenous, initially quiescent gas mixture. In this case, the expansion of burned gases drives the flame forward so that the observed flame speed is approximately $E \cdot V_b$, where E is the expansion ratio associated with combustion at constant pressure (typically of the order of 7 to 8 for stoichiometric burning of common hydrocarbons). V_b is the fundamental laminar burning velocity, i.e., the rate at which the flame front advances relative to the unburned gas ahead. Some typical values for laminar burning velocities for the fastest burning mixture of gas and air at normal temperature and pressure, as derived by NFPA, are shown in Table 1 [35].

Table 1- Burning velocities for use in venting assessments [35]

Gas	Laminar Burning velocity (m/s)
Methane	0.40
Ethane	0.47
Propane	0.46
Butane	0.45
Pentane	0.46
Hexane	0.46
Ethylene	0.80
Acetylene	1.66
Hydrogen	3.12

Flame speed is the rate of flame propagation relative to an external observer (i.e. $E \times V_b$). However, much literature often refers to laminar flame speeds when they mean burning velocities. Burning velocities and flame speeds can be reasonably well predicted by detailed modelling of the heat transfer and (appropriately simplified) combustion kinetics in the flame. Figure 6 shows an example comparing modelled and measured values. Note that the researchers in this study have also confused flame speed and burning velocity [36].
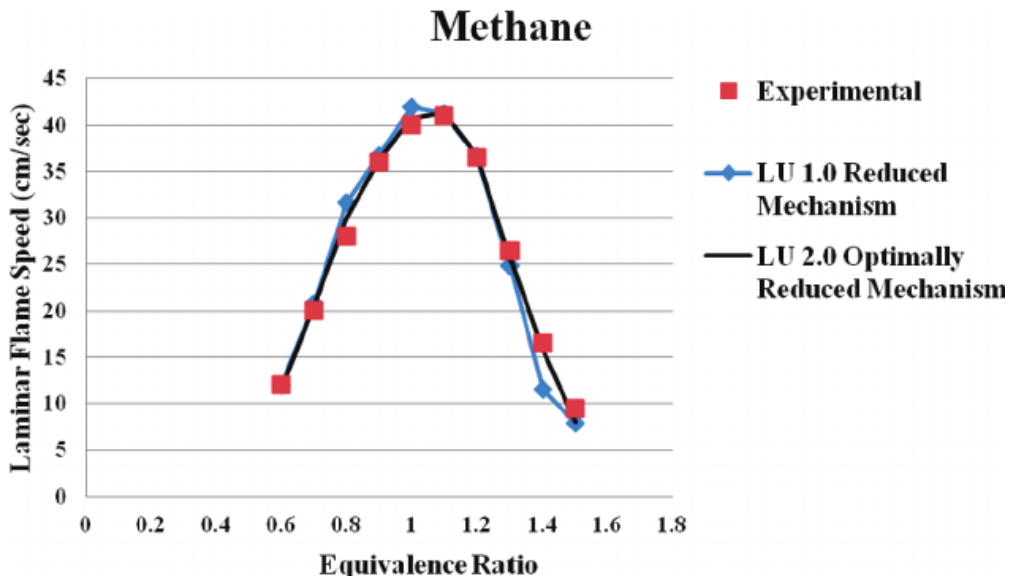
Figure 6 - Experimental and theoretical laminar burning velocities [36]

The effects of pressure and temperature on laminar flame speed have been extensively studied experimentally and theoretically [37 & 38]. Typically, isothermal increases in pressure reduce the flame speed, and isobaric increases in temperature markedly increase flame speeds, as shown for methane and propane in Figure 7.

These behaviours are critical to flame acceleration in confined and unconfined conditions and the severity of the resulting explosions. In particular, the effect of adiabatic compression is to increase both pressure (tending to reduce flame speeds) and temperature (tending to increase flame speeds). The balance of these two effects varies considerably between common gaseous fuels and has a marked effect on the explosion risk associated with each gas. This is explained in more detail later.
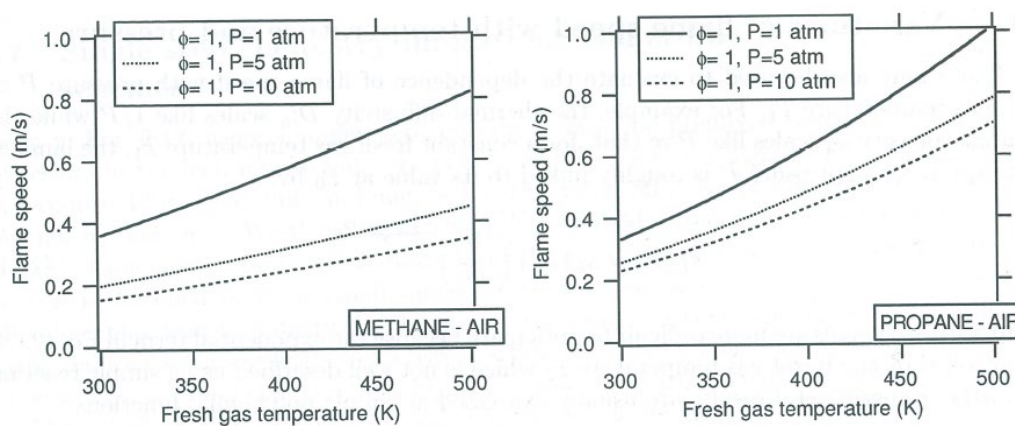
Figure 7- Variation of laminar burning velocity with pressure and temperature [37]

2.1.2 Quiescent Gas – Large Scale

Experiments in large plastic tents and balloons showed a radial flame speed of around 10 m/s for stoichiometric propane [39]. Since the expansion ratio is ~7, this indicates a burning velocity of ~1.4 m/s. This is 2-3 times the laminar burning velocity because of the flame front's natural instability (wrinkling) at a larger scale caused by Darrieus–Landau instabilities [40-46]. This distortion of the flame front gives the flame a cellular appearance and

provides additional surface area over which the flame can spread. Much of the research into the instabilities of premixed flames has been in the form of Bunsen burner experiments. However, research suggests that propane instabilities will start at a radius of around 300 mm, depending on pressure [47 & 48].

2.1.3 Stirred Gas

Agitation of the mixture before ignition can increase the turbulent burning velocity of an unobstructed flame to a value roughly 10-20 times greater than the laminar flame speed. The resulting turbulence increases the distortion of the flame front and the total surface area over which the flame can progress into the unburned mixture. At extremely high rates of agitation, the distortion of the flame becomes so extreme that the burning rate declines and the flame may be quenched [49].

2.1.4 Flame Propagation Around Obstacles (Congested Flame Propagation)

Turbulent burning velocities may be further increased by introducing solid obstacles that divide the flame and cause turbulence in the unburned gas being driven ahead of the flame front by expansion of the burned gases (

Figure **8**). An idealised situation involves a flame propagating through one or more regular grids of obstacles, with square or hollow obstacles [50-58].

The combined effect of additional turbulence and flame area may increase the effective local burning rate to 50 – 70 m/s, i.e., over 100 times the laminar flame speed. The observed flame speed depends on geometry, where the burned gas can only expand in the direction of the flame movement, such as a confined flame in a tube or channel [53, 59-64]. A burning velocity of 50 m/s corresponds to the overall flame speed of order 350 m/s, similar to the speed of sound. In this case, high pressures are inevitably produced.

The flame speed is initially less in less confined geometries (e.g., linear or pancake-shaped, congested gas clouds). A flame speed of approximately $\sqrt{E}.V_b$ 140 - 180 m/s is typical for the highest values of burning velocity V_b = 50-70 m/s [65]. Such flame speeds may not be stable for fuels such as

propane because the pressure associated with adiabatic compression of unburned gas at the flame front increases the laminar burning rate, increasing the turbulent burning velocity and pressure. Such flames may accelerate to a high-speed, high-pressure regime and may undergo deflagration to detonation transition (DDT). For less congested clouds, steady flames with a speed of less than 150 m/s are possible [66]. The laminar flame speed of methane increases much more slowly during adiabatic compression. Much higher densities of obstacles are required to trigger high-speed burning [67].

Experimentally, it has been demonstrated that when the congestion level decreases, the flame speed also rapidly declines [5].

| Laminar flame | Turbulent flame | Stirred gas | Congested gas cloud |
| V_{lam} | 2-3 V_{lam} | up to 10-20 V_{lam} | up to 100-150 V_{lam} |
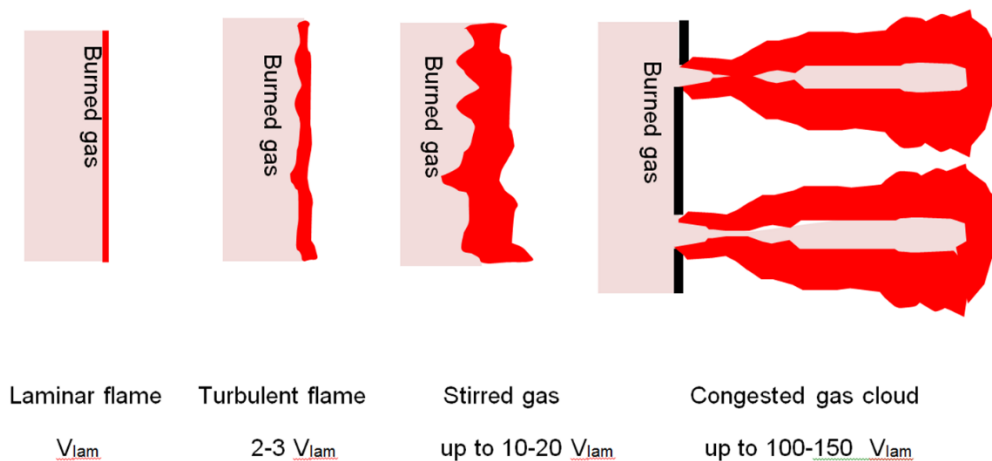
Figure 8 - Increasing burning velocities for laminar, turbulent and obstructed flames

2.1.5 Effects of Thermal Radiation

Some researchers propose that the same methods used to predict laminar flame speeds in the case where the unburned gas has negligible capacity to absorb thermal radiation can be extended to treat the case where fine particles are suspended in the unburned gas [68-72]. Such particles absorb thermal radiation from the flame and transfer it very efficiently to the surrounding (unburned) gas. This pre-heating of the unburned gas increases the laminar flame speed. Some typical results from Liberman et al. are shown in Figure 9 [72]. For fast flames like hydrogen/oxygen, radiative heat transfer makes relatively little difference in flame speed. However, the laminar flame speed increases by around five times to over 2 m/s for

methane. This means very large, dusty methane mixtures will have a turbulent burning velocity well above that of acetylene [73]. The time required for pre-heating is 1-2 milliseconds, which is relatively short compared with the typical residence time of unburned gas within a very large-scale turbulent flame brush.

Therefore, it is expected that wherever gases such as methane and propane are contaminated with particulates ahead of the arrival of the flame, they will exhibit substantially enhanced apparent reactivity.
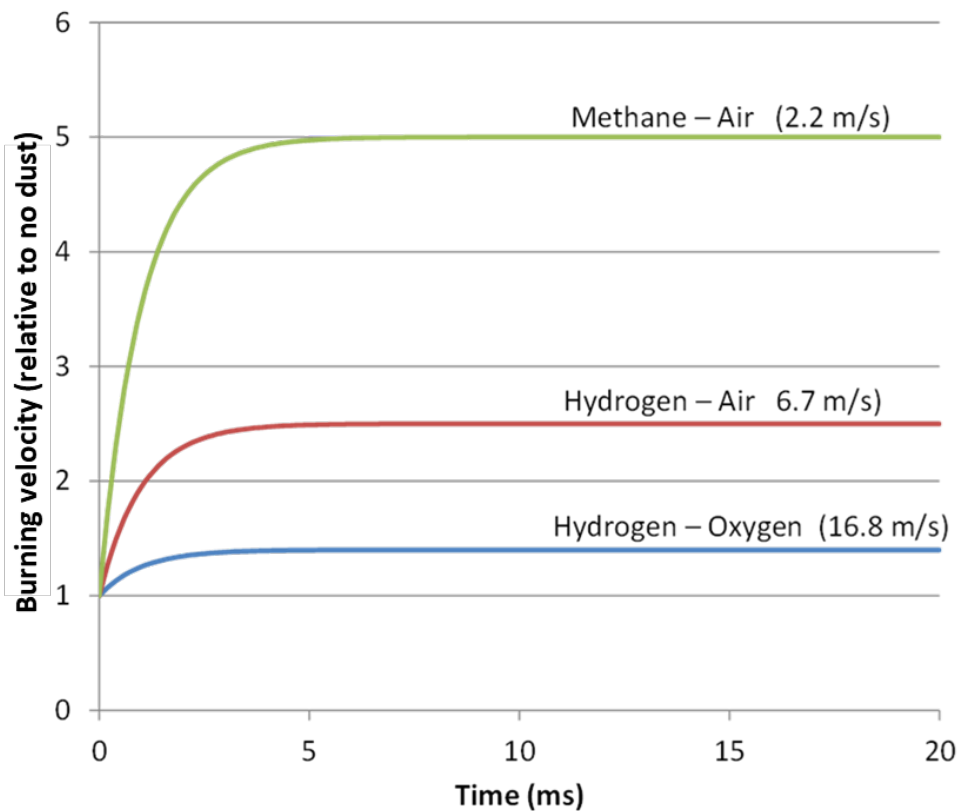
Figure 9 - Effects of dust contamination on laminar burning velocity, derived from Liberman et al. [72]

A better understanding of the physics of nested ignition sources is vital in the potential effect of dust contamination on flame speeds in vapour cloud explosions. A phase of rapid burning triggered by such an explosion induces a pressure wave that may be capable of disturbing layers of dust on the ground, pipework, or vegetation ahead of the flame front. The burning rate could be enhanced when the flame encounters parts of the gas cloud that are contaminated in this way.

A similar process produces secondary dust explosions: an initial blast disturbs dust, fuelling a subsequent explosion [74]. A sequence of blasts may occur as successive blasts disturb dust in more distant areas, allowing the flame to spread unsteadily. The mass loading of dust required to enhance the burning of large-scale pre-mixed gas clouds is at least an order of magnitude less than that needed to sustain a dust explosion, so the effect may be significant in environments where contamination levels are relatively low. With pre-mixed gas present, the dust particles need not be combustible; rust particles, soot and mineral dust will efficiently transfer the energy in thermal radiation to an unburned gas cloud [72].

2.1.6 Effects of Scale and Cloud Concentration

The experiments referred to above were conducted at a laboratory scale or in plastic-covered gas tents filled with controlled gas mixtures [68-74]. Some of these tents were many tens of metres long, but they were typically only a few metres in height and width. The total gas mass involved ranged from a few grams to tens of kilograms.

Some more extensive experiments were carried out in the 1970s and early 1980s, typically as part of dispersion trials, for example, at China Lake, Maplin Sands and Musselbanks [75-77]. These tests involved more considerable amounts of gas (1,000 - 25,000 kg), but the clouds were generated from a localised source by natural dispersion in the wind. Flame speeds were generally low, and substantial congestion and confinement were required to generate any measurable overpressure.

Because of the wind-driven dispersion, these clouds would have been highly inhomogeneous, with substantial areas where the concentration was above and below the flammable range. Even within the area where the average concentration was close to stoichiometric, wide variations in instantaneous concentration would have taken the cloud outside the flammable range.

Between this early work and the Buncefield incident in 2005, it was almost universally accepted that the risk of a severe explosion affecting open, unconfined areas was extremely low. This seemed reasonable because even in gas tent tests (where near-stoichiometric mixtures could be sustained), flame speeds decayed rapidly as the flame emerged from

congested areas [78]. It was argued that the gas concentration would be far more variable and less likely to sustain high flame speeds in real-world clouds. This line of reasoning was developed into explosion assessment methods, e.g., the TNO Multi Energy Method (MEM) [79] and the BakerRisk method [80]. In these schemes, attention is focused exclusively on the propagation of the explosion within congested areas. Although the vapour cloud generally extends more widely, combustion in uncongested regions is assumed to not contribute to pressure effects. This assumption and the corresponding methods were widely adopted by industry and regulators.

The experimental evidence underpinning this aspect of methods such as MEM is, in fact, rather weak. The combination of very large cloud size and high levels of cloud homogeneity had not been examined. Increasing the size of a homogeneous cloud (by three orders of magnitude) or removing inhomogeneity from very large clouds for experiments was seen as impractical, particularly as it has been assumed that this would not show any new combustion physics.

A related, simplified approach to the dispersion of flammable gas was also widely adopted by industry and regulators. This approach represents the range of potential weather conditions by a small number of standard windy conditions, typically 2 m/s (stable) and 5 m/s (neutral). Again, there was no empirical evidence or theoretical justification for this. It was simply assumed that calm conditions, in which vapour transport was gravity-driven, would be rare and not necessarily more problematic so that they would not contribute to overall risk.

Over the last decade, it has become clear that this latter assumption about dispersion was flawed: most major VCE incidents have occurred in gravity-driven clouds [6]. In calm conditions, these typically grow to cover an area hundreds of times greater than would be produced by the same release in windy conditions. The increased risk of ignition within such a large area far outweighs the relative rarity of the weather conditions in determining overall event frequency.

Gravity-driven flows provide a mechanism for generating near-homogeneous clouds covering hundreds of acres, and this can occur even for relatively

small rates of loss of containment, which occur more frequently [81]. This undermines one of the most important foundations of the MEM and similar methods, namely the assumption that very large, homogenous clouds will not usually occur. The lack of experimental evidence about the explosion behaviour in such clouds now appears to be a potentially dangerous weakness.

Many such events have occurred during industrial incidents, and forensic analysis of the consequences is currently the best evidence of likely behaviour.

2.3 Buncefield Vapour Cloud Explosion

As the Buncefield incident drives this research, it is essential to understand how the incident occurred and the issues associated with the investigation.

2.3.1 Cloud Formation

The cloud formation was gravity-driven at Buncefield (2005) and is very similar to that of subsequent severe VCEs: Jaipur (2009), Amuay (2012), and San Juan (2009); this is due to the long durations of release and weather conditions at these incidents. Dispersion at Buncefield occurred while importing winter-grade petrol from a long-distance pipeline. The failure of a tank process level indicator and automatic high-level shut-off system led to a tank being overfilled for 23 minutes. The loss rate was 550 m^3/h, rising to around 900 m^3/h for the last 8 minutes.

Apart from the area immediately around the tank and in the pumphouse lagoon, the vapour cloud reached a depth of no more than 2-3 metres. Cloud development was extensively recorded on CCTV (see an example in Figure 10). This development of the vapour cloud was caused by the way the petrol poured out of the breather vents at the top of the tank and cascaded downwards at the tank wall [9]. The vaporisation rate was around 19 kg/s, and because there was no wind, this vapour accumulated around the tank, only spreading away because of gravity. This form of vapour cloud production has been studied and replicated [82] (Figure 11) using hexane

and other volatile solvents. It has been shown that the cloud is relatively homogenous apart from a stably stratified, laminar layer at the top.

In fact, it is not necessary for the wind to be zero for wind-driven entrainment to fall to a very low level. For example, apart from a small area at the upwind edge, the lower 75% of a cloud of depth 2 m will be undisturbed by a surface wind of 1.3 m/s [6 &8 3] (Figure 12).

Figure 10 - CCTV footage showing the cloud development [12]

Figure 11 - Recreation of Buncefield release mechanism using hexane [82]
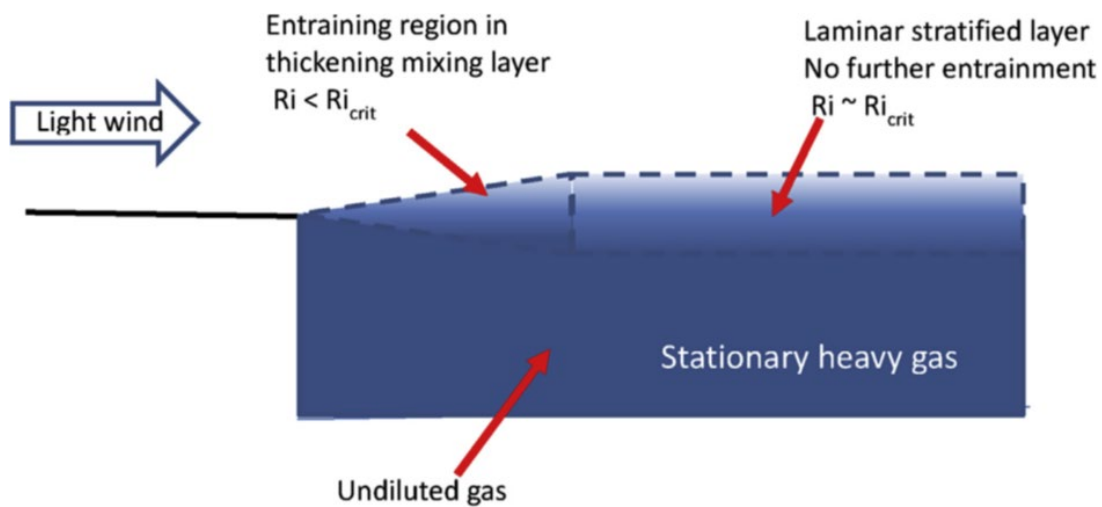
Figure 12 - Detrainment of a heavy gas by a light wind [6]

2.3.2 Ignition of Cloud

The ignition source was determined to have been within the emergency pump house [84] (Figure 1). This building was constructed of a steel framework clad with lightweight steel panels attached to purlins and a partial-height brick back wall. This building housed a diesel pump, which was started as part of the site's emergency procedure. The weight of evidence shows that the ignition occurred inside a steel electrical control box that housed the controls to start the pump (Figure 13). The steel box would have

acted as a small but strong form of containment for the initial ignition. The building itself would be pretty weak [85]; the steel cladding sheets are fastened to the purlins via self-drilling Tek screws. These types of buildings are designed only to withstand wind loading from the outside, and the cladding will detach with very low levels of internal overpressure [86], 2 kPa to 5 kPa. The main methods of detachment being the fastening pulling out of the purlin or the cladding sheet being pulled over the fastener.

The distribution of pumphouse cladding panels was recorded after the explosion (Figure 14). The symmetry of the distribution around the axis of the building suggests that the flight of these panels was determined by the initial explosion rather than the effects of the wider explosion. The range of sheets and the fact that every sheet was simultaneously displaced suggests rapid pressurisation in the pumphouse.

Figure 13 - Buncefield diesel pump electrical control box [84]

Figure 14 - Final location of cladding panels from the Buncefield pump house [84]

2.2.3 Investigation of Incident

Many of those involved in the investigation [5] and following research work believe that the explosion transitioned to a detonation at some stage after the initial explosion in the pump house [87-90]. This would explain the high overpressures observed across the area covered by the cloud because detonations, once stable, do not require congestion to sustain high flame speeds. It has been shown that very linear arrays of densely packed brushwood can trigger detonation, and there were overgrown hedgerows around the Buncefield site [19].

On the other hand, others claim that damage caused by the Buncefield explosion is inconsistent with what is expected in a detonation, which can generate overpressures that easily exceed 1 MPa [6,12, 91-94]. In particular, detonations are associated with very high dynamic pressures on the upstream side of impacted objects. Detonation tests result in highly directional deformation of lightweight steel enclosures like cars, drums, boxes, etc [12]. This was not observed at Buncefield or in other similar incidents. This is, however, also disputed by some studies [88-90].

Experimental detonations and other incidents which can be confidently identified as detonations (e.g., Flixborough) also produce characteristic drag damage to lightweight posts and poles [95]. The very high forces associated with an impinging detonation lead to increases in kinetic energy on a short timescale compared with the transit time of flexural waves from points of constraint. Slender steel posts are left in a continuously curved form, i.e., plastic strain is continuously distributed along the length rather than being concentrated in plastic hinges. Such curved objects have not been documented at Buncefield or in similar incidents.

CCTV records from the explosion show the duration of intense illumination and pressure waves from the explosions. Both data sets are difficult to reconcile with a detonation but are consistent with an explosion that progressed (on average) at a subsonic speed [33 & 91]. Similar CCTV data has been obtained from other explosions where the flame's progress was visible.

2.3 Forensic Analysis of Explosion Damage from Events Before Buncefield

It seems unusual that for several decades, the assumption that severe explosions would not propagate into open areas survived in the face of evidence from multiple incidents. There are many reasons for this, including strong legal and socio-economic difficulties affecting the process of investigation and analysis. In many cases, investigations into costly and fatal incidents focused on immediate causes of loss of containment and issues of responsibility rather than on a dispassionate comparison with existing models of explosion physics. Access to data from explosions has also routinely been tightly controlled for legal reasons (especially in the US), and this problem persists.

There have also been critical technical barriers to the appropriate investigation of VCEs.

2.3.1 Unreliable Overpressure Markers

The effects of overpressure on most important objects damaged by VCEs are generally too complex to analyse from first principles. Forensic work at incidents referred to tables of overpressure damage markers - a typical example of which is shown in Table 2.

Table 2 - Overpressure/damage markers

Damage	Overpressure
Typical pressure for glass failure	1 kPa
Minor damage to house structures	4.8 kPa
50% destruction of brickwork of house	17 kPa
Rupture of oil storage tanks	27 kPa
Severe crushing of cars	34 kPa
Loaded train box cars completely demolished	62 kPa
Probably total destruction of buildings	69 kPa

The most comprehensive and influential of these pressure/damage tables were generated during the testing of nuclear weapons [96]. The problem with such an approach is that the duration of the positive phase of the atomic explosions, in which the effects were noted, was several seconds. The duration of the impulse from a low-lying vapour cloud is at least two orders of magnitude shorter. For many of the objects listed, the pressure required to produce the listed effect in such a short time is much higher. For example, testing following Buncefield has shown that to severely crush a car in the circumstances of a VCE takes an overpressure of at least 200 kPa.[5] Similar problems apply to other types of objects and structures.

2.3.2 Application of Models Based on Hemispherical Blast Waves

The spherically symmetric decline of blast overpressure from a central explosion is straightforward and has been extensively studied for high explosives [97]. Investigators tended to assume that a vapour cloud could be reasonably represented by a spherical or hemispherical gas volume or an

equivalent TNT charge [98] and that the variation of damage around this cloud could be fitted as P = k/r, where r is the distance to the cloud centre.

Most very large VCEs involve heavy gases and develop over reasonably long periods. A typical cloud shape is like a pancake; the width may be up to 1000 m, but the depth is usually around 2 m. Any spherical or hemispherical blast wave cannot usefully represent the blast wave from such a cloud. [5 & 99] The pressure declines very rapidly at the edge of the cloud, on the length scale of the cloud depth (2 m) rather than its width (1000 m).

The Flixborough explosion provides a clear example of the difficulties associated with forensic work in the era before Buncefield. Estimates for the overpressure indicated by particular objects at ground level, e.g., crushed vessels, cars, snapped poles, etc, varied from >2000 kPa [100] to 50 kPa [101]. Sadee et al. [101] proposed that the pressure effects across the site could be represented by a TNT charge with an elevation of around 50 m. Unfortunately, the pressure levels on which this analysis was based were typically in error by an order of magnitude, and the effort required to force the data into this form obscured the real qualitative lessons that could be learned [92].

Although the incident was thoroughly investigated, an opportunity to recognise that a severe ground-level explosion occurred that affected all of the area covered by the cloud (mostly uncongested) and other similar opportunities were missed [3]

2.4 Developments since Buncefield

All of this changed with the Buncefield incident. Early efforts were made to correlate the damage with a central TNT explosion and to apply the MEM method to congested hedgerows. However, the extent of the cloud could be precisely determined from the burnt areas, and the site was rich in pressure-sensitive targets, so the pressure effects across all of the area covered by the vapour cloud could be compared with those in the areas immediately outside the cloud and beyond [92].

The data clearly showed that similar severe pressure effects (>200 kPa) were sustained across all of the area covered by the cloud (mostly completely uncongested). The severe pressure effects were confined to areas with about 10 m of the cloud edge, consistent with what is expected for a pancake cloud that suffers a severe explosion throughout.

When this type of damage pattern had been clearly identified, a review of previous incidents showed that many more previous incidents were also of this sort [5].

Several other very large VCEs have occurred since Buncefield, and all closely corresponded to the same pattern. The damage sustained to cars, drums, trees, etc., was indistinguishable from the examples documented at Buncefield. The extensive data sets gathered in these incidents provide a clear empirical record of what happens in a large VCE.

However, the question of why these explosions became so severe remains open. Taking a lesson from the subject's history, it is worth studying the circumstances of the actual vapour clouds to establish what features might have played a role in the transition to a severe explosion.

This research, therefore, focuses on the ignition at the Buncefield incident.

2.5 Research Relating to Incidents

The focus of this research is to look at the ignition mechanism at Buncefield to address its effect on the overall explosion. Evidence suggests that the initial ignition event was enclosed in a small, relatively strong box within a building [84]. This will have led to a vented explosion into the cloud within the building, which in turn would have led to a vented explosion into the external cloud. There is a lot of published research into vented explosions, but this focuses on the effect on the confined part of the explosion rather than the ignition of a larger cloud by a venting explosion. There is also the divergence of views over the actual explosion severity at Buncefield and in other large VCEs, which needs to be understood.

2.5.1 Explosion Severity of Vapour Cloud Explosions

There is still active discussion over whether or not transition to detonation, known as a deflagration-to-detonation transition (DDT), occurred in some of the incidents such as Buncefield, with many insistent that it did [5, 19, 88, 89, 93 ,94 & 102-105]. Johnson et al. have gone further and stated that all vapour cloud explosions of the size seen in the incident will detonate simply because of their size and that DDT should be included in risk assessments for these types of sites [88 & 89]. The San Juan incident at the Caribbean Petroleum Corporation, Puerto Rico, is another example in which DDT is openly contested, with some insisting the evidence points to a deflagration and others a DDT [87-90, 106-107]

Atkinson's recent review of incidents [12] also found no evidence that any very large VCEs involving petrol had been flash fires; they had all been severe events.

One possible response to this incident experience is to assume that DDT can occur with high probability and prepare for this as a worst-case scenario [88 & 89]. However, the danger is that if these incidents did not involve DDT, we may not have seen a recent detonation of a pancake cloud on this scale. If this is the case, and if DDT does occur in a future event, then the consequences could be much more severe than those observed recently.

Sites may consider themselves prepared for a detonation event based on the damage in past incidents that have yet to be uncontroversially proven to be one. Also, a longer-term objective should be to control the risk through appropriate plant design. The experience of repeated events with similar consequences suggests that whatever triggers the transition to a severe explosion is a common feature of many sites. If the explosions are not, in fact, detonations, mitigations designed to control the risk may be ineffective.

The presumption that DDT is occurring arises from the presumption that there are only three possible scenarios for a VCE: flash fire, deflagration, or detonation. There is almost universal agreement that the incidents were severe explosions with peak overpressures >200kPa. Still, there is some doubt that the observed damage is consistent with a pressure of around 2000 kPa that would occur during a detonation.

A study by Taveau [108] looks for other explanations for the overpressure seen. In contrast, another study [109] states that they have generated similar damage to objects seen at Buncefield with lower overpressures but longer impulses than in the Buncefield JIP tests [5]. However, no photographic evidence is offered for this.

A review [95] studied photographs from large VCE events, looking for evidence of the continuous curvature of slender metal objects such as scaffolding seen at Flixborough and in detonation tests. No evidence of this was seen in the VCEs, which have very detailed photographic records, i.e., Buncefield, Jaipur, and San Juan.

Researchers reviewed various blast damage evidence to drums, cars, posts, etc., in detonation tests and incidents and found substantial qualitative inconsistencies (Figure 15, Figure 16) [6]. In all cases, the damage observed in incidents could be explained by pressures of order 200 kPa (Figure 17).

Figure 15 - Damage to empty drum in a detonation test – end caps pulled out of plane by severe deformation of upstream face [12]

Figure 16 – Typical examples of damage to empty drums in incidents - end caps remain in plane [12]

Figure 17 - Left - Typical damage to nominally full drum in the incident. Right – results of static pressure tests at 200 kPa [12]

Much of the research on DDT has been based on detonation in tubes, which differ from unconfined regimes and field-scale experimental rigs. The rigs

used so far in VCE testing have only been a tiny fraction of the size of the clouds in any of the large VCE incidents [5, 19, 94, 109 & 110]. Much of the larger scale work uses rigs comprised of repeated rows of congestion. In recent studies, the rig configuration described as lightly congested consists of repeated rows of vertical and horizontal members (Figure 18) [94, 111 & 112].
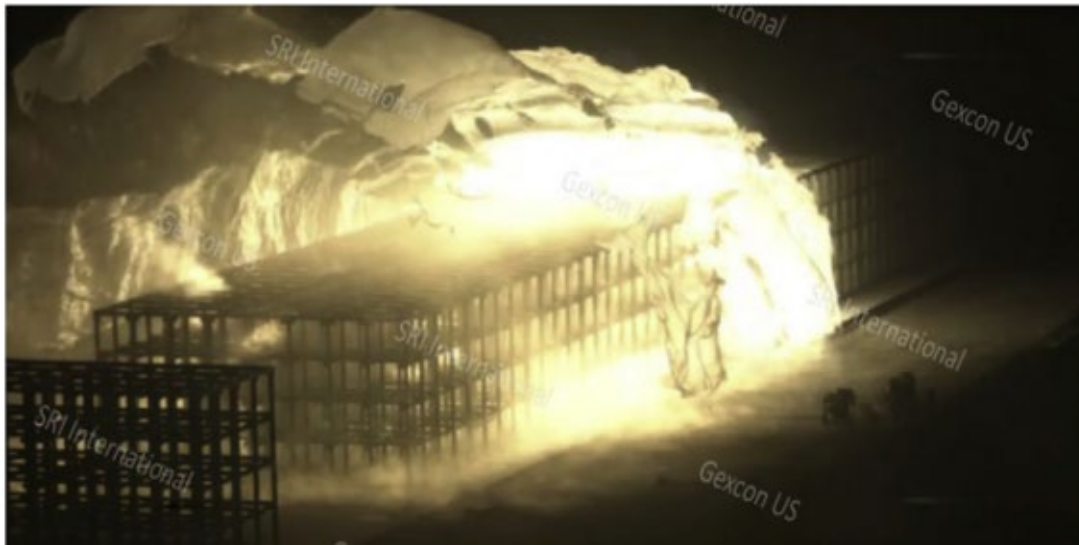
Figure 18 – Large-scale test rig described by Davis et al. as low congestion [94]

Bradley et al. offer another theory of fast deflagration or quasi-detonation [33]. Atkinson and Cusco suggest that the apparently inconsistent observations of sub-sonic average flame speed and high local overpressures can be resolved if the flame's progress is unsteady [91]. They have proposed that events like Buncefield are unsteady or episodic deflagrations, rather like a series of secondary dust explosions.

One hypothesis, discussed briefly in Section 2.1.5, is that an initial violent localised explosion induces vortices in the cloud ahead of the flame front [68-73, 113-115]. These vortices are contaminated with environmental particles such as rust, soot, mineral dust, cellulose fragments, etc., and are heated by the considerable flame front radiation. Heat is rapidly transferred to the surrounding unburned gas by conduction. The radiative heat transfer to unburned gas pockets increases as they roll up in the burning vortex. Pre-

heating of the gas increases the laminar flame speed, causing a local violent explosion as the vortex burns out. Such rapid burning would generate pressure waves that could drive further vortex formation.

Another hypothesis, which takes this further, is that high thermal radiation levels are sufficient to cause multiple spontaneous ignition points in the gas ahead of the flame or within burning vortices [116-118]. This process is due to the radiative heating of blackened dust to temperatures sufficient to ignite the surrounding gas. Recent work by Li and Lindstedt [115] on flammable clouds laden with inert dust adds some weight to the multiple ignition theory [115]. They demonstrate that it is possible that the turbulence caused by an explosion can entrain particles such as soot and that radiation-induced ignitions may occur in an unstable way, leading to an episodic event. One concern with this theory is that organic particles will vaporise before causing the ignition of surrounding gas, so these particles would not be effective in driving ignition.

Some researchers enthusiastically refute the idea of such episodic explosions, convinced that very large VCEs will almost certainly transition to detonation [104 & 105]. However, this argument has aired in peer-reviewed publications and conferences for over a decade.

2.5.2 Vented Explosions

During a contained stoichiometric explosion, the initial combustion raises the pressure until the containment fails or all the gas is consumed, at which pressure reaches its maximum before cooling and condensation of the produced water vapour, which is around 800 kPa for propane, depending on which study [119-121]. If the containment fails, the explosion becomes vented; the internal explosion will push out the remaining unburnt gas, which could be around 80% of the original volume for weak enclosures. Unless the unburnt gas is removed or diluted before the flame exits, it will be ignited by the flame coming out of the enclosure and explode outside the enclosure. The flame will follow the shape of the vented gas plume. In most cases, with a large enough vent aperture, the gas will form a rolling vortex bubble; the flame will then burn that gas, assuming the typical mushroom shape [122 & 123], as demonstrated in Figure 19. This effect will be seen as changes in

the enclosure pressure [124-131]. The pressure will rise to the point of failure and then drop before rising again as the vented gas explodes externally; Figure 20 is a typical pressure trace from such an event. In this instance, the peak marked PFV is the point of vent failure, PEXT is the external explosion, and P_{MFA} is the point of maximum flame area or most intense combustion [128]. P_{REV} and P_{AC} were described as peaks associated with reverse flow and acoustic oscillations; however, they are likely a combination of these, along with Taylor instabilities and reflected pulses contributing to P_{MFA} [132]. The severity of the external explosion is dependent on several factors, such as the size and strength of the enclosure, the severity of the internal explosion, size, speed of flame as it exits and the behaviour of the gas as it vents [125-128, 132-144] in Figure 20 the external explosion is dominant.
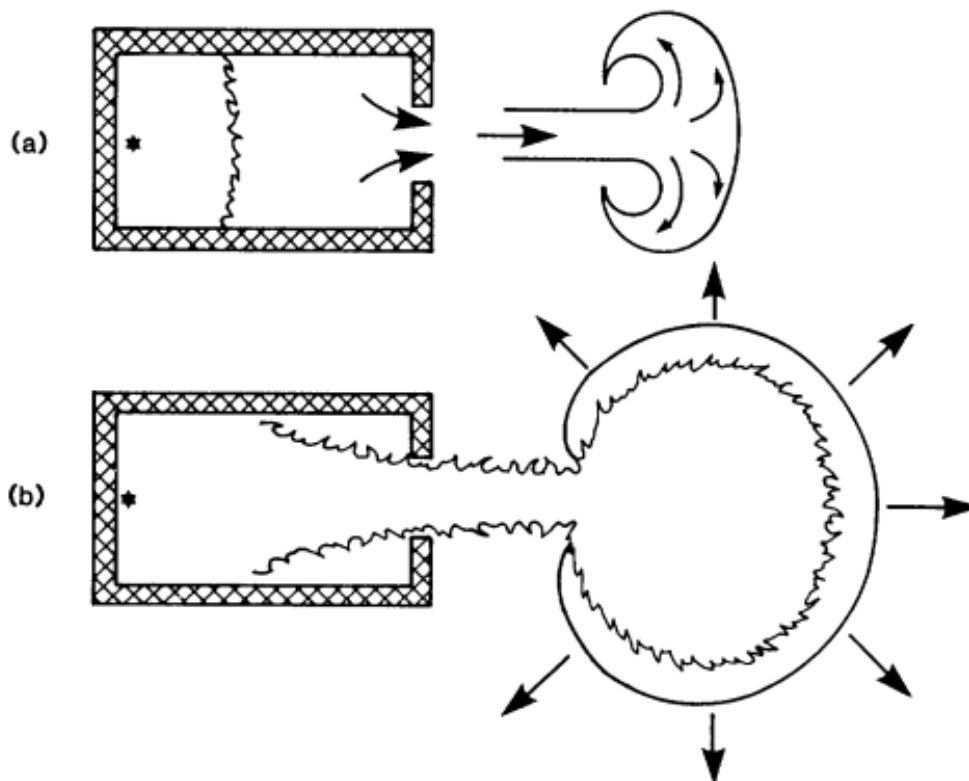
Figure 19 - Diagram of the shape of the vented gas plume and then the resultant flame shape or a typical vented explosion [145]
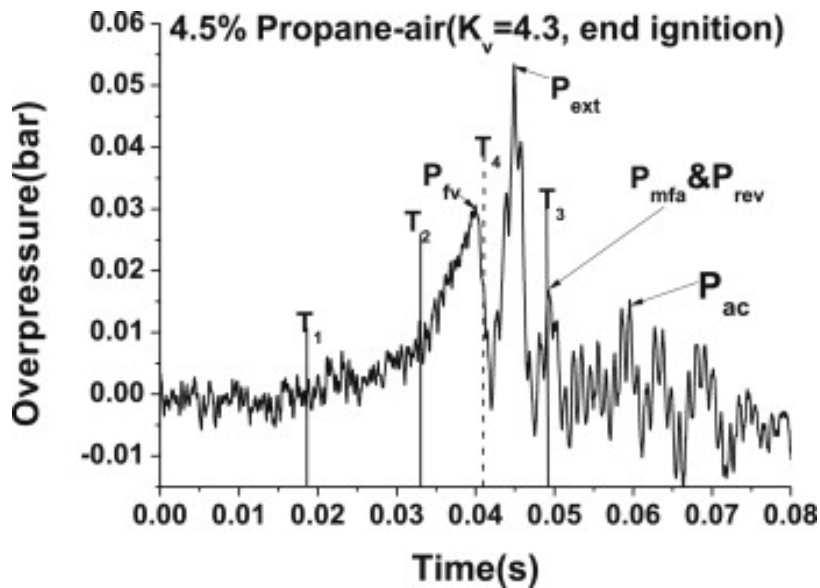
Figure 20 - Typical pressure trace of a vented explosion [128]

Research by Tomlin [130] discovered that in natural gas explosions, the vent size, as well as the degree and location of congestion within the enclosure, affected pressure, although in this study, the pressure measurements reported were from a pressure transducer at the back of the enclosure away from the vent. The maximum pressure reading at an internal pressure transducer during the external explosion is the sum of the pressure wave from the external explosion, the reflected pulse and residual pressure oscillations set up within the enclosure by the internal explosion. Consequently, using internal transducers to monitor the strength of external explosions may be somewhat unreliable. If the timing of the external explosion means there is particularly strong coherence with internal pressure oscillations, then higher peak pressures are recorded at devices within the enclosure. External flame speed measurements may be a more reliable indicator of external explosion strength.

The research by Tomlin also showed that when the vent was restricted, the flame speed near the vent could increase to more than 600 m/s. Most of the increase in speed is likely to result from the gas outflow stretching the flame towards the vent (Figure 21). It was also shown that for ignition at the rear of the enclosure, congestion towards the back of the enclosure had a more significant effect on increasing the flame speed than congestion close to the vent. This was thought to be caused by a combination of two related effects: firstly, the flame surface area increases as it distorts around the obstacles,

increasing the burning rate and, therefore, flame speed and secondly, the unburnt gas is forced through the obstacles causing a turbulent region for the flame to travel into, further increasing the burning rate and flame speed.
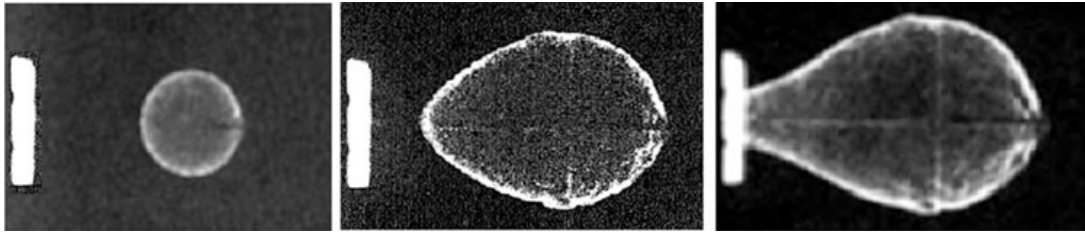
Figure 21 - Images of the stretching of a flame towards an open vent [146]

As venting an explosion to outside is a methodology used in industry to protect vessels there is a lot of literature on the effects of vent location and nature and the presence of ducts on the severity of the internal explosion [137]. But even though there is a European standard for this methodology, there is still a lot of disagreement, with some saying that the approach used in the standard to reduce the effects of the internal explosion is wrong, as it relies on static burst pressures when explosive burst pressures tend to be higher [147 & 148].

The way that the explosion vents to the outside substantially affects the severity of the subsequent external explosion, with turbulent jet venting causing increases in overpressure [127]. It has been discovered that circular vents can enhance this effect [125].

Another factor affecting the strength of external explosions is the proximity of vents when there are multiple vents. Research on dust explosion relief ducts has shown that if the vents are close enough that the venting streams interact, the external explosion will be more severe [149]. This is because there will be an area where the streams of flammable atmosphere ahead of the flame front mix, causing turbulence without being excessively diluted.

2.5.3 Vented Explosions into a Flammable Atmosphere

During a vented explosion, the flammable mixture driven out of the compartment or vessel in the initial stages is subject to some dilution by external air. Turbulence generated by instabilities in the shear layers around the jet is mainly responsible for this entrainment and mixing process. If the

explosion vents into an existing flammable atmosphere, such as an external vapour cloud, turbulence can be created without dilution. Consequently, if a vented internal explosion ignites a VCE, the explosion event will be much more energetic. This is known as a bang-box ignition, and while its effects are known and have been utilised in studies to form an energetic ignition event, there is little research into real-world bang-box hazards [5 & 150]. Most research has been focused on the jet-flame ignition of clouds, as a jet-flame can be an outcome of a vented explosion when the vent area is restricted [151-156]. As the ignition at Buncefield is known to have been confined, Bradley called for more research into bang-box ignitions in 2012 [33].

Researchers at INERIS, in 2017, undertook research to investigate the effects of bang-box ignitions with a particular focus on Buncefield [34]. A strong box with two different vent sizes was used to vent an explosion into a larger tent containing a flammable cloud of propane/air. It was found that with a larger vent, the vented explosion forms a vortex. The explosion resembles a classic bubble shape described by Maxworthy in 1975 (Figure 22), which interacts very little with the surrounding cloud [34 & 122]. With a smaller vent, the vortex breaks down, and the explosion forms into a jet (Figure 23), creating more turbulence in the external cloud, resulting in much higher overpressures. This is well known for circular vents and well-studied [135, 157-159]. However, an opening door does not result in a round vent aperture.
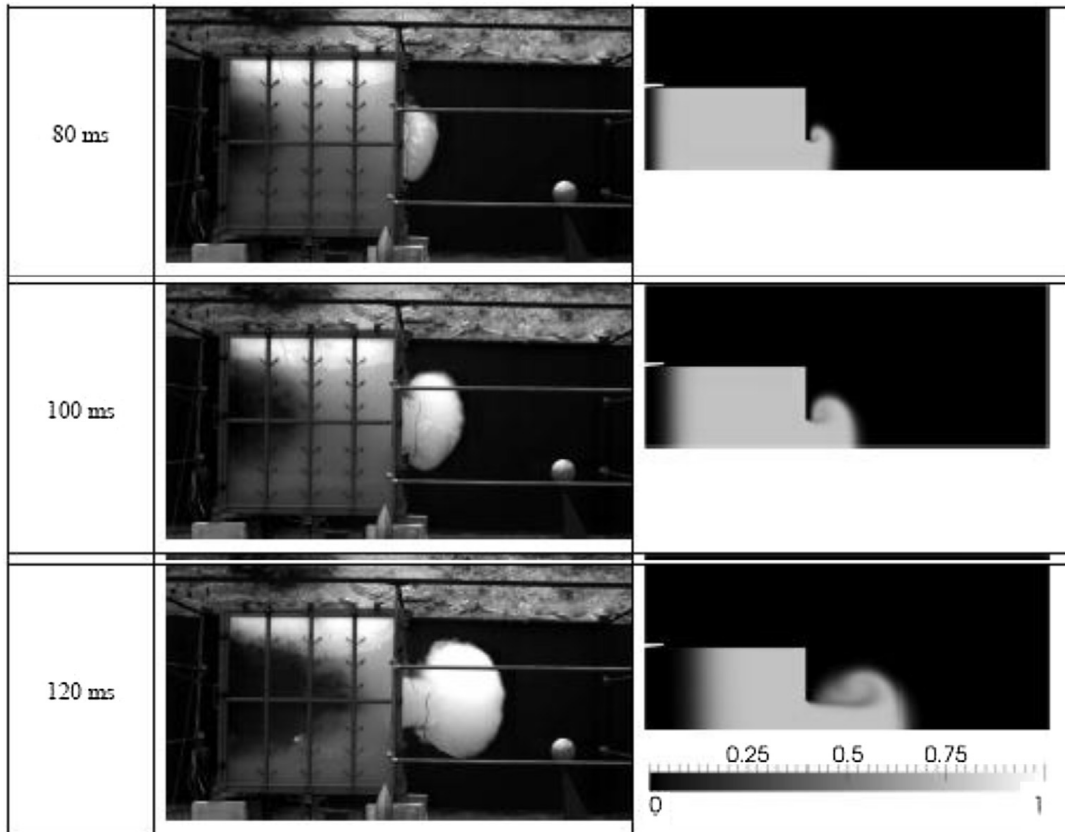
Figure 22 - Bubble formed during the large vent tests [34]
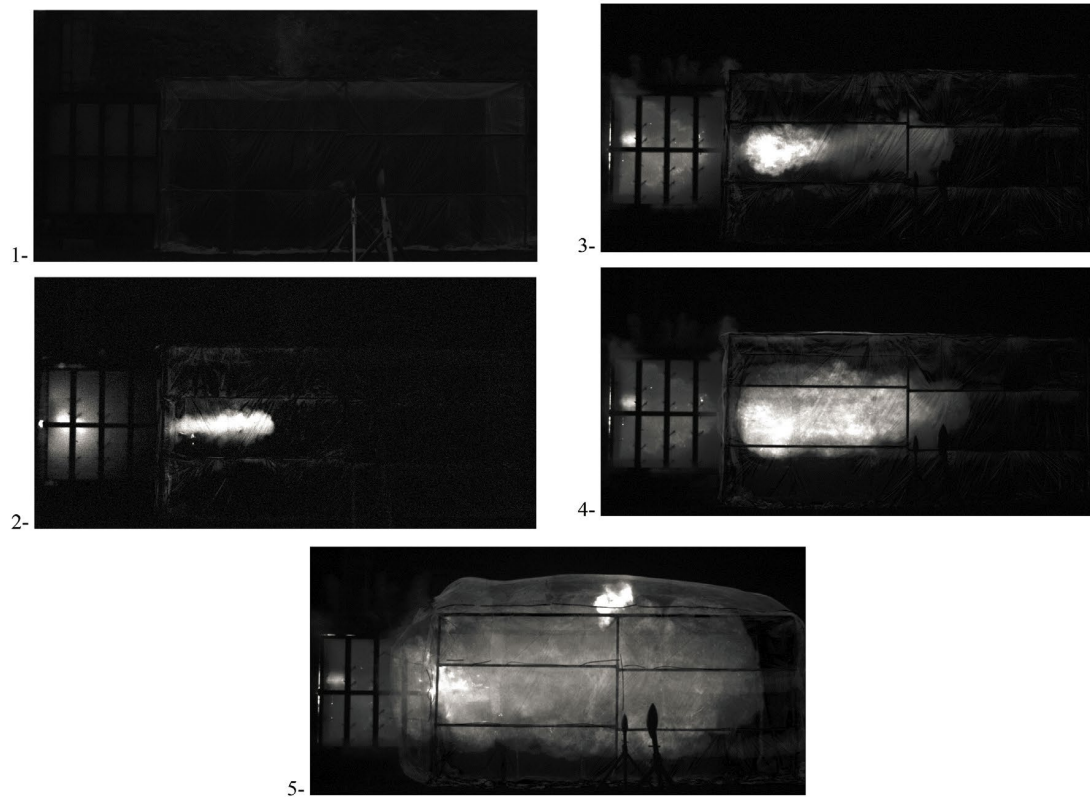
Figure 23 - Jet formed during the small vent area tests [34]

An issue with this study is that the assumption that the ignition event at Buncefield was a simple confined explosion that vented into a cloud is incorrect. The introduction to the paper states that the pump house resembled a concrete bunker. Still, as previously discussed, the ignition source was likely in a small, strong steel box inside a weaker steel-clad building with a moderate level of congestion.

2.5.4 Discussion of Relevant Previous Research

Much has been made of the potential for vegetation at Buncefield to act as congestion and increase flame speeds [19]. However, a more detailed analysis of the character of the pump house explosion in the ignition mechanisms is needed. Daubech's work does not consider all the events in play during the Buncefield ignition [34].

The main issue with previous research into vented explosions is that the focus has been on the nature of the vent orifice; size, geometry, position, etc. and there is little on the effect of the vent covering on the explosion; it is tacitly assumed that the vent covering disappears and plays no significant role as soon as the explosion is initiated or the cover failure pressure is reached. In reality, the vent cover does not disappear, and the details of the mechanism of cover failure and subsequent trajectory of the cover may strongly affect the course of the explosion.

For example, at Buncefield, the switch box (Figure 13) in the pump house was a standard electrical control box consisting of a five-sided box with a hinged door held with a catch. During the internal explosion, the door would have flexed and started venting around seals and holes before the weakest components (catch or hinges) failed. The door would have flown off or violently swung open. Each of these events would have induced turbulence in the gas within the pumphouse, and the point at which the flame exits would have governed the flame shape and exit location. At Buncefield, this event occurred in another confined and congested area. Again, in the early stages of this explosion, the light steel panels of the pump house walls would have flexed, bowing outwards as the internal pressure increased and gas was forced out of the building. The large observed displacements of all the cladding panels suggest they failed almost simultaneously before being

driven violently outward through the surrounding vapour cloud. Gas would have been driven out through the gaps developing in the sheets, and the detached sheets would then have moved rapidly long distances through the wider flammable gas cloud. Each of these processes would have induced turbulence, leading to the acceleration of the external flame.

Chapter 3
Methodology

3.1 Experimental Facilities

The work was undertaken at the HSE Science and Research Centre. This facility is a 550-acre site in Derbyshire that has been used for large-scale explosion research since it was opened as the Safety in Mines Research Establishment in 1947. Since it was taken over by HSE, various blast ranges, bunkers, and explosion vessels have been developed for explosion experiments.

This study used two experimental rigs: one for the steel cladding experiment and one for the control box experiments. These were located on blast ranges designed to accommodate more severe explosions than expected, which had the services to allow the experiments to be controlled from a safe distance.

3.2 Steel Cladding Experiments

These experiments were designed to achieve objective 1 from Section 1.6.

3.2.1 Experimental Rig

The author designed and built all the gas delivery systems and control systems. The rig used for these experiments was repurposed from vessels used in previous Buncefield-related research to assess vehicle damage caused by external explosion overpressures [5]. The vessels were steel cubes with a nominal internal dimension of 2.5 m and had two open faces with 250 mm flanges to allow them to be bolted or welded together modularly. The rig was constructed from three modules welded together with a single end plate, resulting in a vessel with nominal dimensions of 2.5 m x 2.5 m x 7.5 m and a single 2.5 m^2 vent aperture (Figure 24). The rig was mounted on concrete blocks that provided 460 mm clearance from the ground.

Purlins with a Z-section 140 mm wide were bolted to the flange to provide industry-standard support and fixing medium for the steel cladding panels. These were bolted to the top and bottom flange and across the centre of the aperture.

The purlins were framed with a 150 mm deep timber flange to either attach a plastic sheet cover for the baseline experiments to the vent or tape the edges of steel cladding panels to provide a gas-tight seal. The timber protrusion increased the volume of the vessel by a maximum of 1.09 m^3, depending on the nature of the vent covering. The plastic sheeting for the baseline experiments was attached by screwing a timber frame over the sheeting to the timber flange.

For the steel cladding experiments, 0.5 mm galvanised 32/1000 box profile sheets were used (Figure 25). Panels were attached to the purlins using 50 mm long light section self-drilling Tek screws with 19 mm washers. The cladding panels were designed to overlap and provide a cover width of 1 m, excluding the overlap. The aperture sizing allowed for three overlapping panels 3 m long to be attached with the overlap excess width cut from the third panel. The manufacturer's guidance is to apply a fixing in every valley of the sheets. However, it is common practice to use far fewer screws, for example, in every other valley, as this reduces build time and material costs. Both systems were investigated, and specifications for each are provided in the test schedule, Section 3.2.8.

Figure 24 - Experimental rig with purlins and timber flange attached and with cladding panels attached
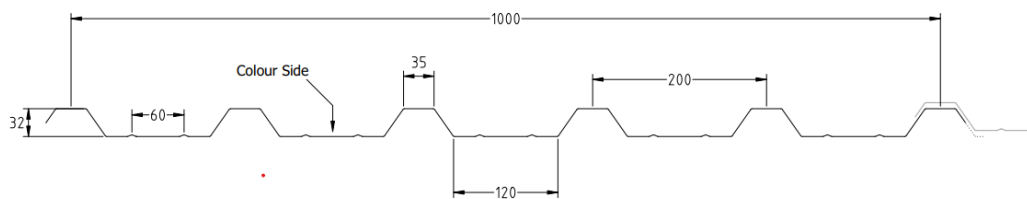
Figure 25 - Diagram of 32/1000 box section steel cladding panel profile [160]

3.2.2 Pressure Measurement Techniques

The sponsor for this research was primarily interested in understanding the sheet failure mechanisms' effects on the overpressures generated by the explosions. Therefore, the focus for measurements was overpressures. Three Kistler type 4043A2 piezoresistive absolute pressure sensors, 0-2 bara range, were used. These sensors transfer external pressure to a silicon load cell via a thin steel diaphragm using a transmission medium of silicone oil. These silicon load cells have a micromechanically produced diaphragm structure. It contains implanted piezoresistive resistors connected in a Wheatstone bridge. The applied pressure unbalances the bridge and produces a proportional output signal [161]. These pressure transducers

(PTs) are high accuracy and high-speed and have in-line amplifiers that condition excitement voltages and amplify sense output signals to provide a sense voltage of 0-10 volts over the 0-2 bara range.

The signals from the PTs were measured using a National Instruments cDAQ 9188 chassis [162] with an NI 9223 voltage input card [163]. This data acquisition system can sample at a rate of 1 million samples a second (1 MHz); however, this research used a rate of 100 kHz.

As the pressure signals are voltage signals and the data logger was located around 20 m away, there is a potential for voltage drop; therefore, calibration was carried out on the entire system. This was done by applying a series of known static pressure loads to the sensors with UKAS traceable calibrated equipment and measuring the voltage outputs with the datalogger. The results produced a calibration curve for converting the voltages to a millibar output in the data acquisition software.

The PTs provided absolute measurements, including atmospheric pressure. To account for atmospheric variations between tests, the initial step in data processing was to zero out this pressure, converting the readings to overpressure measurements instead of absolute pressure.

Two PTs were positioned inside the rig and a third outside, see Figure 26. The internal PTs were mounted flush to the vessel's interior at a nominal height of 1.25 m above the compartment floor. The external PT was mounted in a frame and offset from the compartment axis to avoid damage by missiles, but it was at a height aligned with the vent's midpoint.
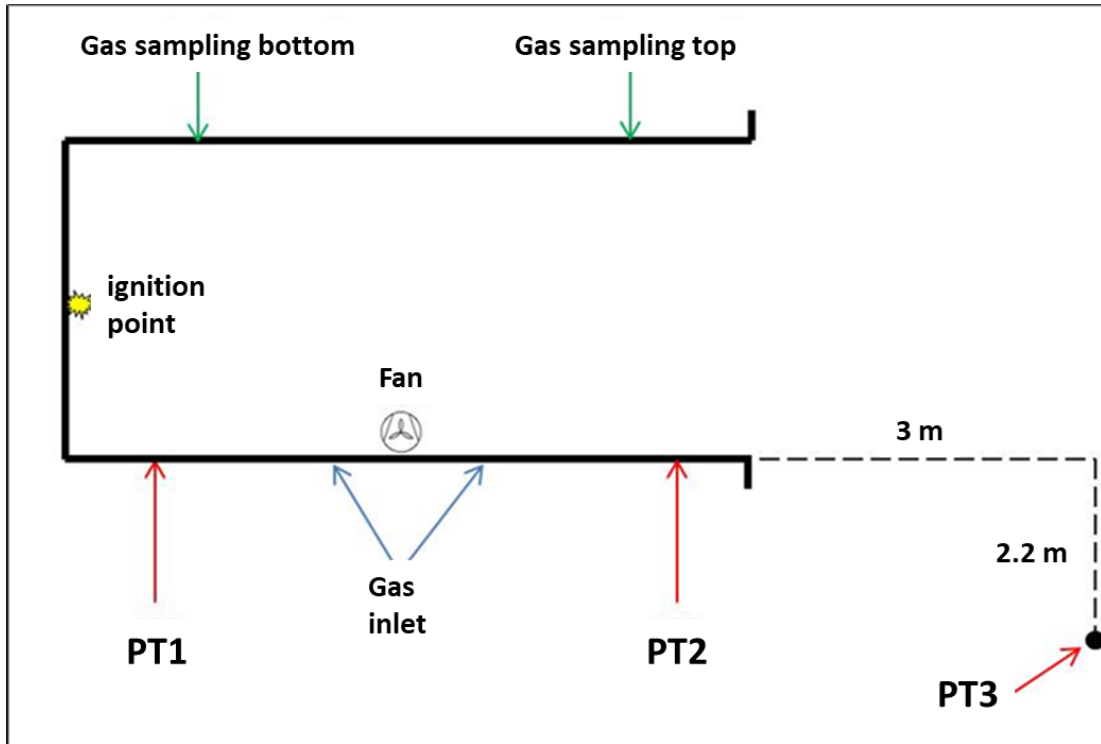
Figure 26 - Diagram of the experimental rig with locations of instruments, ignition, gas inlets and sampling points (Plan view)

3.2.3 Gas Filling, Mixing, and Monitoring

A 230 VAC centrifugal fan (Figure 27) with shroud casing removed was mounted on the vessel with the impellers located inside the vessel. The squirrel cage impeller dimensions were nominally 280 mm OD and 100 mm width, the designed air movement rate inside a duct sized at 260 mm x 195 mm at 230 VAC was 750 m^3/h, in the unshrouded configuration, the fan draws gas into the centre. It blows it out in a 360° spread axially to the impeller, with the flow velocity at the impeller diameter around 2.5 m/s. Two gas inlets were located at the top of the vessel on either side of the fan, with the inlet flow designed to be entrained into the expelled flow from the impeller, thus facilitating as thorough circulation and mixing as possible throughout the vessel.
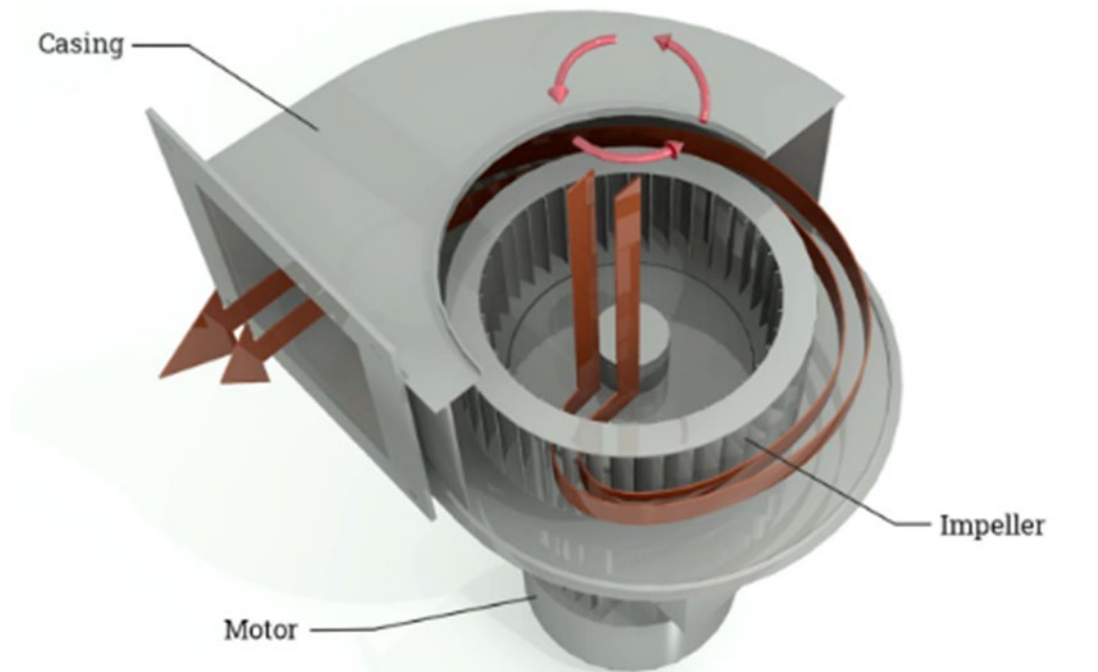
Figure 27 - Representative diagram of the fan before removal of casing [164]

Propane (LPG) was injected into the vessel at intervals. The gas concentration was monitored by sampling from the top and bottom of the vessel on the opposite wall to the fan. The sampled gas was analysed using two ADC MGA 3000 multi-gas analysers with a propane range of 0-10%. The analysers operate using infrared absorption: a pyro-electric detector is used to measure the difference in energy between a reference zero (no infrared absorption) condition and that with the gas present; the concentration is then derived. A reliable concentration measurement can be obtained by calibrating with a known zero and a known concentration of span gas [165]. The analysers were calibrated with nitrogen as a zero and 8.4% propane span gas calibrated each test day. Linearity was checked using a 4.2% propane span gas.

The 4-20 mA output signal of the analysers was connected to the NI datalogger for remote monitoring from the control room, which was situated outside the exclusion zone. If the required concentration was overshot, the gas inlets could deliver air from a compressed air cylinder pack to reduce the gas ratio. Once the analysers indicated the specified concentration, the fan was left running, and the gas concentration was monitored to ensure homogenous mixing had occurred. Once the gas concentration was

confirmed stable, the fan could be turned off if the test conditions called for static gas.

3.2.4 Videography

All experiments were filmed in high-definition 50 fps video to provide a record of the experiments. Due to the results of the experiments, high-speed video was used for tests 8 and 9; this was recorded with a Phantom Miro LC320s camera at a speed of 1500 fps. The purpose was to understand the mechanism of steel cladding detachment from the vessel; the intention was for visual confirmation, not for analysis of flame or missile speeds.

3.2.5 Ignition System

J-Tek 1 J electric matches were used to ignite the gas. The reason for the selection was specifically down to safety. The matches were fired using 24 VDC and have a very low ignition failure rate. Due to the vessel being metal and located outside, attempts to install a spark ignition resulted in a system with high unreliability or interference with the instrumentation.

The ignition system was installed at the beginning of the test before the vessel was filled. When in safe mode, the firing system was a short circuit so that the match head could not activate prematurely. Arming the system opened the circuit to allow the firing current to be applied.

3.2.6 Safety

The proposed work and procedures underwent a peer-reviewed risk and DSEAR assessment. Hazards were mitigated, notably by eliminating the use of mains voltage equipment. Where elimination was unfeasible, risks were reduced to as low as reasonably practicable (ALARP). Experimental tasks, including gas filling, were performed remotely.

The primary safety issues were due to the scale of the experiments, with particular concerns regarding sound levels and projectiles generated by the explosion tests.

The experiments had to be conducted with an exclusion zone to ensure that no personnel would be allowed close enough to the experiment to be subjected to peak noise above the L_{Cpeak} 135 dB action limit [166].

The exclusion zone was set based on the results of previous vapour cloud explosion experiments on the range and as a further safety measure based on this programme's experimental results. For the first experiment, the exclusion zone was set at a 350 m radius; the experiment was the predicted worst case for noise. Noise measurements were taken from two locations using Brüel & Kjær type 2270 sound meters. Based on the results, the first sound meter (SM1) was located at the edge of the expected exclusion zone. (see Figure 28). The second meter (SM2) was situated next to the control room. A large earth bank protected the control room. The L_{Cpeak} sound measurement results for the first test were 132 dB at SM1 and 122 dB at SM2. Sound meter readings were taken at SM1 for each experiment so the exclusion zone could continually be reassessed based on the results.

The second main concern was projectiles, such as the steel cladding panels and fixings when forcibly removed by the explosion. The vessel was located in a valley, with the opening toward the valley slope. Any projectile fired from the vessel opening would hit the bank within 20 m. This distance was significantly smaller than the exclusion zone needed for sound.

A lookout with views extending beyond the exclusion zone was deployed for each test to control the area and ensure it was safe to proceed. They would provide details of activity beyond the exclusion zone before the start of the test and ensure that the exclusion zone was clear for the entirety of the experiment.

To account for unplanned events, all valves were designed to fail safe if a loss of power or control was experienced. A multicylinder pack of compressed air was connected to the gas inlet; the supply could be switched between this from the propane if there was a need to abort the test and purge the vessel of flammable gas.
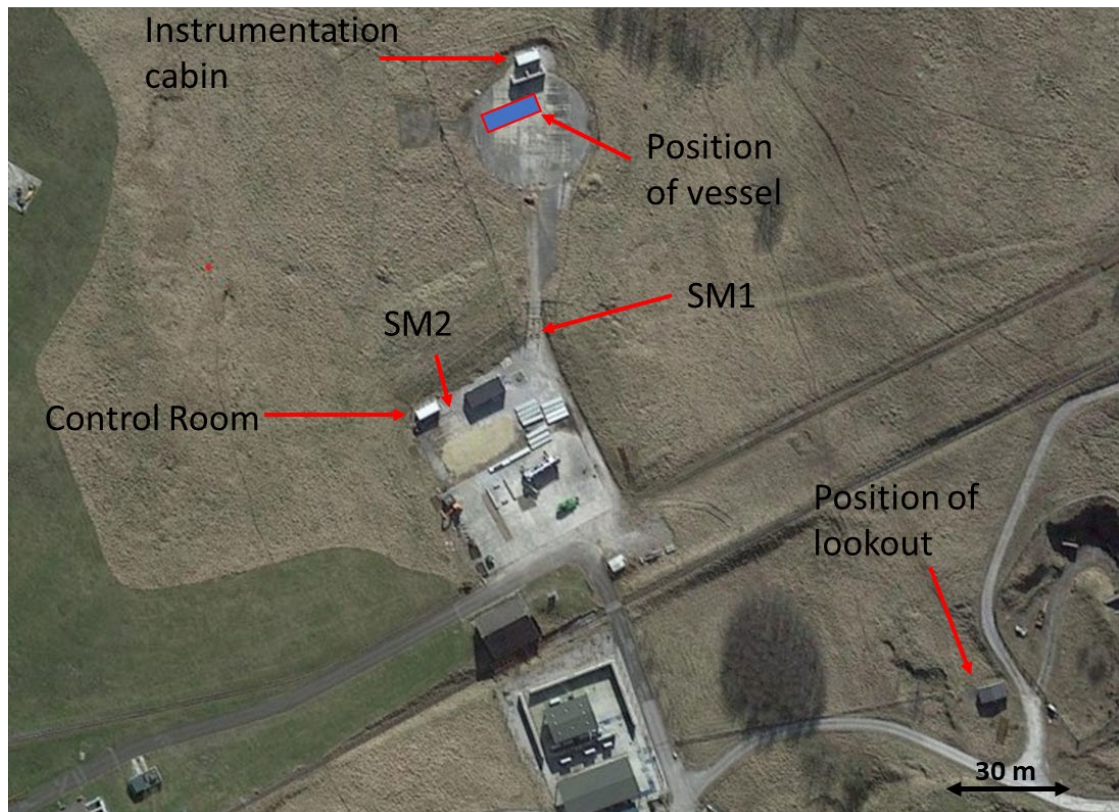
Figure 28 - Overhead view of test range with position of buildings, vessel, sound meters and lookout marked on (Google Earth)

3.2.7 Experimental Protocol

For these experiments, the procedure was:

1. Install vent and seal
2. Install ignition system and clear exclusion zone
3. Lookout to confirm all is clear
4. Turn on the fan and open the propane valve
5. At a measurement of 3.5% propane, stop filling and wait 5 minutes
6. If the final concentration is not nominally 4.2%, open the propane valve for 1 minute, wait 2 minutes, and repeat until 4.2% is achieved.
7. If the fan is to be off, turn off and wait 2 minutes
8. Confirm all clear with the lookout
9. Arm highspeed data trigger and fire

3.2.8 Experimental Test Schedule

All experiments in this program were to be conducted with the propane concentration at 4.2%; the variables for these experiments were the vent covering and the fan being on or off during the ignition, see Table 3. The purpose of leaving the fan on was to create a reproducible, lightly turbulent atmosphere for the explosion.

For vent coverings, "full strength steel system" indicates three cladding panels attached to the purlins using a screw in every valley. The "weak system" indicates fixing in every other valley. Polythene sheets were used for baseline tests; a 120 micron sheet was compared to a 60 micron sheet, which, was preferred due to lower opening pressures and ease of covering the vent aperture.

Test 9 was added to assess if a deliberate weakness could provide a potential mitigation.

Table 3 - Experimental programme for steel cladding experiments

Test Number	Fan	Vent cover
1	On	120 micron polythene
2	Off	60 micron polythene
3	Off	60 micron polythene
4	On	60 micron polythene
5	On	Full strength steel system
6	Off	Weak steel system
7	Off	Weak steel system
8	On	Weak steel system
9	Off	Strong steel system with weak centre panel

3.3 Electrical Control Box Experiments

These experiments were designed to investigate the flame propagation mechanisms from commercially available electrical control cabinets with a hinging door, per objective 2 discussed in Section 1.6.

3.3.1 Experimental Rig

The author designed and constructed a purpose-built enclosure for all experiments involving electrical control boxes, along with the gas delivery and control systems.

An 8 m^3 frame rig measuring 2 m on every edge was constructed from mild steel angle (Figure 29). The back wall of the rig was a 5 mm thick steel plate with four gas ports. An electrical control wall box could be mounted to fit flush with two of the ports (Figure 30).

The electrical control boxes used were high-quality, commercially available Schneider Spacial S3DEX ATEX wall box enclosures [167] 600 mm high, 400 mm wide and 250 mm deep, with a nominal volume of 0.06 m^3. The boxes had a full steel door with a mass of 3.29 kg (Figure 31). The door was attached by two 50 mm long hinges. The door had a soft foam rubber gasket that fitted around the lipped flange of the box. The closing mechanism was a 15 mm wide plastic catch that engaged with the inside of the flange on the longest wall when the removable external handle was rotated. Protruding from the catch were two 5 mm diameter steel bars that engaged with the inside of the flange at the top and bottom; these were stabilised near the door with weak plastic supports. The shape of the flange leaves an actual opening of 365 x 560 mm. The entire closing mechanism was designed to be easily removed by the user to allow for the replacement of the handle with an aftermarket key-locking handle. The door and hinges were designed to be easily removed and inverted by the user. During these experiments, the door and hinge pin were replaced with new ones after each test. The hinges were changed if they became damaged because of the previous experiment, and the box was also changed if it became distorted.

For some of the tests, the door was removed completely, and the opening was covered with a membrane to establish base explosion characteristics

with a bursting-type vent covering. Due to the shape of the aperture, designed to seal on the door, the membrane was taped to the flat surfaces of the box with duct tape. The left side wall of one box was cut away and replaced with a 5 mm polycarbonate sheet for viewing purposes.

Control boxes are usually full of equipment which will act as congestion elements. The contents of these boxes are highly varied depending on their use. There may be large and small electrical components, cabling, and pneumatic tubing. The boxes are also available in a wide range of sizes and styles. Generally, the economic driver will be to utilise the space within the smallest possible box for the required task.

To limit variables, only one style and box size was used for testing in this work. For tests where congestion was added, the aim was not to recreate a specific installation but to produce a robust, easily reproducible, and consistent configuration between tests. Commercially available Schnieder NSYMR64 monobloc perforated chassis plates were used (Figure 32). These are designed to fit inside the box and be used to attach equipment. Up to four of these chassis plates were bolted together with a spacing of 50 mm and attached to the inside of the box with the intended mounting bolts. The grid had rectangular holes and an area blockage ratio of 21.5% in the centre, with a solid border around the edges and mounting points. When fitted, there is a 25 mm gap around the plate. The mounting points of the three forward grids were cut away to facilitate the array fitting as a single piece. In testing, the flame kernel was expected to travel through the central gridded section before vent failure.
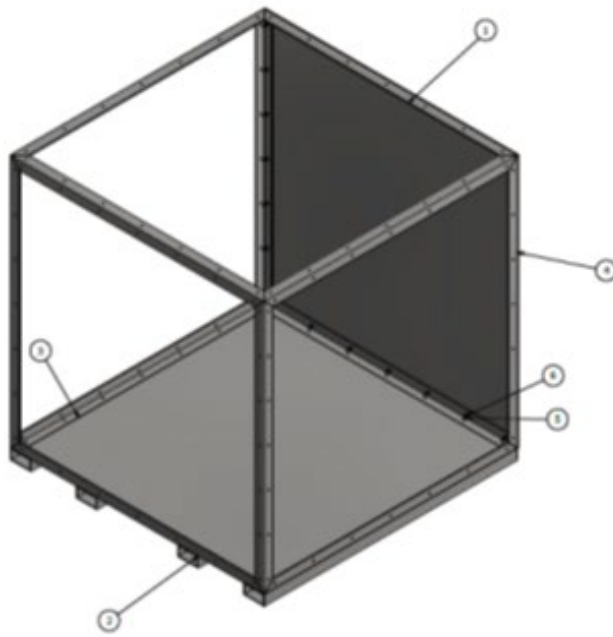
Figure 29 – Technical drawing of Steel frame rig

Figure 30 - Steel frame rig with electrical control box mounted

Figure 31 - Electrical wall box doors 3-point locking system

Figure 32 - Chassis plates used for congestion, as received and fitted into the wall box

3.3.2 Pressure Measurement Techniques

Calibration and pressure measurement techniques were discussed in Section 3.2. Figure 33 shows the layout of the transducers. Experiments were conducted with PT1 in different locations within the control box; the results showed that positions A and B recorded identical pressure results. Therefore, these positions were considered interchangeable during experiments.

For some door experiments, PT2 was moved to a position 250 mm perpendicular to the box, in line with PT3; for these tests, the PT2 is referred to as PT2a.

3.3.3 Flame Speed Measurement Techniques

Flame speeds were initially measured using 1 mm diameter K-type thermocouples with an exposed tip. The voltages of the thermocouples were recorded using a National Instruments NI 9205, a high-speed voltage card with a ±0.2 V range. The change in the potential difference at a millivolt level caused by the temperature change as the flame arrives at the thermocouple was recorded by the datalogger. This provided a point-to-point flame speed. The thermocouple (TC) positions are shown in Figure 33.

In addition, medium and high-speed videography was also utilised in some tests using a GoPro Hero 5 at 240 fps and a Phantom Miro LC320s at 1000 fps; as the work progressed, HSE purchased a higher specification Phantom V2640 camera that offered higher resolution at a higher frame rate. The video output was analysed to measure the flame speed, and the number of frames the flame travelled over set distances was used to calculate the point-to-point flame speed. The locations of the cameras are shown in Figure 33.
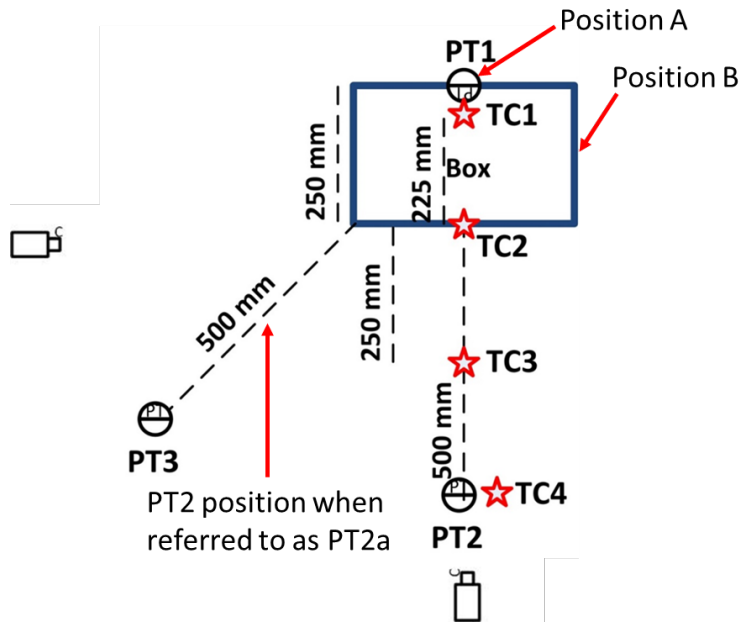
Figure 33 - Layout of pressure transducers and thermocouples

3.3.4 Gas Filling and Monitoring

The gas filling system was designed to cover all planned tests, including those in which the frame rig and box would be filled with a flammable atmosphere. For this reason, a purge-fill method was decided upon. The piping and instrumentation diagram (P&ID) for this is shown in Figure 34. The rig had four ports with pneumatic actuated ball valves attached, two aligned with the control box and two into the remaining volume of the rig. The upper valve was an outlet, and the lower valves were inlets for gas filling (Figure 35). The outlet gas flow was sampled using ADC MGA 3000 multi-gas analysers with a propane range of 0-10%. A single sample line was used, and this could be switched between the two outlets with pneumatic ball valves.

Bronkhorst IN-FLOW thermal conductivity mass flow controllers (MFCs) were used to meter the air and propane into the downstream pipe work. Four calibrated MFCs were used:

- 5000 l/min Air
- 20 l/min Air
- 200 l/min propane
- 10 l/min propane

The gas flow quantities were set on the MFCs to supply a mixture of 4.2% propane in air at a flow rate of 20 l/min. Once five volume changes of the control box had been achieved, and the propane concentration flowing out of the box gas outlet was stable at 4.2%, all the valves were closed, and the gas flow was stopped. As the control boxes were airtight at ambient pressure, the internal concentration remained stable indefinitely.

The closed valves at the rig offered protection against unintentional ignition and flashback of the flammable atmosphere in the gas system. However, as further protection, a flashback arrestor was located just after the valves. Where the compressed air and propane flows enter the supply system from the MFCs, one-way check valves were situated to prevent back contamination of either stream. The propane stream was further protected by another flashback arrestor with an integral check valve. The check valves limited the maximum possible flow to below the reported maximums of the MFCs. However, this compromise was acceptable to protect the instruments from flashback.

Instrument List

Label	Description	Connection Size	Pressure rating	Manufacturer	Model
I-1	5000 l/min Propane Flow Meter	25 mm Swagelok comp	100 bar	Bronkhorst	In-flow
I-2	200l/min Air flow Meter	12 mm Swagelok comp	20 bar	Bronkhorst	In-flow
I-3	200l/min Propane Flow Meter	12 mm Swagelok comp	8 bar	Bronkhorst	In-flow
I-4	3.5l/min Propane Flow Meter	12 mm Swagelok comp	8 bar	Bronkhorst	In-flow

Connector details

Connector type	Working pressure	Maximum pressure in system	Manufacture	Series
Compression	125 Bar	10 Bar	Swagelok	ss-mo
Push fit	20 Bar	10 Bar	legris/ITM	LF3000/ITM metric
threaded	10	Negligible 0-<1 bar	RS pro	ANSI s20

Label	Description	Line Size	Working Pressure rating	Max actual pressure in system	Manufacturer/supplier	Model
V1	propane regulator	12 mm	10 bar at inlet cylinder at 7.5 bar 20 DegC outlet 4 bar		BOC	Series 6000 Single-stage
V2	N/C AA ball valve	1/2 inch	8 bar	4 bar	Valbia	Valpres Art. 703000
V3	N/C AA ball valve	1/2 inch	8 bar	4 bar	Valbia	Valpres Art. 703000
FBA1	Flashback arrestor	N/A	30		BOC	41542
V4	Manual Ball Valve	12 mm	103 bar	4 bar	Swagelok	Series 40
V5	Manual Ball Valve	12 mm	103	4 bar	Swagelok	Series 60
FBA2	Flashback arrestor	12 mm	5 Bar	Nominal 0 to <1 bar	Witt	85-20
FBA3	Flashback arrestor	1 inch	17.7 Bar	Nominal 0 to <1 bar	Elhardo	DTA-101-5/8-660R-6
V6	Air regulator	12-25mm	210bar at inlet cylinder at 180 bar max outlet 10 bar		Concoa	622 series
V7	Pressure relief Valve	12mm	17 Bar	10 bar	Norgren	V74G
V8	Manual Ball Valve	12 mm	103 Bar	10 bar	Swagelok	Series 60
V9	Manual Ball Valve	25 mm	103 Bar	10 bar	Swagelok	Series 60
V10	Check Valve	25 mm	103 Bar	10 bar	Swagelok	Series 60
V11	N/C AA ball valve	1/2 inch	68 Bar	Nominal 0 to <1 bar	Acuation Valves and controls LTD	Custom built
V12	N/C AA ball valve	1 inch	68 Bar	Nominal 0 to <1 bar	Acuation Valves and controls LTD	Custom built
V13	N/O AA ball valve	1/2 inch	68 Bar	Nominal 0 to <1 bar	Acuation Valves and controls LTD	Custom built
V14	N/O AA ball valve	1 inch	68 Bar	Nominal 0 to <1 bar	Acuation Valves and controls LTD	Custom built
V15	N/O AA ball valve	1/4 inch	68 Bar	Nominal 0 to <1 bar	Acuation Valves and controls LTD	Custom built
V16	N/C AA ball valve	1/4 inch	68 Bar	Nominal 0 to <1 bar	Acuation Valves and controls LTD	Custom built
P1	Propane Line	12 mm	68 Bar	Nominal 0 to <1 bar	Acuation Valves and controls LTD	Custom built
P2	Air line	12 mm	15 Bar	4 bar	Bearing Boys.co.uk	BS EN 12449/BS 2871
P3	Air line	25 mm	15 Bar	10 bar	Parker	NTM12/100c
P4	Stainless steel 12 mm tube	12 mm	300 Bar	10 bar	Hose world	NV-25/20
P5	Stainless steel 25 mm tube	25 mm	200 Bar	10 bar	Swagelok	SS-T12M-S-1.5M-6ME
P6	BS6501 1 inch hose	1 inch	50 Bar	Nominal 0 to <1 bar	JF hoses	SS-T25M-S-2.0M-6ME
P7	BS6501 1/2 inch hose	1/2 inch	200 Bar	Nominal 0 to <1 bar	JF hoses	Custom built

Figure 34 - P&ID of gas filling system.

Figure 35 - Back wall of the rig with valves attached

3.3.5 Ignition system

A method of ignition was required that did not impart significant kinetic energy into the surrounding gas or produce any flaming debris to cause secondary flame kernels in the box. The aim was to produce a smooth initial flame kernel without flame wrinkling or turbulence. Therefore, it was decided to use Talon hotwire firework ignitors; these have no pyrotechnic material and are designed to clip onto a consumer firework fuse. For these experiments, part of the clip was removed to expose the wire; the wire heats up when initiated, and ignition occurs when the temperature reaches the auto-ignition temperature of the fuel gas (Figure 36).

The igniters were taped to the rear wall of the box and initiated with a 12 VDC ignition circuit. The ignitors proved to be 100% effective. Any failed ignitions were due to issues with the circuit, such as animal attacks or corrosion. However, a pre-test ignition system check was successful in identifying these issues.

Figure 36 - Talon Ignitor - as received, with the clip removed and energised

3.3.6 Safety

Before the rig design, the work was subject to a HAZOP (hazard and operability) study. The output of this study was used to build a peer-reviewed risk and DSEAR assessment for the experiments. Hazards were eliminated where possible. Where elimination was impossible, the risk was reduced to as low as reasonably practicable (ALARP). The experimental activity, including gas filling, was conducted remotely from the control room.

The rig was located on a blast range previously used for blast exposure testing of passive fire protection. This blast rig was a 12 m long tube of greater volume than this rig and was used to subject samples to strong deflagrations with overpressures up to 2 bar. Initially, the exclusion zone for noise was set using the exclusion zone for the blast rig (Figure 37). The reasoning was that it was highly conservative and offered convenient locations for lookouts. As per the previous experimental programme, sound measurements were taken for each change of condition to adjust the exclusion zone if necessary. The results showed that using the blast range

fenced compound as an exclusion zone was sufficient and convenient for all tests.

The other consideration was the door and components forming projectiles; with the doors having much weaker catches than hinges, complete displacement of the door was considered unlikely. However, the door's weight and energy available in the box were used to evaluate the potential range of a projectile in a worst-case scenario. This showed that no personnel or safety-critical equipment were in danger from projectiles with the rig in the chosen orientation.

To cover a loss of control, all valves were designed to fail safe; the fill valves failed to close, and the vent valves failed to open. A sufficient inventory of compressed air was maintained to purge the rig of flammable gas if needed.
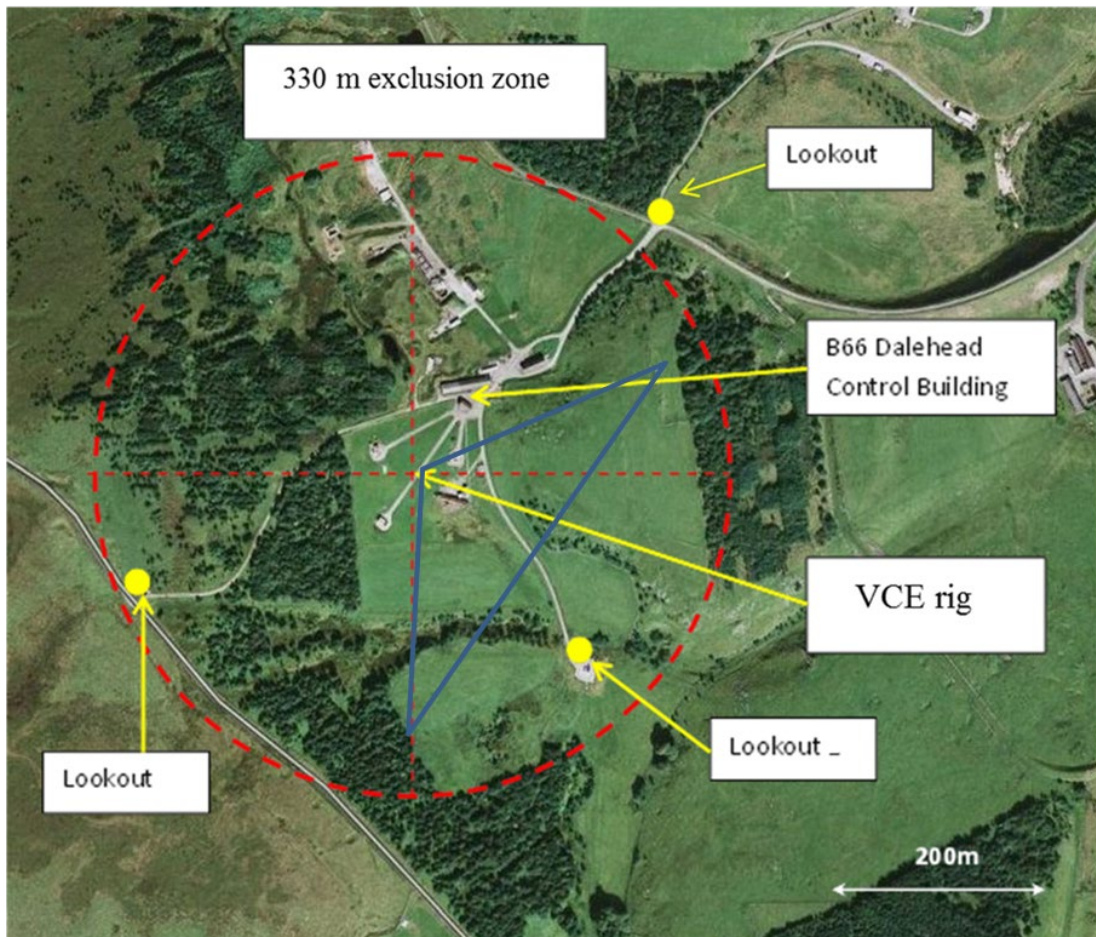
Figure 37 - Maximum exclusion zone and location of lookouts

3.3.7 Experimental Protocol

A comprehensive operating procedure, with an aid memoir check box, was written for the experiments; an example is attached in Appendix A.

3.3.8 Experimental Programme.

The experimental programme was designed to be conducted in five stages, with all experiments using 4.2% propane and air.

1. Empty box with PVC cling film covering the opening
2. Empty box with foil covering the opening
3. Empty box with door on
4. Box with congestion and foil covering
5. Box with different levels of congestion with door on

The full test schedule is given later in this Chapter.

3.4 Electrical Control Box Inside Covered Frame Rig or Tent

These experiments were designed to investigate the effects on explosion severity in an 'unconfined' volume of pre-mixed gas when ignited by an explosion propagating from a control box as per objective 3, as discussed previously in Section 1.6. To investigate effectively, it was required to undertake baseline tests to understand the effects of explosions in the control box on the tent when filled with air and to understand the explosion characteristics of an explosion initiated in the tent filled with 4.2% propane and air.

3.4.1 Experimental Rig

The rig used was as previously discussed in Section 3.3.1, except that the outer frame provided a tent containing an external volume from the control box. A 2 m2 piece of 4 mm clear polycarbonate sheeting created a viewing window. This was attached to the front of the frame to provide a clear view of the front of the electrical box and the flame's progress for the high-speed camera. Clear plastic sheeting was used to provide a gas-tight seal for the remaining three sides of the frame.

Previous tests showed that the flame direction travels transversely from the door opening. To allow the maximum possible travel distance for the flame, the control box was located on the edge of the back wall at a central height instead of the centre of the back wall (Figure 38). This allowed a distance of 1550 mm from the door opening to the plastic film on the outside of the rig.

3.4.2 Pressure Measurement Techniques

Calibration and pressure measurement techniques were discussed in Section 3.2. Figure 39 shows the layout of the transducers.

Figure 38 - Rig configuration for propagation experiments.
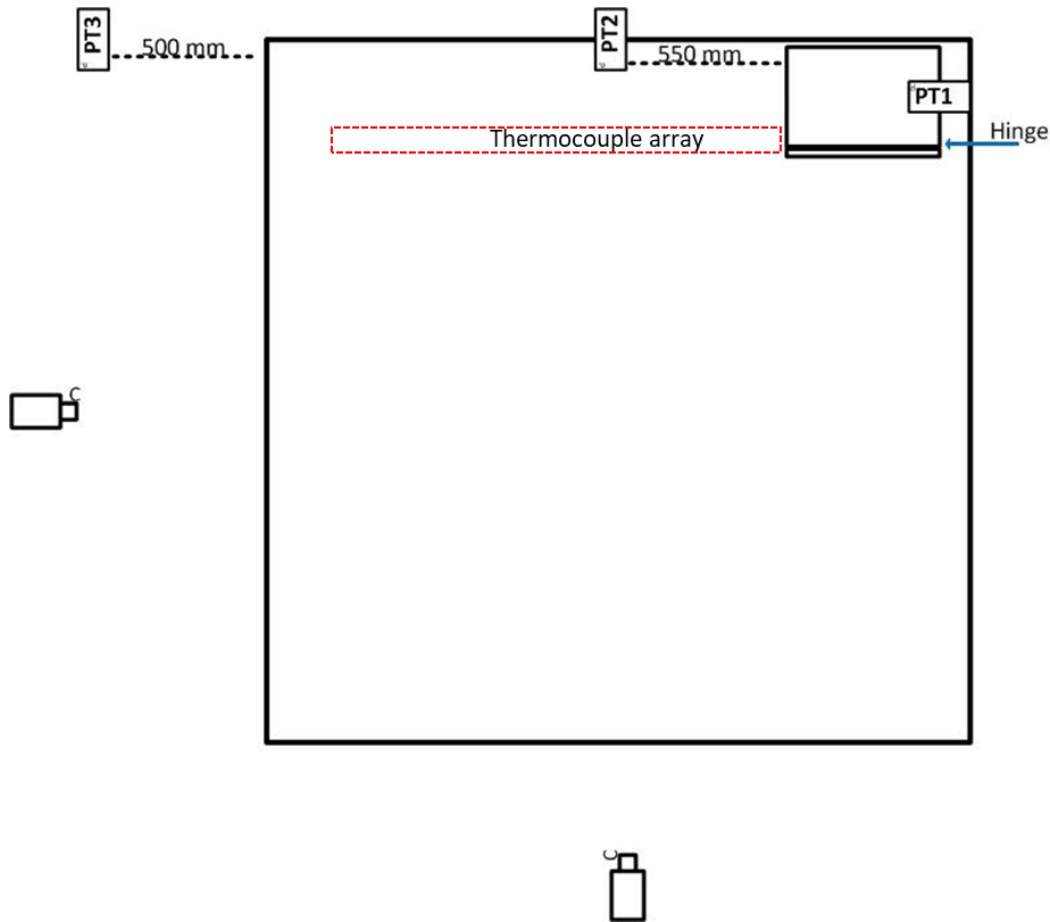
Figure 39 - Layout of highspeed cameras, pressure transducers and the thermocouple array

3.4.3 Flame Speed Measurement Techniques

The primary method of flame speed measurement was via high-speed videography using a Phantom V2640 camera with a frame speed of 10000 fps. As a secondary method, a thermocouple array was constructed so that 3 mm diameter thermocouples with exposed tips could be positioned at set distances with the exposed tips in line with the door opening. The thermocouple data was acquired as detailed above in Section 3.3.3.

3.4.4 Gas Filling and Monitoring

For some tests, the outer tent was not filled with a flammable atmosphere; this was to allow baseline tests of the dynamics of the box venting into a sealed tent.

The gas filling and monitoring method was as detailed above in Section 3.3.4. The control box was filled first, and as the boxes were gas-tight, the

concentration remained stable while the outer tent was filled. The outer tent was filled using the higher-range MFCs.

3.5.5 Ignition System

The ignition method was as described above in Section 3.3.5.

3.5.6 Safety

The safety procedures for the control box experiments, detailed above in Section 3.3.6, were designed to include these experiments.

3.5.7 Experimental Protocol

For the experiments, a comprehensive operating procedure with an aid memoir check box was written; an example is attached in Appendix B.

3.5.8 Experimental Test Schedule

The experimental program was designed to be conducted under five different conditions. Each experiment has four rows of congestion in the box, and ignition is in the box unless stated otherwise.

1. Box with 4.2% propane and air, tent with air
2. Tent with 4.2% propane and air, ignition source in tent
3. Tent with 4.2% propane and air, a box with no door
4. Tent with 4.2% propane and air, a box with a door and 4,2% propane and air
5. Tent with 4.2% propane and air, a box with a door and 4,2% propane and air, a congestion array external to the box inside tent

Chapter 4
Explosions Vented by Standard Steel Cladding Panels

4.1 Introduction

These experiments were designed to investigate any effects on the severity of explosions venting from a building covered in lightweight steel cladding panels, per objective 1 from Section 1.6.

Buildings made from lightweight steel cladding panels attached to a frame and purlin structure are easy and convenient to build. The structural strength of the building is within the frame; the cladding is weather protection. Therefore, the strength of the cladding fixing is designed around its ability to withstand wind loading to the external face. Should an explosion occur in such a building, it is likely to be significantly damaged. If the pressure rises rapidly (i.e., high internal flame speeds), the explosion might remove a large proportion of the panels. This work aimed to investigate how the magnitude of the external explosion is affected by the mechanism of the building failure and jet outflow of unburned gas and flame. The cuboidal experimental vessel (Rig 1) used has an aspect ratio of 3:1, with only the smaller, square end face clad in profiled steel panels. This means that the explosion scenario in which all boundaries of an enclosure fail simultaneously cannot be studied. Still, the likely long-axis acceleration of the flame before venting provides a conservative test for these geometries. The rig does offer the opportunity to study the mechanism of detachment of a series of panels and how this affects the gas outflow and explosion intensity. The purpose of the polythene sheet experiments is to characterise the explosion in the vessel with a very weak vent covering, which is likely to fail in a bursting-type mechanism.

4.2 Pressure Development

Explosions in vessels with a large vent area are multi-staged events with peaks and falls in pressure. A typical pressure trace from Rig 1 with the peaks highlighted is detailed in Figure 40. The origin of different peaks from

vented explosions has been widely discussed; there is a vast amount of variability depending on factors such as vessel shape, size and congestion level, ignition location, vent size and geometry [132, 168-176]. Mostly, there is a consensus regarding the causation of the first two peaks; comparable pressure traces are described by Tomlin et al. [130] for methane-air explosions and Carcassi et al. [173] for hydrogen-air mixtures. On ignition, the flame development induces a pressure rise within the vessel. The rate of pressure rise may be initially offset as a plastic vent stretches under the increased pressure, effectively increasing the rig's volume. The pressure reaches a peak (shown as P_1 in Figure 40) corresponding to the failure pressure of the vent. After the vent opens, the pressure will fall or plateau, depending on the efficiency of the vent, as the unburnt gas is driven out of the vessel ahead of the flame front.

As combustion and expansion of the flame continue, the rate of excess volume production in the flame will typically exceed the capacity of the vent, and pressure rises again. Eventually, there is likely to be a second peak in pressure at the point when flames rather than unburned gas start to exit the vessel. This is shown as P_2 in Figure 40. This fall in internal pressure corresponds to a rapid drop in the density of gases passing through the vent. For a given rate of volume expansion of the flame, a lower density requires lower internal driving pressures, or and more appropriately for these test conditions, a given pressure difference will result in higher volumetric out-flow for burnt gases than for unburnt and thus, when burnt gas venting begins the pressure in the vessel drops at a faster rate. The exit of flames from the vessel may also correspond to a decline in the potential for the flame to spread internally, especially if ignition occurred towards the back of the box- and this also leads to a reduction in pressure. If the vent is substantial (as in Rig 1), the inertia of gas moving towards the vent may lead to a significant negative phase, i.e., pressures below ambient. The cooling of gases internally also contributes to this decline in pressure.

As the flame exits the vessel, it ignites any vented unburnt gas around the vent, leading to an external explosion, shown as the maximum peak on PT3, the external pressure transducer, in Figure 40.

Where there are some differences in results and interpretation are the peaks after P_1 and P_2. Some results show two further peaks, one corresponding to the external explosion and an additional peak. Many researchers discuss the further peak corresponding to the maximum flame area, which, in the work of Tomlin et al., occurred after the external explosion peak [130]. Corresponding to the maximum flame area is a period of intense burning of residual gases within the vessel. There is a difference of opinion in the literature as to the cause of this intense burning phase; one opinion is that Talyor instabilities are caused by the acceleration of the unburnt gases out of the vessel, destabilising the flame and increasing the burning rate [130]. Van Wingerden and Zeeuwen discuss the maximum flame area as being caused by standing acoustic waves within the vessel, which induces an enhanced burning rate in gases that exhibit spontaneous cell structure, such as propane [176]. They successfully reduced or removed this peak by acoustically dampening the vessel.

McCann et al. investigated a combination of Taylor instabilities and acoustic interactions, along with the effects of the flame re-entering the vessel to ignite pockets of unburnt gas and the effects of pressure wave-induced oscillations all breaking the flame into a cellular structure to increase the burning rate [177].

In this vessel, Rig 1, the P_3 peak (corresponding to the external explosion) at the pressure measurement locations inside the vessel are superimposed on the effects of internal pressure oscillations and flame instabilities. The rig is a large steel box, so the damping of acoustic oscillations will be weak, and these are seen in the pressure trace in Figure 41 after the three main peaks. The experiments are deliberately carried out with a rear ignition so that only limited pockets of unburnt gas remain as the flame front moves through the vessel. Also, the vent opening pressure is low, which limits the strength of the pressure waves that can drive instabilities. However internal resonant effects cannot entirely be eliminated, and these may infer constructively or destructively with the effects of the external explosion. In these investigations, the external explosion is the feature of most significance, as it determines the likely damage to surrounding structures and the potential for triggering severe explosions in a larger cloud. The pressure recorded at the

external transducer PT3 gives the clearest indication of the severity of the external explosion as it is coupled least strongly to internal pressure oscillations.
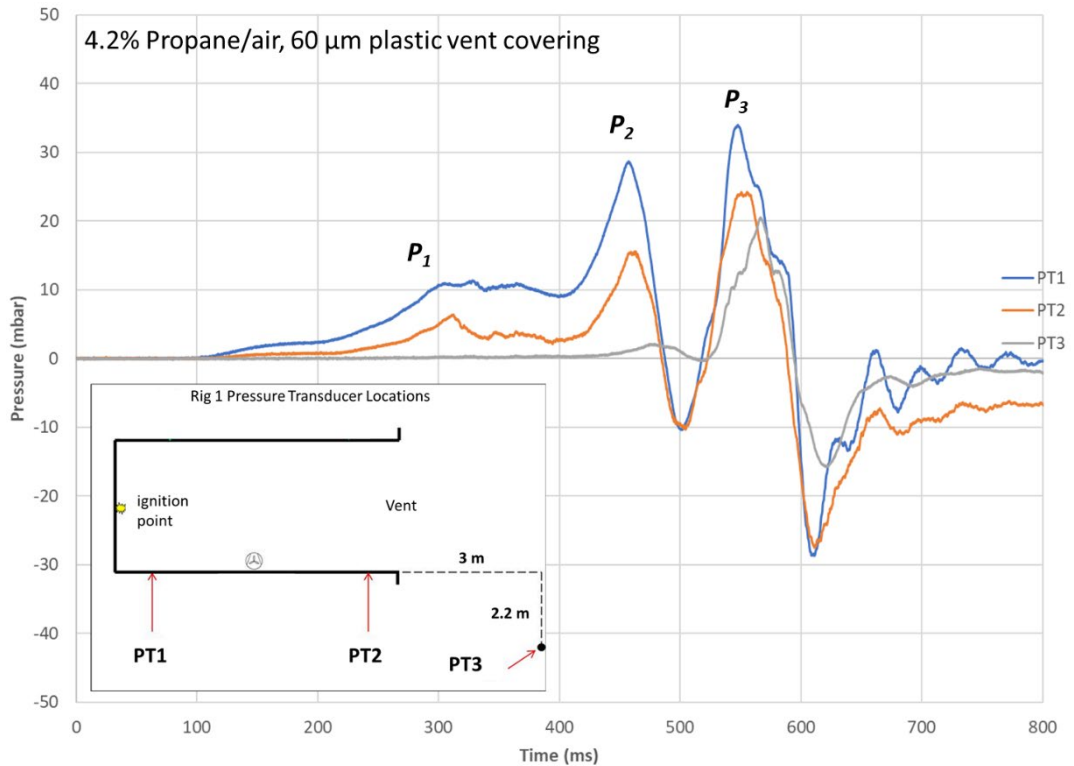
Figure 40 - Typical pressure trace from an explosion in rig 1 with a weak vent covering

In these experiments, the ignition source is on the back wall; therefore, the flame travels towards the vent. Approximately 6/7th of the unburned flammable mixture is vented out of the vessel ahead of the expanding flame. When there is a plastic membrane, it typically bursts and moves rapidly and completely out of the way of the gas outflow; the vent is largely unobstructed for most of the outflow process. As the vented gas forces its way into the outside atmosphere, it will likely form a rolling vortex bubble, as described by Maxworthy [122]. There will be little turbulence generated and low levels of dilution; unless there is a strong crosswind, most of the unburnt gas will be available to contribute to the external flame, which is typically like a mushroom in shape (Figure 41 and Figure 22).
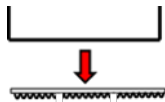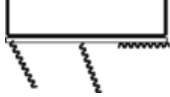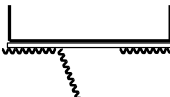
**Figure 41 - External explosion of plastic film test showing mushroom-
shaped cloud**

4.3 Overview of Results

The primary findings of the experiments are summarised in Table 4,
showcasing the notable overpressures observed. It also summarises the
initial cladding failure patterns in the experiments with cladding panels
attached, representing the venting stage configuration before complete
panel removal, except for Test 9, where the panel remained attached.

Table 4 - Results of Experiments 1-9

Test	Conditions	P_1 at PT 2 (mbar)	P_3 at PT3 (mbar)	P_3 at PT2 (mbar)	P_3 at PT1 (mbar)	Pattern of initial P_1 sheet failure, during initial venting
1	120 µm plastic, fan on	23	38	110	74	n/a
2	60 µm plastic fan off	11	20	33	24	n/a
3	60 µm plastic, fan off	12	23	47	34	n/a
4	60 µm plastic, fan on	20	22	80	50	n/a
5	Full strength steel fixing, fan on	135	41	59	44	All three panels removed together with centre purlin
6	Weak steel fixing, fan off	36	38	70	62	Central panel removed completely, edge panels hinge open

Test	Conditions	P_1 at PT 2 (mbar)	P_3 at PT3 (mbar)	P_3 at PT2 (mbar)	P_3 at PT1 (mbar)	Pattern of initial P_1 sheet failure, during initial venting
7	Weak steel fixing, fan off	26	71	156	131	Two adjacent panels hinge open, third remains attached
8	Weak steel fixing, fan on	42	103	170	153	Two adjacent panels hinge open, third remains attached
9	Strong steel fixing, week centre panel fan, off	41	46	70.1	64	Central panel hinges open, all panels remain intact

4.4 Reproducibility

Tests 2 and 3 were conducted on the same day with the same test parameters, 60 μm polythene with the fan off during ignition to explore the reproducibility of base explosions within the experimental chamber. Because the tests were done together, external factors such as temperature and humidity were also similar.

The pressure traces show a reasonable level of repeatability. The pressure rise to the peaks P1 and P2 at the two internal pressure transducers is very similar in both tests, both in the pressure reached and the overall timescale of the explosion propagation, with a slight offset in the timing of the initial pressure rise (Figure 42).

Internal pressures recorded later in the explosions varied more significantly. In Test 3, the P3 part of the trace, broadly corresponding to the external explosion, separates into a smaller initial peak at a time similar to the peak in Test 2 and a more prominent later peak. As noted previously, pressure variations during this part of the explosion are driven by several different effects, corresponding with external explosion and internal resonance. Small changes in the strength and timing of these processes will substantially affect the overall maximum pressure reached.

This suggests that the later phases of the two tests should be more similar when measured by an external transducer that would be less strongly coupled to internal combustion instabilities. The data in Figure 43 show that this is indeed the case. The external explosions recorded with PT3 appear very similar, although there is a slight offset in timings traceable to the earliest stages of pickup after ignition.

Analysis of the video (standard speed) shows the only noticeable difference in the events was that the vent tearing was cleaner in Test 2 (Figure 44) than in Test 3 (Figure 45).

The maximum pressure for the external explosion (P_3) recorded by the internal gauge PT1 was 34 and 48 mbar for Tests 2 and 3, respectively. The corresponding pressure at the external gauge PT 3 was 20 mbar for Test 2 and 23 mbar for Test 3. This suggests that the maximum internal pressures are increased because of internal acoustic effects and that the strength of these resonances is comparable with the effects of the external explosion. The results show that the events last a similar time. The pressure measurements demonstrate an average flame speed between the ignition point and the end of the rig was around 20 m/s, which, allowing for expansion, corresponds to a nominal burning velocity of about 20/6 = 3.5 m/s.
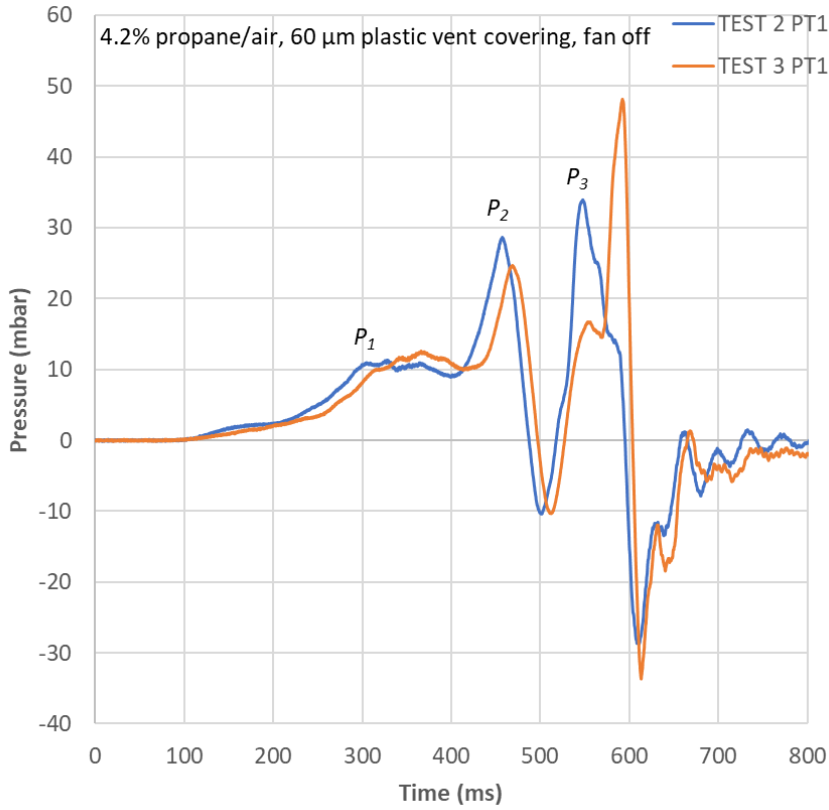
Figure 42 - Comparison of PT1 trace for Tests 2 and 3
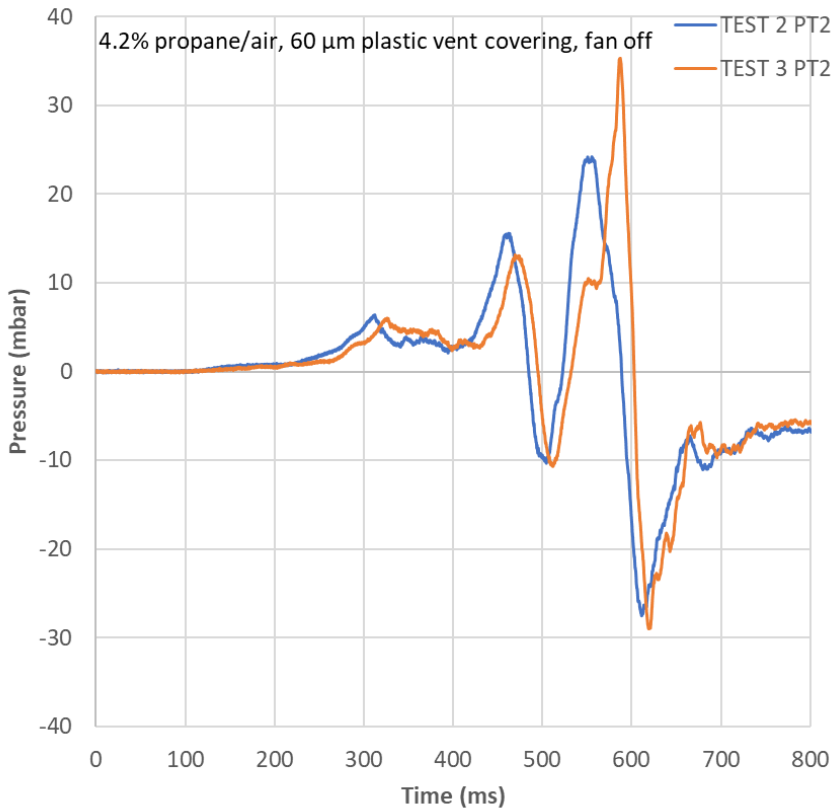
Figure 43 - Comparison of PT3 traces for Tests 2 and 3

Figure 44 - Vent tearing of Test 2

Figure 45 - Vent tearing of Test 3

4.5 Effect of Vent Covering Thickness in Plastic Film Tests

The opening pressure of a vent covering depends on the strength of the material and its fixings, its plasticity, and the covering's resistance to displacement from the vent aperture, i.e., inertia. A vent covering that clears the aperture will lead to more efficient venting. Any blockages could lead to turbulence generation within the vented gas outflow.

Researchers widely use polythene sheeting as a vent covering, as it tears easily and has negligible mass, therefore little inertia and can be used as a

baseline against real-world vent coverings [178-184]. Test 1 was conducted with 120 µm plastic covering, and the fan on, and Test 4 was conducted using lighter plastic at 60 µm but again with the fan on. The pressure traces look similar; however, as expected, the opening pressure, P1, for the lighter plastic is lower than the heavier plastic. The rate of initial pressure rise at PT2 is similar in both tests (Figure 46), meaning that the flame speeds were similar in the early stages. However, the lower opening pressure with the lighter plastic leads to venting starting earlier, bringing forward the flame exit, the P_2, and the P_3 peaks.

McCann et al. discuss how a higher opening pressure leads to increased pressure oscillation interactions with the flame, increasing the burning rate of the maximum flame area [177]. This may be one factor driving the increase in the P_3 peak for the stronger plastic. The flame exit peak pressure, P_2, is nearly identical for both tests. However, P3 for Test 1 was significantly higher than Test 4 with the light plastic, especially at PT3, the external pressure transducer (Figure 47). This could be due to several factors. It would be evident that the thinner film has less mass, so it will have moved out of the way of the aperture, once torn, more quickly. Therefore, there will be less restriction at the aperture, allowing for freer venting and an earlier flame exit, potentially resulting in less turbulent venting and a less severe external explosion than in Test 1. However, video analysis shows that the film was moved cleanly from the aperture in both tests. It is noted that in Test 4, there is no negative phase once the flame exits as some enhanced burning has already begun to result in a pressure rise, which can be seen on PT3 as a gradual rise up to 400 ms when the external explosion causes a high rate of pressure rise.

Whether the presence of a negative phase in Test 1 affects turbulence with the unburnt gas cloud or instabilities in the flame is unknown. It is the case that both days were windy with a southernly wind; on the day of Test 1. the wind was 39 km/h (10.8 m/s), and on Test 4, it was 24 km/h (6.7 m/s). In the video, the flame for Test 4 appears to elongate in a northern direction; there is a potential that the wind could have removed some of the vented flammable gas from the aperture. Furthermore, PT3 was located downwind of the vessel; if the position of the explosion shifted due to the available

flammable cloud moving from the vent, the distance to the pressure transducer would be different. These factors and the higher opening pressure leading to higher speed initial venting need to be considered.
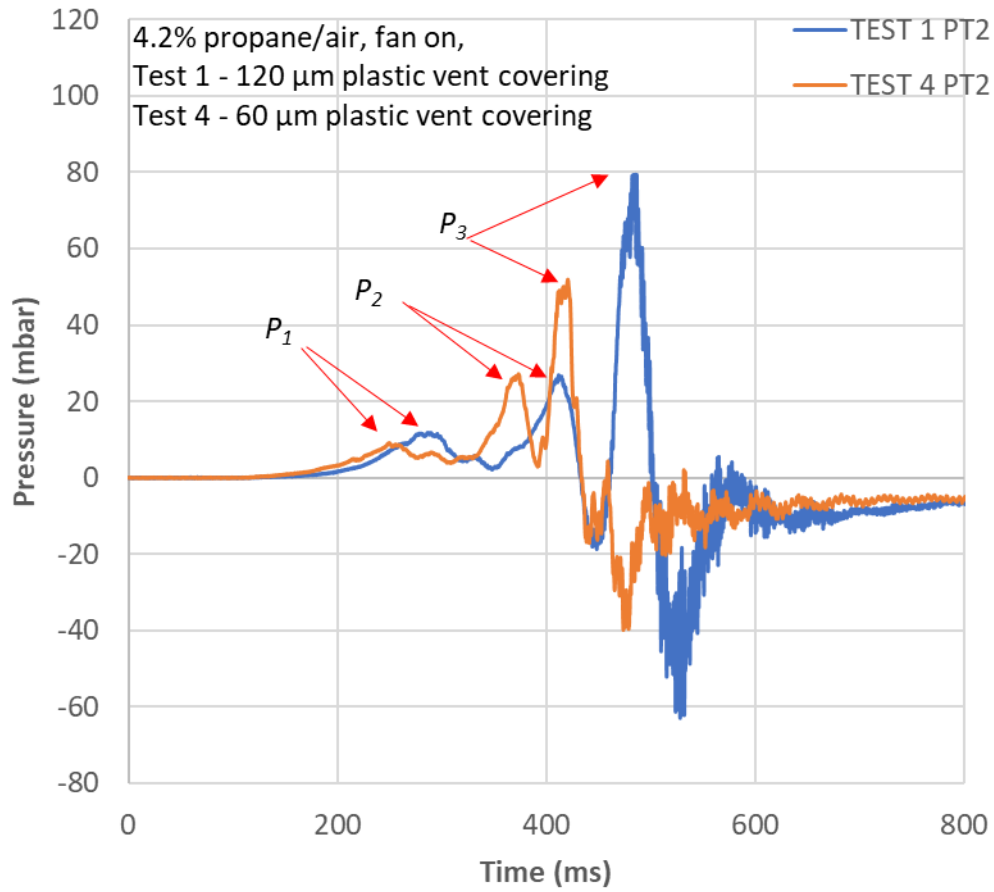
Figure 46 - Comparison of PT2 for Tests 1 and 4
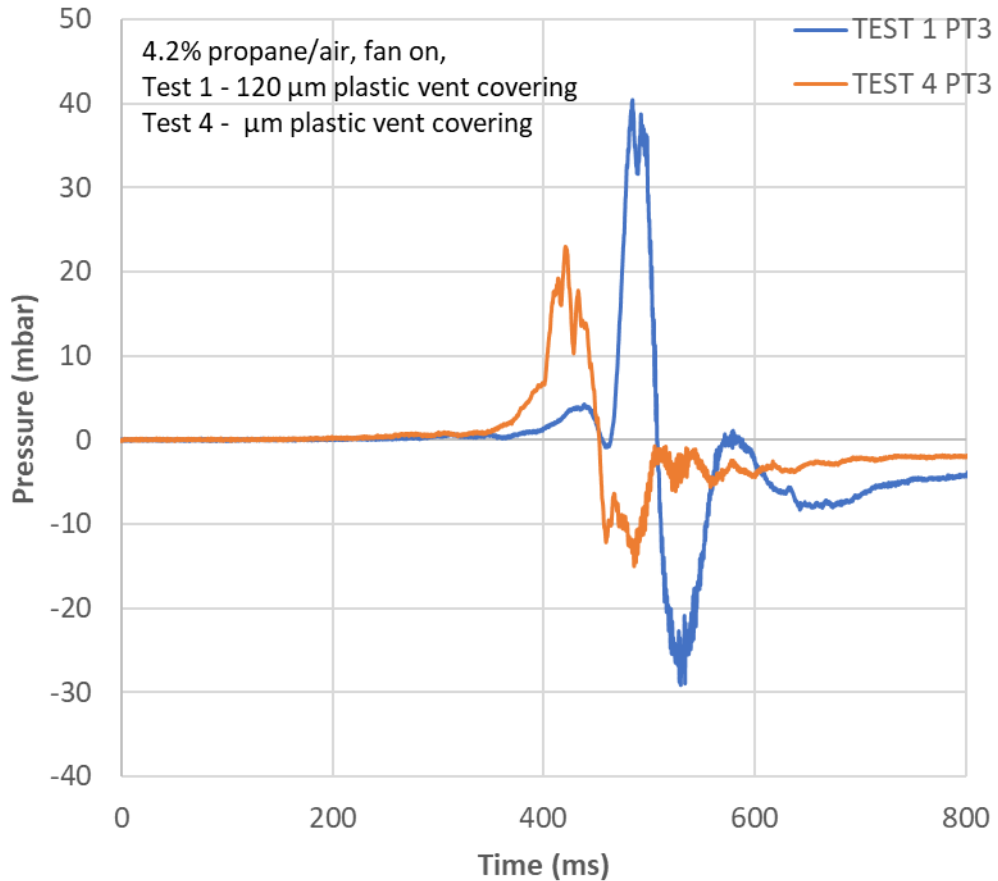
Figure 47 - Comparison of PT3 for Tests 1 and 4

4.7 Effects of Light Turbulence Caused by the Fan

Tests 3 and 4 were performed with the same conditions, except for Test 4, the fan for gas mixing was left running to allow for a lightly turbulent regime for ignition. The results show that the event was significantly faster with the fan running in Test 4 than without in Test 3 (Figure 48). The rate of pressure rise for P_1 was considerably higher, and as a result, the peak for Test 4 occurred around 120 ms before Test 3 (Figure 50); this translated to all remaining peaks. The overall peak pressures recorded within the vessel were higher for the fan being on.

Research on ignitions into turbulent gas regimes generally focuses on turbulence induced by jets [185 & 186]. However, the effect of light turbulence caused by the fan in these experiments is likely similar to light

congestion inside the vessel, introducing flame instabilities and increasing reactivity in both circumstances.

The pressures recorded by PT3, which only captures the external explosion, were almost identical, with the fan-off pressures being nominally higher at 23 mbar compared to 22 mbar (Figure 50). It might be expected that external burning in Test 4 (fan-on) would be higher as the gas is vented at a higher speed and, consequently, higher turbulent velocities induced in the rolling vortex [122]. The results suggest that this is perhaps less important than the timing of the mixing process and the flame's arrival, although there may also be significant wind effects.
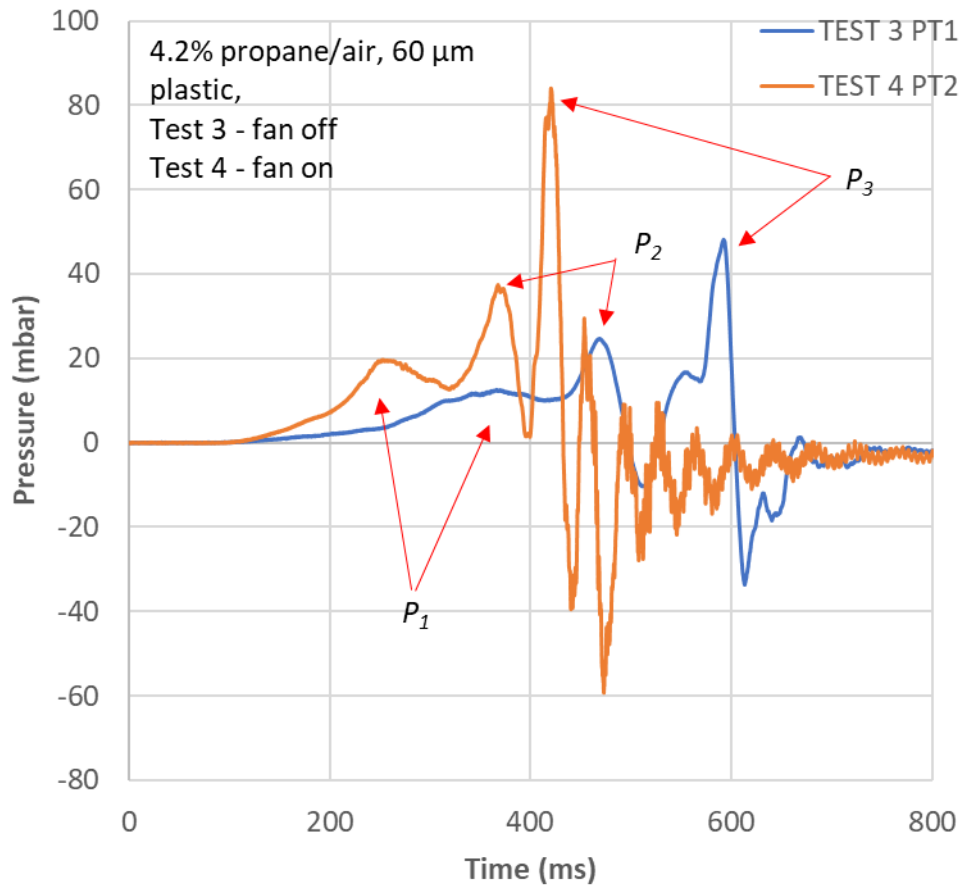
Figure 48 - Comparison of PT1 for Tests 3 and 4
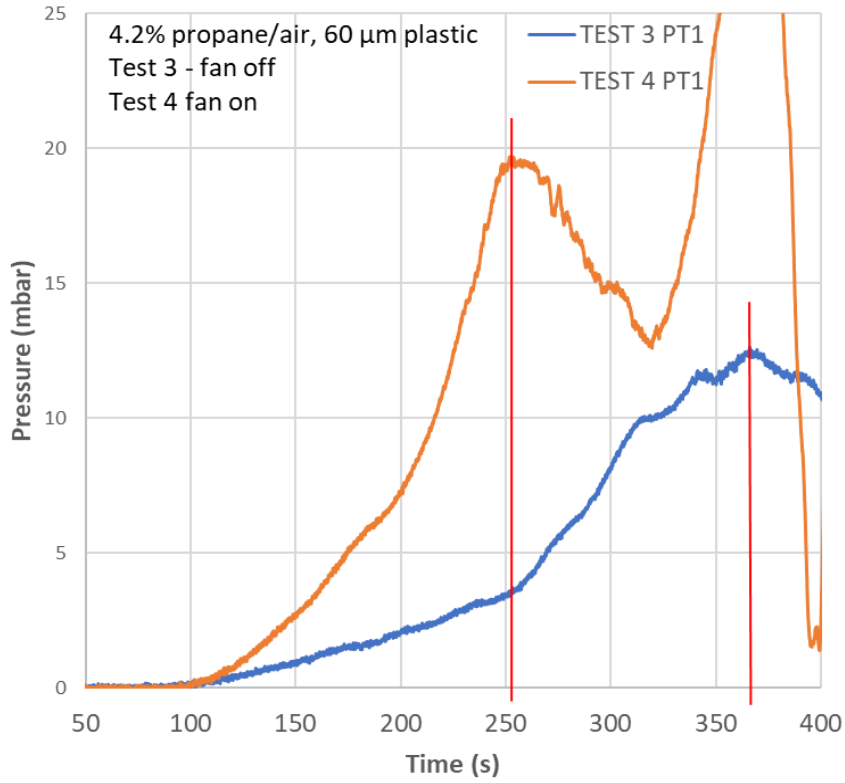
Figure 49 - Timing of P_1 peak for Tests 3 and 4
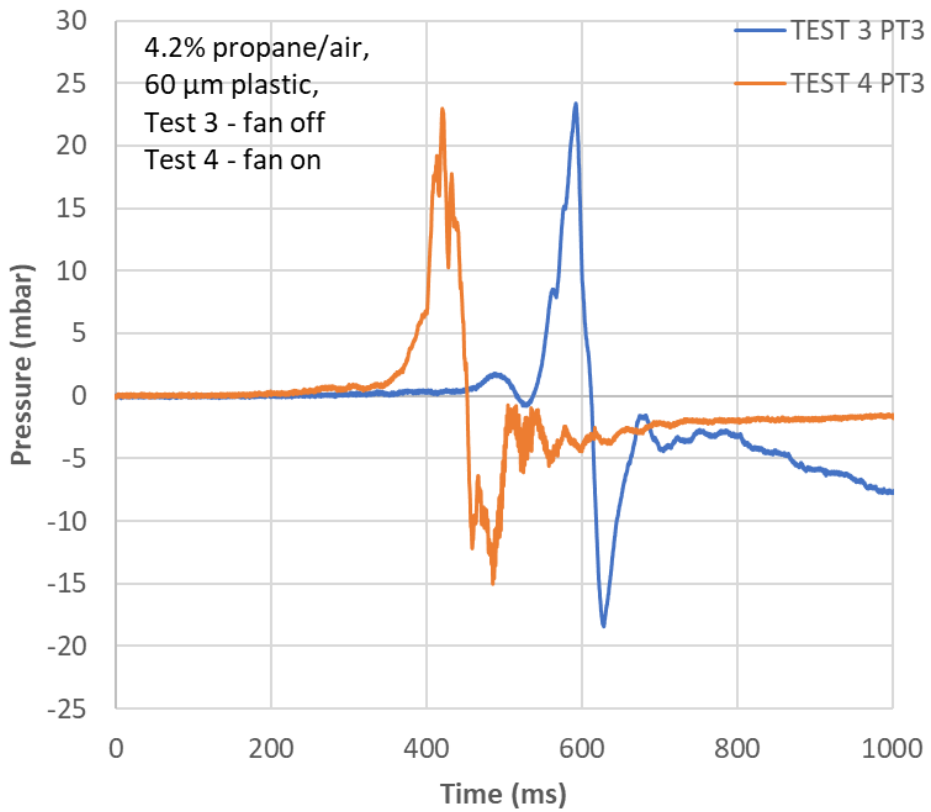
Figure 50 - PT3 traces for Tests 3 and 4

4.8 Explosions with a Full-Strength Steel Panel Vent Covering

Test 5, the cladding panels were attached with a screw in every valley; this is the recommended method. However, it is not always followed for economic reasons. Usually, purlins are long and attached to several of the building's structural frame columns. Due to the vessel aperture's limited span, the central purlin could only be attached at two points, one on each end. The fan was on during the test to provide a lightly turbulent mixture for the experiment. The test was designed to be worst-case for confinement strength and pre-ignition turbulence.

In this test, the central purlin detached from the vessel with all three cladding panels still attached. The complete assembly was propelled upwards and landed 27 m away from the rig. Out of the 30 screws used to fix the panels to the top and bottom purlins, 17 were pulled out of the purlins, and 13 of the screws were left in the purlins with the washers and heads pulled through the panels. This mixture of failure modes reflects the fact that screws, washers, and sheets are designed to resist similar loads. In this test, the high number of cladding fixings meant that the cladding system was stronger than the fixings of the central purlin to the vessel flanges. Since the aim of the experiment was to measure the effect of panel failure on the external explosions, further tests were conducted using fewer fixing screws, as is often common practice. This provides a means to compensate for the reduced strength of the central purlin fixing.

The pressure measurements (Figure 51) show that the explosion was again multi-staged; however, the opening pressure was significantly higher due to the system's strength than plastic. The internal pressure peaked until the cladding was sufficiently removed from the aperture, allowing the pressure and unburnt gas to be vented freely. From the point of free venting of the vessel, until the flame exits to ignite the vented gas, there is a period of around 100 ms. The internal overpressure before the removal of the cladding assembly was higher than the overpressure caused by the explosion of the unburnt gas vented from the vessel.

The available video shows that the centre purlin detached very early in the venting process, and the panels were in motion before the flame exited. There was no interaction between the flame front and the vent covering until after the flame exited the vessel (Figure 52).

The pressure data shows that the explosion was not well developed before the pressure was sufficient to start the removal of the vent panels. The data shows a slight reduction in the rate of pressure rise at around 38 mbar, seen at PT2, annotated in Figure 52, closest to the vent and visible at PT1, close to the back wall, around 15 ms later when the pressure is at 60 mbar. This is likely to indicate when the vent starts to open. The video shows some flex in the side panel before the central purlin detaches from the vessel flange, as shown in Figure 52. The pressure continues to rise as the panel assembly is still causing a blockage to the vent area, and the rate of rise exceeds that of venting. Once it has moved away from the aperture, the pressure drops as the gas is freely vented. PT2 appears to be close enough to the vent to be affected by the movement of the panel assembly, and PT1 appears to provide a clearer indication of the pressures deeper within the vessel.

The flame exit peak pressure (P_2) and the external explosion peak pressures (P_3) appear in close succession; there is no time for a negative phase to P_2; in fact, the pressure has not peaked in the chamber as the external explosion starts.

The external explosion peak pressure is significantly lower than the opening pressure, which contrasts with the results of the plastic sheet experiments.
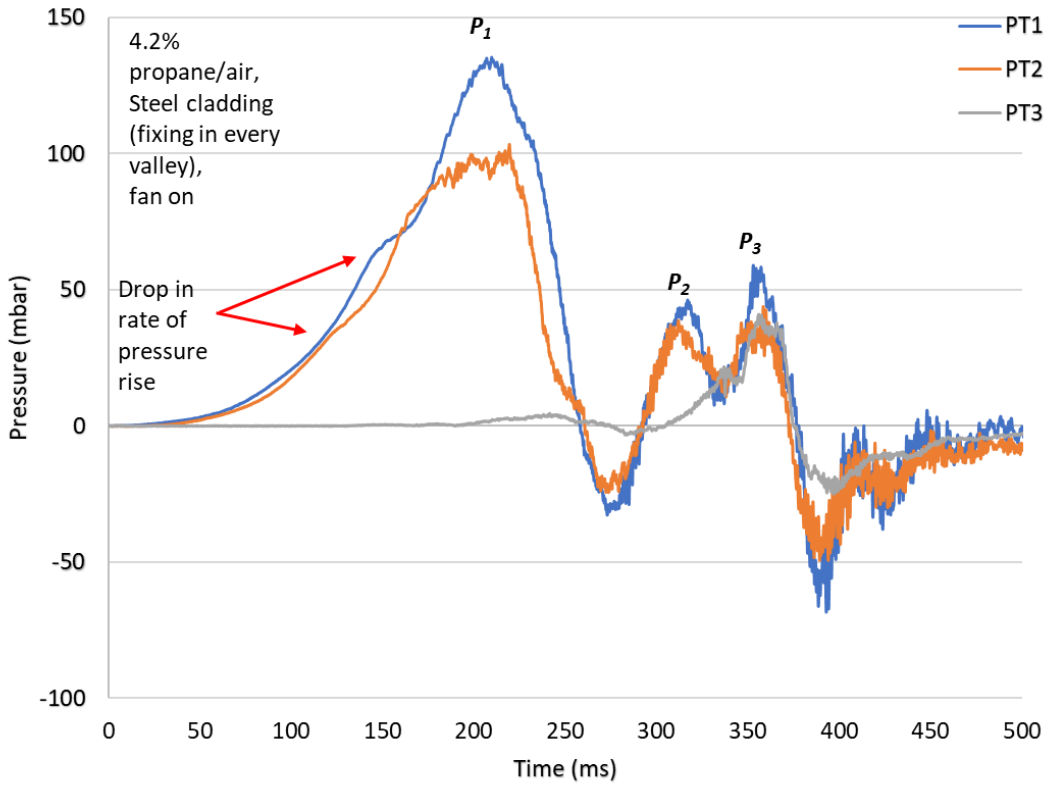
Figure 51 - Pressure measurement from Test 5 (fixing in every valley of the steel panel)

Figure 52 - Collage of frames from the video showing vent opening and flame exit (frame speed 24 fps)

4.7 Effects of Steel Cladding Panel Opening Configuration

Tests 6, 7 and 8 were conducted with the panels fixed in every <u>other</u> valley. The pressure development inside the vessel is very similar to the plastic tests, with the same three pressure peaks visible. The difference is that the opening pressures are higher, and the event is slightly quicker. Tests 6 and 7 are duplicates (with the fan off) to gauge reproducibility. Test 8 had the fan running.

The results of Test 6 (Figure 53) and Test 7 (Figure 54) show some significant differences in the balance of the peaks: In Test 6, all peaks are very similar at around 40 mbar, while Test 7 shows much lower pressures for the first two peaks and almost double for the external explosion.

The conditions for the two tests were identical, but the video analysis showed that the sequence of panel fixing failures might explain the differences in results.

In Test 6, the central panel detached, and the two outer panels hinged open, still fastened to the outer edges of the aperture (Figure 56 and the diagram in Table 4) until after the flame exits the vessel. This left a largely unobstructed opening across the whole area of the vent.

In Test 7, one of the side panels remained fully attached during venting, whilst the central and the other side panels hinged outwards from the same side (See Table 4). This meant that the vent was partially restricted, and the central hinging panel divided the jet outflow, acting as an obstruction or congestion element during the venting stages of the explosion. This accounts for the anomalously severe explosion in this case.

Since all the fixings are nominally identical, it is unsurprising that subtle changes in installation practice or manufacturing tolerances might lead to significantly different failure and sheet detachment patterns. Anything that increases the number of adjacent hinged failures will substantially increase external explosion strength, especially if the structure is in an engulfing cloud.

In Test 8, the fan was left running to provide pre-ignition turbulence. The cameras were repositioned to give a clearer view of the front of the rig. This showed the panels hinged open similarly to Test 7, with two panels hinging and one remaining intact until the flame exits (Figure 57). Higher speed videography was also utilised; this showed that not only did the central panel hinge in a manner that created congestion, but it also oscillated and remained moving as the gas flowed past it, as did the edge panel hinged open. The pressure trace (Figure 58) shows a marked difference from Test 5 (Figure 51), with the fixing in every valley, because the opening pressure was no longer dominant. Test 8 trace is in keeping with the other tests with

pre-ignition turbulence; the event is much faster; however, in this case, the external explosion was significantly higher than Test 7. This shows that with a restricted vent and panels acting as congestion elements in the outflow, the higher internal pressures have an escalating effect (Figure 59) on the severity of the external explosion. This reflects that the combination of partial obstruction and higher velocity through would result in higher turbulence downstream in the gas before it is ignited.
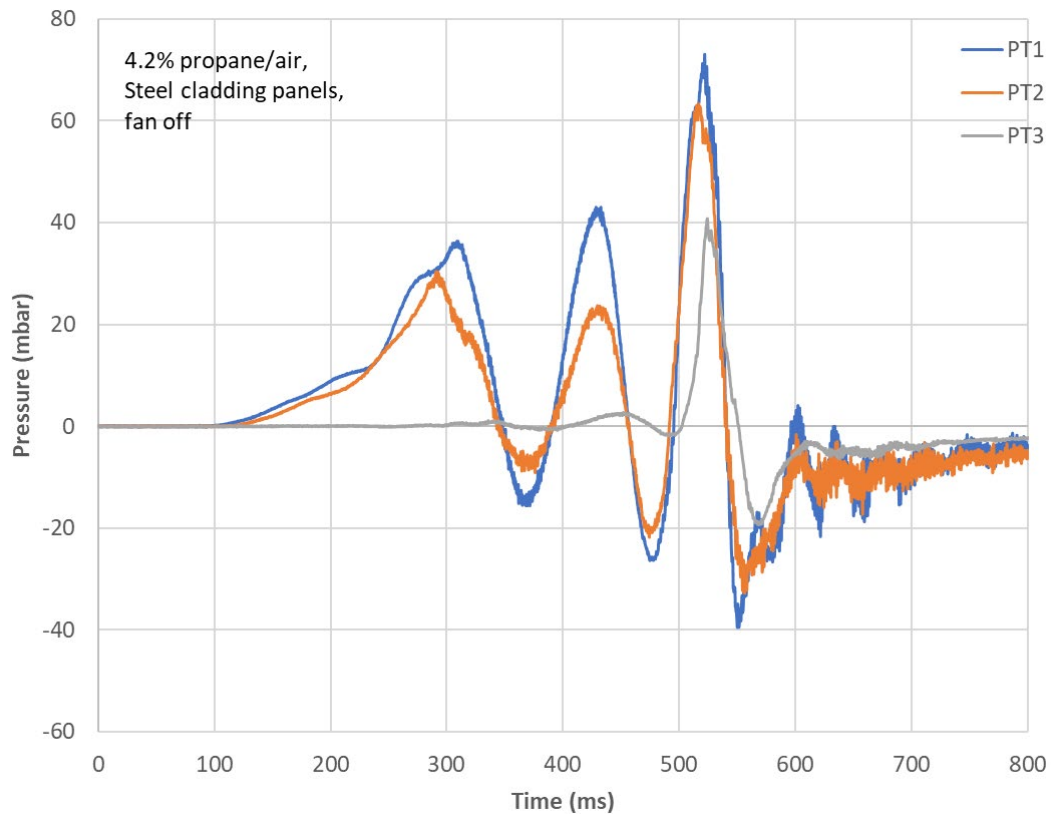
Figure 53 - Pressure trace for Test 6 in which the central panel detached
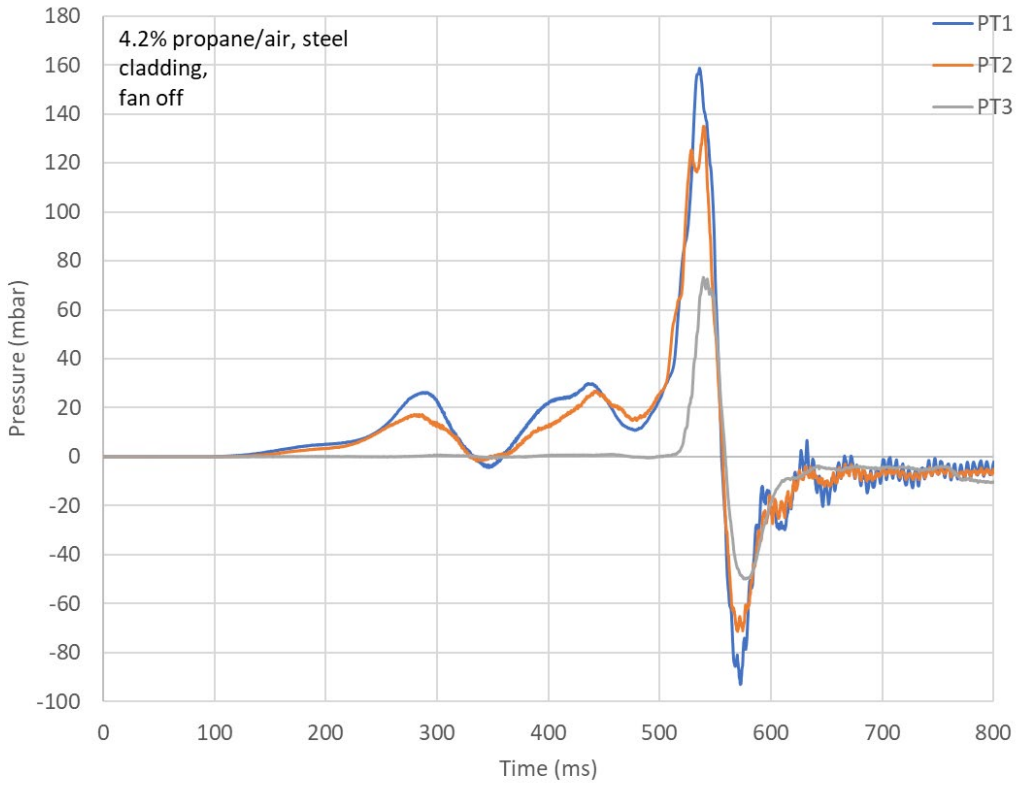
Figure 54 - Pressure trace for Test 7, in which two panels hinged open

Figure 55 - Montage of video frames showing Test 6 panel opening configuration

Figure 56 - Frame from Test 7 video showing panel opening configuration in shadow on the ground

Figure 57 - Montage of video frames for Test 8 showing panel opening configuration
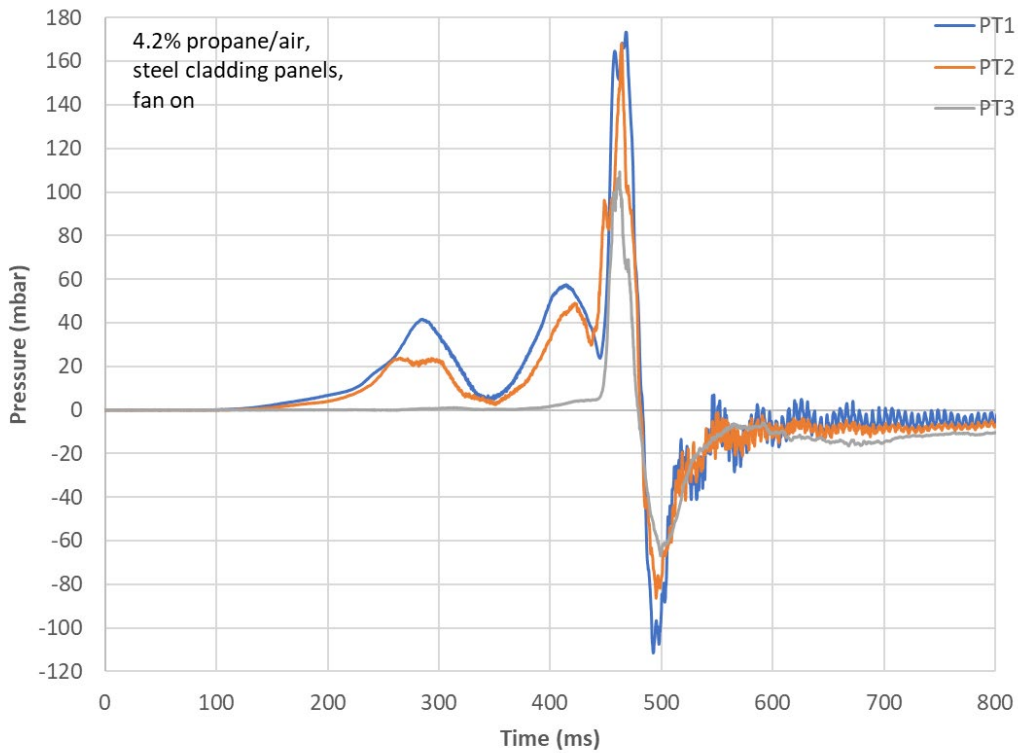
Figure 58 - Pressure trace for Test 8, in which two panels hinged open
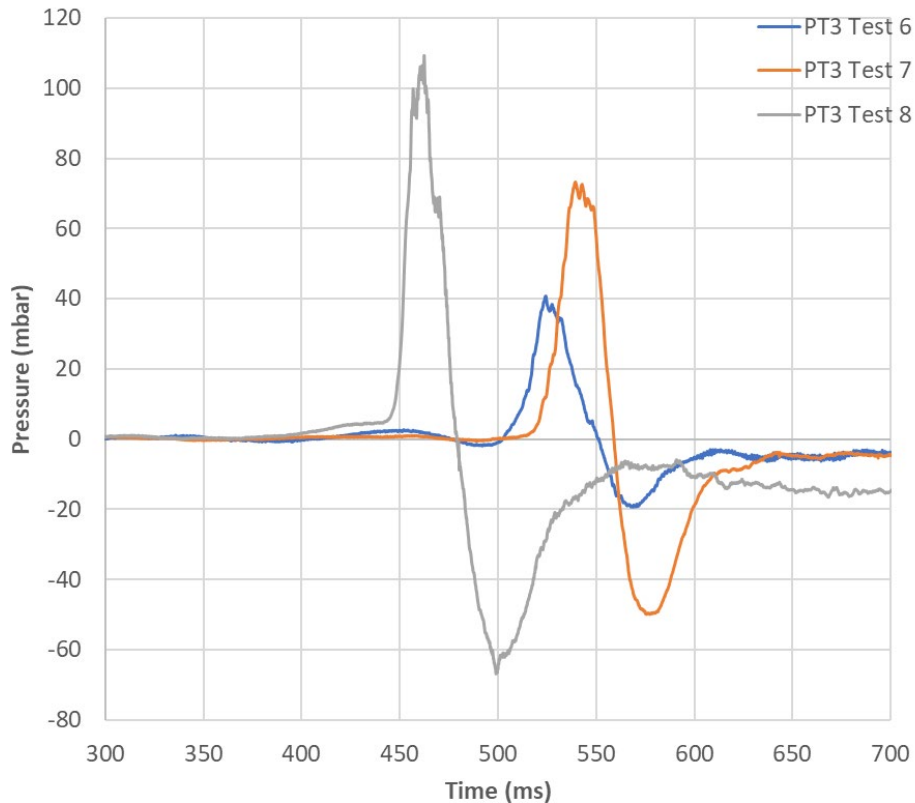
Figure 59 - Comparison of PT3 pressure traces from Tests 6, 7 and 8

4.8 Effect of Introduced Weakness to the Steel Cladding System

Test 9 was conducted with an introduced weakness in the steel cladding panel system. The edge panels were fixed with a fixing in every valley, and the central panel was fitted with a fixing in every other valley. The aim was to investigate whether the reduced vent area increased explosion severity or if there was a potential means of controlling the opening configuration of the panels.

The pressure measurements (Figure 60) show that the overpressures measured were no more severe than Test 6, in which the central panel was removed, and the remaining two panels hinged open to expose nearly the entire vent area of the aperture. The venting process occurred over a longer duration, almost merging P_2 and P_3 for the internal pressure transducers. The video analysis (Figure 61) shows that the central panel hinged open for

the duration of the event, and then the negative phase forces the panel back into position.
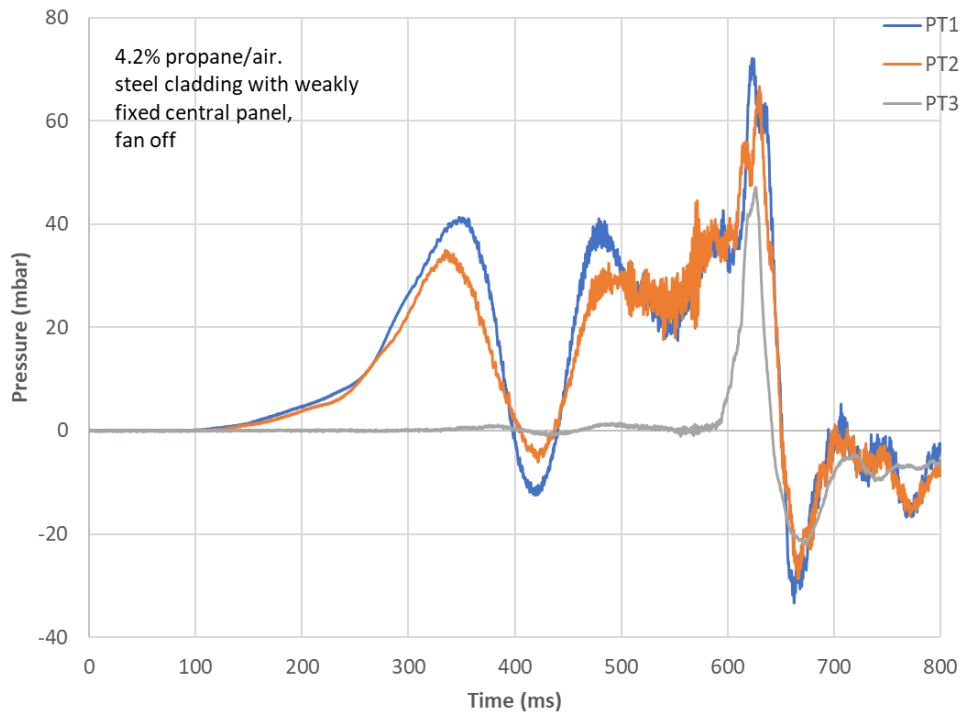
Figure 60 - Pressure trace of Test 9

Figure 61 - Video frame from Test 9

4.9 Comparison of Results to Venting Standards

The highest internal pressures recorded in these tests were around 170 mbar. In this case, the vent size was close to the full (open) cross-section of the test chamber, which is 6.25m^2. It is interesting to compare this observation with the recommendations in NFPA 68 [35] for vent sizes to limit maximum pressure.

4.9.1 Low strength calculation

The required vent size is given by $A_v = \frac{C.A_s}{P^{1/2}}$

 A_s is the surface area of the whole vessel

 P is the maximum (vented) pressure.

C is the standard's venting parameter– 0.052 for stoichiometric propane.

This method is not strictly applicable as the maximum overpressures exceed 100mbar. Still, the nominal recommended size to limit pressure to 170 mbar is 10.5 m^2 as opposed to the actual 6.25 m2 in the experiment.

4.9.2 High strength calculation

This calculation [35] is applicable above 100 mbar. In the limit of vent panels failing at low pressure (in a static test), the required vent area is:

$$A_v = \frac{V^{2/3}}{P^{0.582}}\left(0.0127\, log10(K_g) - \, 0.0567\right)$$

In this case, V is the vessel volume, and K_G is the gas deflagration index (280 bar.m/s for stoichiometric propane in the standard). This gives a basic (low aspect ratio) vent size of 9.2 m^2. However, because the aspect ratio is 3, a 37% increase in vent area is recommended (to a final value of 12.6 m2).

Both values for design vent size are comfortably in excess of the actual vent size, leading to 170 mbar in the tests. This is expected as NFPA is a design standard to protect vessels and incorporates a significant safety margin.

4.10 Conclusions

The experiments show that for this test rig with a full vent area, the explosions have three distinct pressure peaks, The third peak is the only one that is registered on the external pressure transducer and therefore corresponds to the external explosion of the vented gases, as external targets would experience it. On the internal pressure transducers, this third peak is an amalgamation of the external explosion, the maximum flame area and any enhanced or quenched burning rates due to oscillations and reflections introduced from the overall event.

The plastic tests show good repeatability regarding peak pressures and flame speeds. The steel tests show a wide variation in results depending on the fixing methodology and the displacement mechanisms of the panels. The worst-case internal pressure severity is when more fixings are used and the overall fastening of the system is strong. The worst case for the severity of external explosions is when the fixings hinge open and stay fastened on one edge during venting. In these instances, a panel divides the gas. It acts as a congestion element in the vent aperture and offers a smaller venting area and, hence, higher flow velocities. The combination of partial obstruction and higher velocity through would result in higher turbulence downstream of the vent (i.e. externally).

The use of the fan to introduce pre-ignition turbulence causes increased flame speeds and higher internal peak pressures. With plastic sheeting, this does not lead to a more severe external explosion. This is likely because the turbulence introduced by the venting is greater than that caused by the increased flame speed inside the vessel.

The results show that a likely failure mechanism of the lightweight steel cladding panels is for them to hinge open during the early stages of the explosion. The panels are pulled off the fixing, and the fixings are often left in the purlins. Where the panels overlap, the increasing force is sufficient to pull the top panel over the fixing; however, as this occurs, the moved panel provides pressure relief, and the lower sheet is left attached to its fixing, providing a hinge point. The panel hinges on the row of fixings and moves as the pressure causes an outflow of unburnt gas; this acts as a moving

congestion element and introduces turbulence into the outflow, substantially increasing the severity of the external explosion. The panels are only removed as the pressure peaks, just before the flame exits the vessel.

The external atmosphere was air in these experiments, with two panels hinging open, there was only a single point where turbulence occurred without diluting the unburnt gases. On a building, there are countless panels; even a proportion opening will induce a significant amount of turbulence without entraining much air. This shows that assuming the overpressures generated by an explosion in such a building will be governed by the strength of the building construction is incorrect, as the panels are not cleanly pushed off by the rising pressure and interfere with the gas outflow.

A practical implication of the findings from these tests is that the external explosion can be limited/reduced by introducing weakness to the steel panel system. With just a single panel of the three opening, the external explosion severity is comparable to when all three panels open without restricting the vent aperture, and the internal pressure is not increased. This suggests that the increased severity of the external explosion that occurs when the panels hinge open is due to the congestion effect rather than the reduced vent area.

Chapter 5
Explosions in Electrical Control Boxes

5.1 introduction

These experiments were designed to investigate the pressure development and venting mechanisms from commercially available electrical control cabinets with a hinging door and the effect of internal congestion as per objective 2 from Section 1.6.

The electrical control boxes used in these experiments are typical of those present on high-hazard sites. However, they come in a variety of styles and dimensions. For these experiments, a roughly medium-sized box was used with external dimensions of 600 mm high, 400 mm wide and 250 mm deep, and a nominal volume of 0.06 m^3. The boxes are relatively strong with a weak catch and strong hinges; however, they have a full steel door with a mass of 3.29 kg (Figure 31). There has been little previous research on how a vent with a weakly held, high inertia, hinged cover affects venting and combustion mechanisms; previous work has focussed on vents with very low inertia [187].

Experiments were carried out using the supplied door and bursting vent coverings to establish base explosion characteristics in boxes of these dimensions. The bursting membranes used were 240 µm aluminium foil and 10 µm PVC cling film. Due to the shape of the box opening aperture, which is designed to form a watertight seal with the door, the bursting membranes had to be taped to the box.

Further experiments explored the effects of congestion on flame development and overpressures. Chassis plates (Figure 32), available to mount equipment on for installation in the boxes, were used as congestion elements as they have a regular grid pattern. These were fitted at 50 mm intervals. The aim was to use the maximum level of four rows for the later propagation test. However, it was important to understand the effects of different congestion levels and positioning.

The ignition source for the 4.2% propane/air mixture used in every test was a hot wire ignitor positioned centrally on the back wall. This provided an ignition source without imparting significant thermal energy or risking multiple points of ignition.

5.2 Pressure Development

With a foil vent covering and no congestion, the ignition produces a growing hemispherical flame that does not fill the box before the vent bursts, as shown in image A4 of Figure 62 and flame exit, image B4. Given the large vent area relative to the box's volume, it could be expected that if the vent closure was fairly weak, the peak pressure would be dominated by the external part of the explosion [141]. In this case, however, the dominating pressure peak is the rise to vent pressure peak (P_1). The pressure rise is consistent until the vent bursts (Figure 63), and the pressure decays within 3 ms for Test 10. A peak around P_1 was recorded on the external pressure transducers (PT2 and PT3) but is exceptionally low (4-7 mbar); these peaks correspond with the bursting of the vent at a timing consistent with the speed of sound, indicating that they could be the result of acoustic effects of vent bursting.

A second peak (P_2) is recorded on PT2 and PT3, which also roughly corresponds to a second peak on PT1 of around 20 mbar on test 2. This peak is again very low (2-3 mbar) on PT2 and PT3 but corresponds to the start of the ignition of the vented gases, image A5 in Figure 62, the likely external explosion. The third peak (P_3) corresponds to image C5, which appears to be the period of most intense combustion before the residual gases burn, causing heat effects on the pressure transducers.

The pressure development differs from that of rig 1, which is expected due to the different dimension ratios and the box's greater vent area-to-volume ratio.
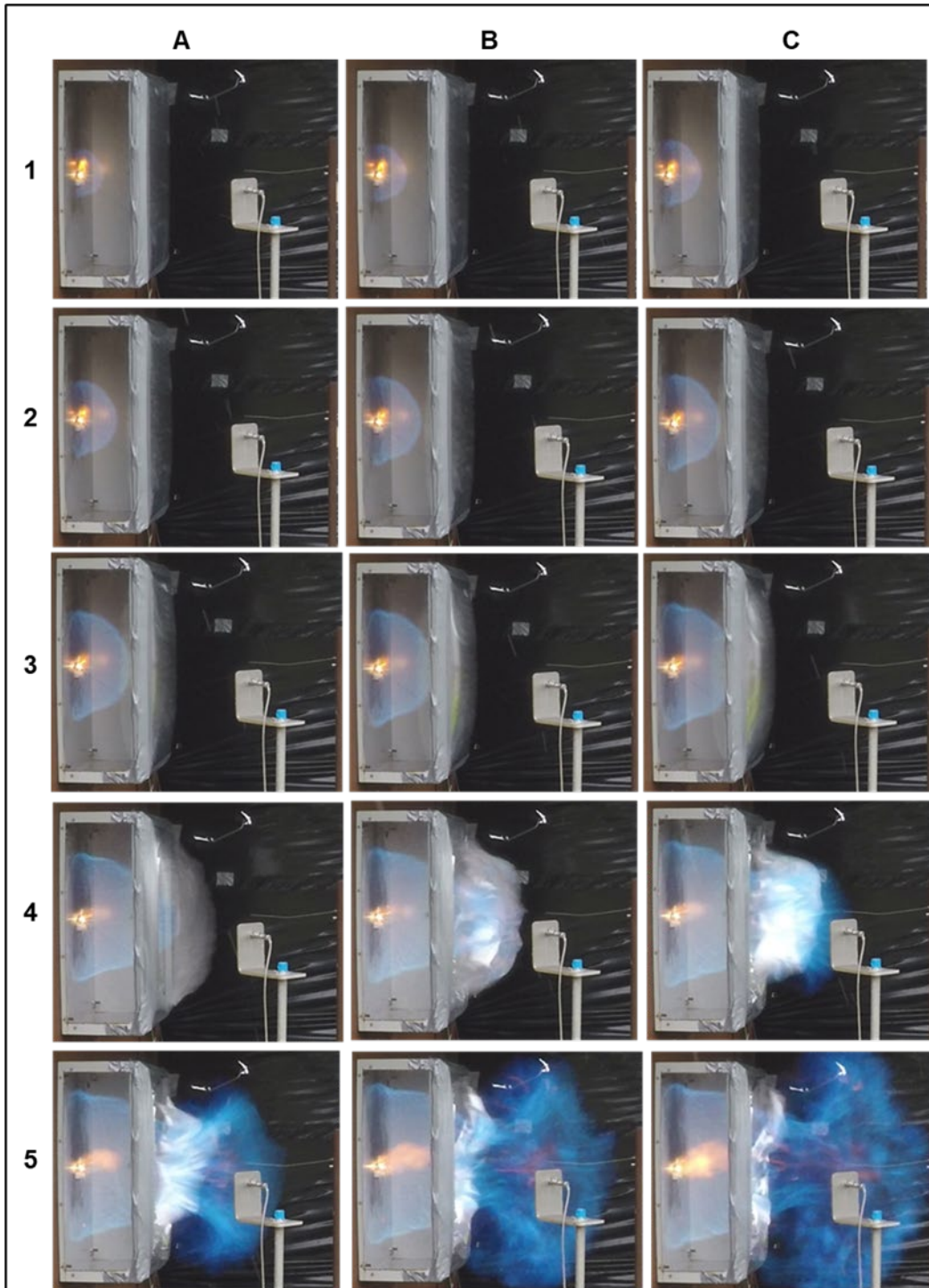
Figure 62 - Flame development in the box with foil vent covering, frame interval 4.17 ms
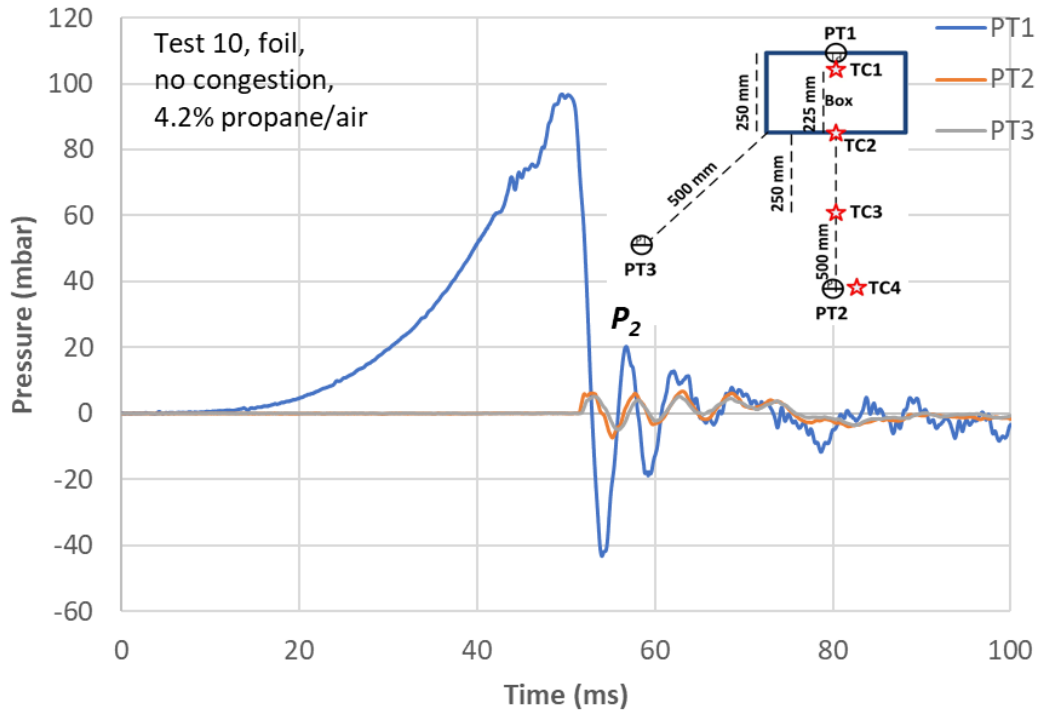
Figure 63 - Pressure trace from Test 10

5.3 Overview of Results

The results of pressure measurements and flame arrival times are shown in separate tables, as flame speed measurements were not made for all tests. The pressure measurements are shown in Table 5. Note that for some door tests, PT2 was moved from 500 mm in front of the box to 250 mm perpendicular to the box on the same line of sight as PT3, which is 500 mm perpendicular to the box (Figure 34). For these tests, PT2 is referred to as PT2a.

The measured flame arrival times and calculated average point to point flame speeds are shown in Table 6.

Table 5 - Pressure measurements for Tests 10 to 35

Test	Vent covering	Number of rows of congestion	P_1 at PT1 (mbar)	P_2 at PT2 (mbar)	P_2 at PT2a (mbar)	P_2 at PT3 (mbar)
10	foil	0	97	5	-	5
11	door	0	90	4	-	7
12	Foil	0	72	3	-	3
13	PVC film	0	9	0	-	0
14	PVC film	0	16	2	-	2
15	door	0	78	2	-	4
16	door	0	86	-	12	8
17	door	0	75	-	9	5
18	door	2	93	-	21	15
19	door	2 (at front)	174	-	31	22
20	door	2	93	-	9	6
21	door	2	81	-	11	6
22	door	3	197	14	-	30
23	door	3	119	-	21	12
24	foil	4	109	17	-	9
25	foil	4	109	15	-	14
26	foil	4	131	20	-	17
27	door	4	289	16	-	41
28	door	4	351	24	-	59
29	door	4	206	-	44	25
30	door	4	201	-	41	23
31	door	4	327	-	78	55
32	door	4	312	-	75	56

Table 6 - Flame arrival times, with calculated point to point average flame speeds

Test	Conditions	TC2 flame arrival (ms)	Av. flame speed (m/s)	TC3 flame arrival (ms)	Av. flame Speed (m/s)	TC4 flame arrival (ms)	Av, flame Speed (m/s)
10	Foil 0 rows congestion	51	4.41	65	17.86	81	15.65
11	Door 0 rows congestion	53	4.25	-	-	-	-
12	Foil 0 rows congestion	44	5.11	69	10	88	13.15
24	Foil 4 rows congestion	28	8.26	36	31.25	42	20.833
30	Door 0 rows congestion	30	7.5	-	-	-	-
31	Door 0 rows congestion	30	7.5	-	-	-	-

5.4 Effects of Different Vent Coverings on Venting and Flame Exit

5.4.1 Effects of Foil Vent Covering

In Test 10, the foil vent covering is stretched taut and outwards, significantly expanding the box's volume, as seen in image C3 of Figure 62. The foil tears and is quickly displaced by the outflow, exposing a significant proportion of the vent area; as the flame exits, it burns through the vented gas and establishes a typical mushroom shape (Figure 64). This shape is characteristic of the vented gases forming a rolling Maxworthy vortex bubble [122&141]. As the flame extends, it forms a second mushroom shape, reinforcing the theory that the rolling vortex bubble venting method applies in this case (Figure 65). The flame extends to near the edge of the 2 m long rig.

In Test 12, the recorded overpressures were significantly lower than in Test 10 with the same conditions; analysis of the video shows that as the foil stretches taut, the tape fails at the edge, and the foil tears horizontally from this breach and only exposes around a third of the vent area (Figure 66). The pressure trace (The Figure 67) differs from Test 10 (Figure 64), showing a disruption in pressure development as the tape fails and a much longer pressure decay, which is expected with a smaller vent area. This also resulted in a reduced-sized mushroom flame shape. The lower pressure vent bursting of Test 12 to Test 10 with a similar pressure rise equates to the vent bursting earlier in the event. This shows as an earlier flame arrival to TC 2, equating to an apparent faster average flame speed inside the box. However, the external flame speeds are lower than in Test 10.
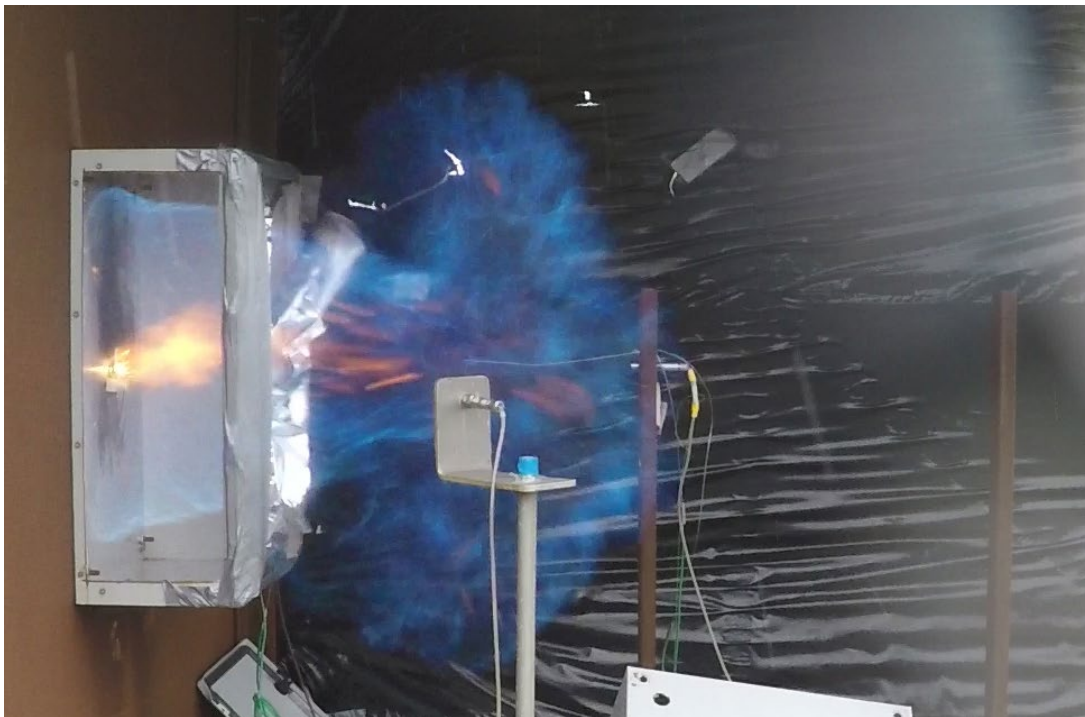
Figure 64 -Test 10 – initial mushroom flame, typical of rolling vortex bubble venting
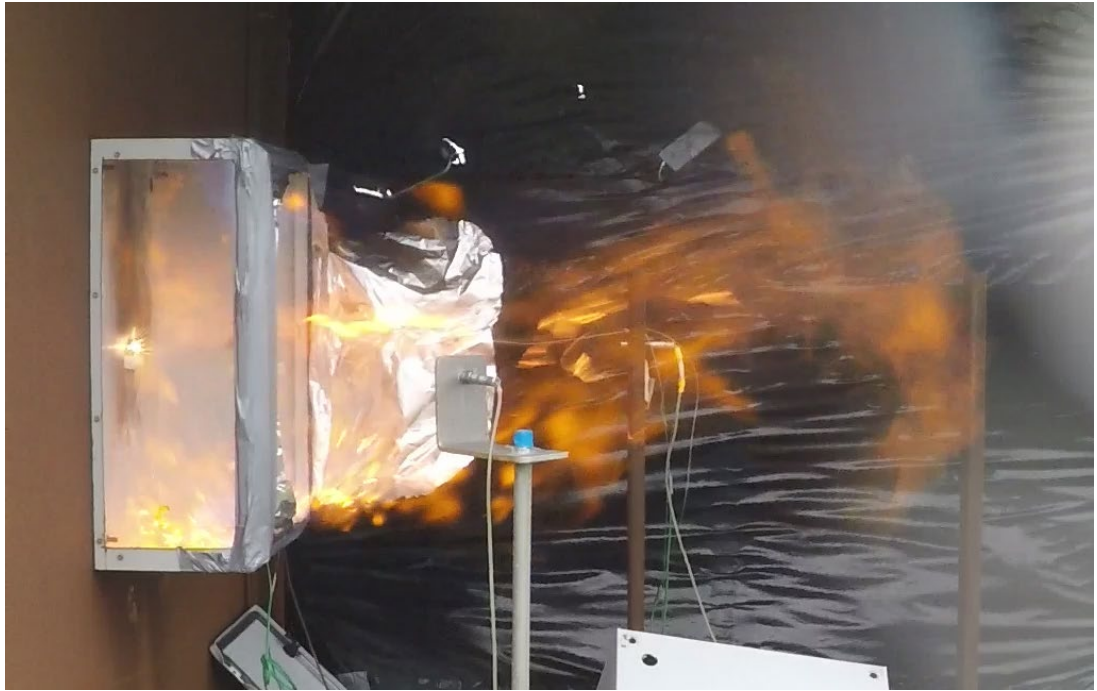
Figure 65 - Test 10 - secondary mushroom flame

Figure 66 - Test 12 - failure of taped edge and tearing of the foil
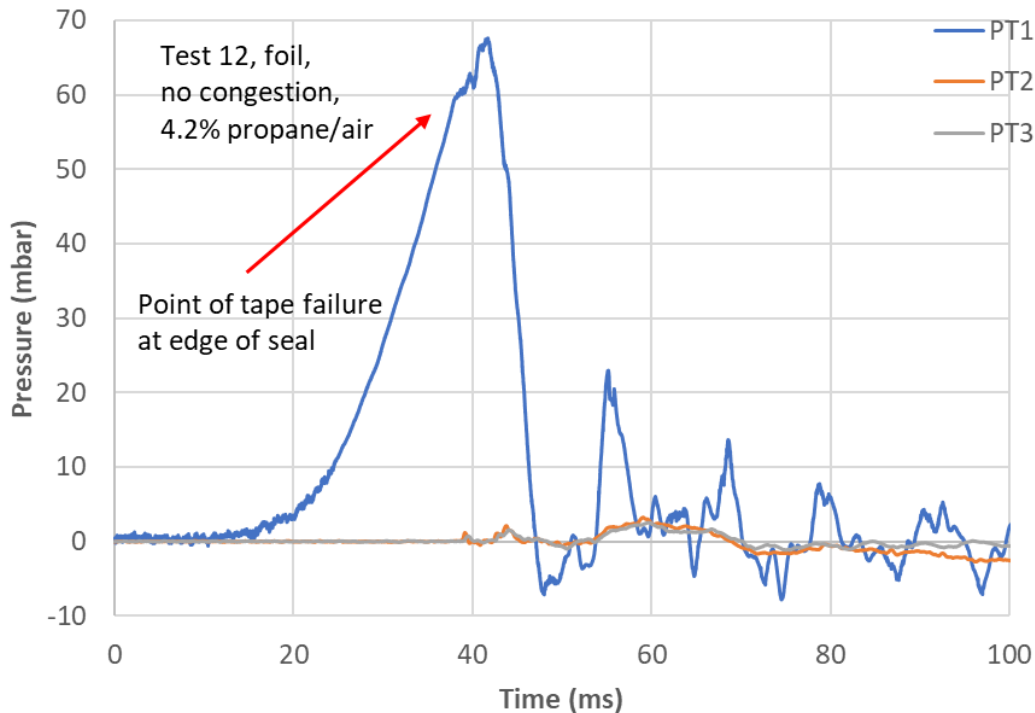
The Figure 67 - Pressure trace from Test 12

5.4.2 Effects of Door

When the door is in place, it appears to flex before the catch is overcome and the door opens; the point of the catch being fully overcome at the top and bottom is image D4 in Figure 68. The door flex, as well as increasing the effective volume of the enclosure, causes a breach of the gas-tight seal of the door; the resultant effects are visible as a stall in the rate of pressure rise on the pressure trace (Figure 69), before the rate of pressure rise exceeds the efficiency of the vent area made available by the door flex. The pressure decay is also slower than with the foil because the door has so much inertia that it is not moved from the vent area and still provides an obstruction during venting. The pressure decay for Test 11 was nominally 10 ms, a significant percentage of the total 68 ms that the pressure took to rise and fall in the peak. These results are consistent with the modelling of the dynamics of the hinged door, see Section 5.8.

The door is only partially open before the flame starts to exit via the widening slot. When the door is completely clear of the vent area, the event is over,

and the only combustion occurring is residual burning within the box (Figure 70). The venting gases are, therefore, forced perpendicular to the direction of venting seen in the foil tests, and as the flame ignites this gas, it shows that the venting is not in the form of a vortex bubble but a quasi-planar jet.
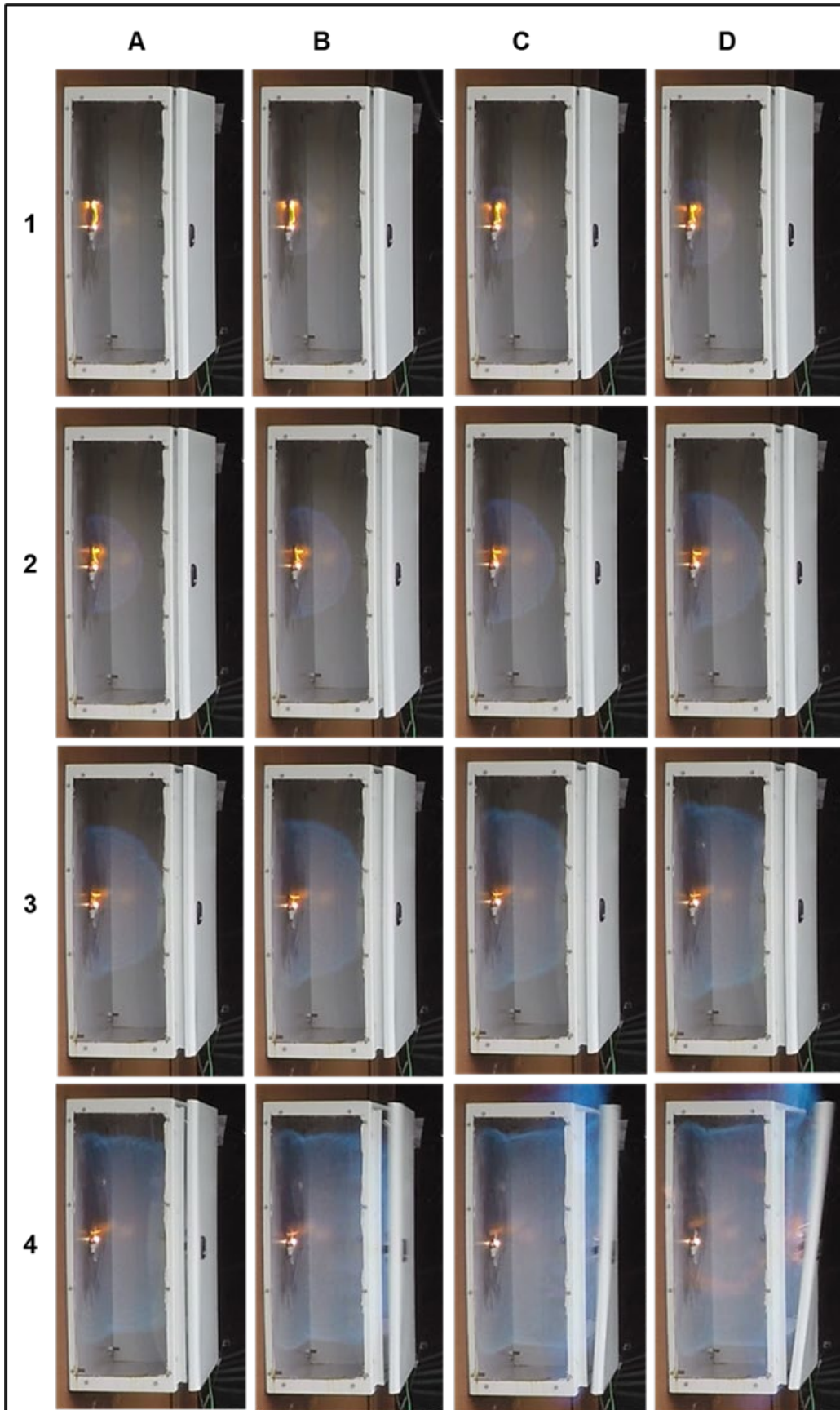
Figure 68 – Flame development and vent opening of the box with door attached, frame interval 4.17 ms
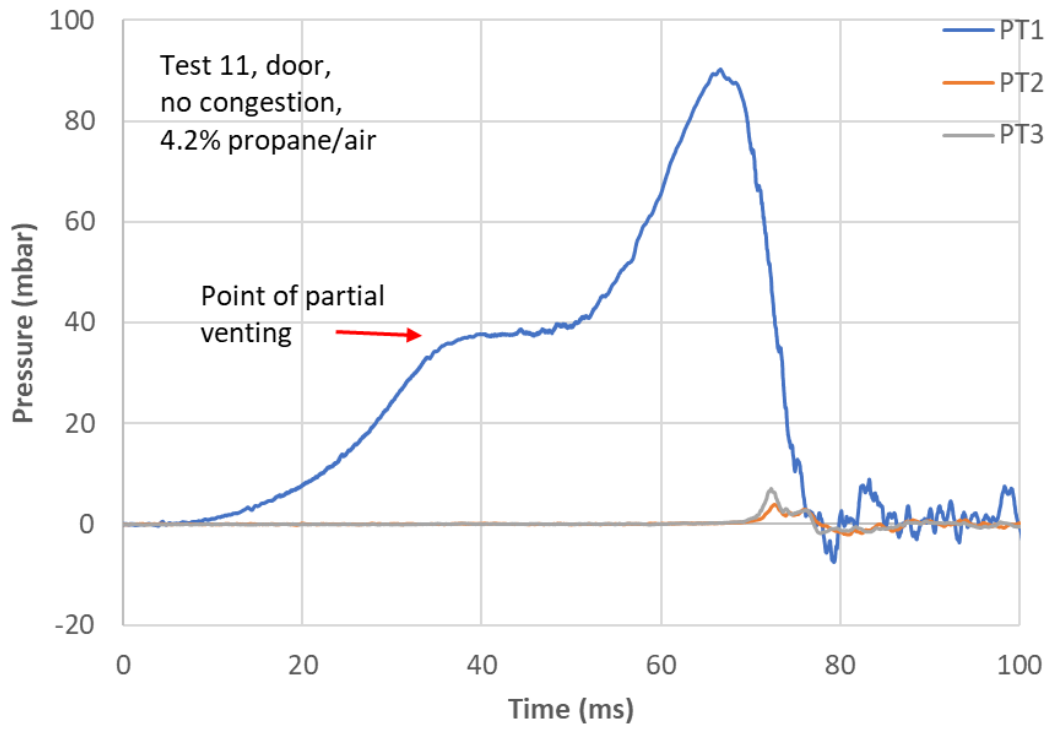
Figure 69 - Pressure trace from Test 11

Figure 70 - Test 11, point door is clear of vent area.

5.4.3 Effects of PVC Cling Film

The PVC film gave rise to very low overpressures (Figure 72), and the rate of pressure rise was slow over the first 40 ms of the event. The video shows the film stretching significantly, almost doubling the volume of the box (Figure 72); the film hits TC3 before it bursts. The significant increase in box volume offsets any potential for compression of unburned gases and pressure rise. Due to this vent-burst mechanism, plastic film was not pursued further in this test programme.
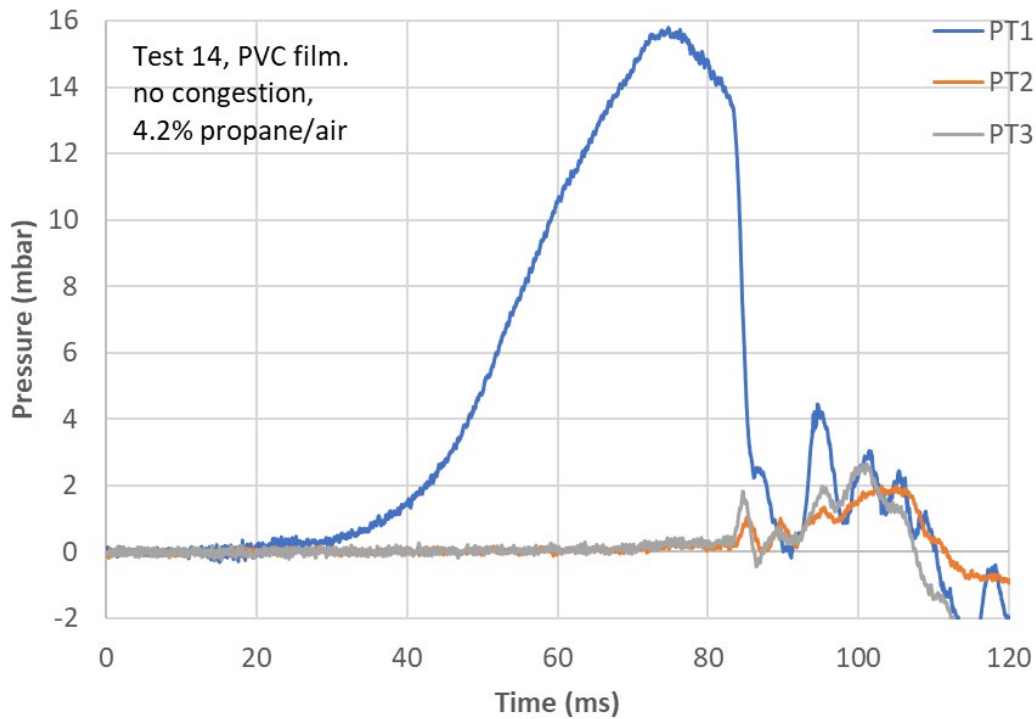
Figure 71 - Pressure trace from Test 14

Figure 72 - Test 14, film before bursting

5.4.4 Evaluation of the Venting Mechanisms and Reproducibility of a Bursting Vent Cover Versus the Door

The door has a mass of 3.29 kg and a surface area of 0.24 m^2; even considering the folded rim of the door, the vent covering will have a greater specific mass than 10 kg m^{-2}. According to EN 14797:2006 [188], vent coverings of this mass "shall be compared to a venting device with a specific mass < 0.5 kg m^{-2} (e.g., bursting foil) of the same size, static activation pressure P_{stat} and geometry without any obstructions".

Tests 10, 11, 12, 15, 16 and 17 showed that the peak overpressures achieved in the box without congestion with both foil and the door are comparable, ranging from 72 to 97 mbar (Figure 73); the door results fall between the two foil test results. However, the reality is that in Test 12, the foil was not sufficiently sealed to the box, and therefore, the peak pressure was lower than in Test 10. Thus, the indication is that the P_{stat} for the foil is higher than that of the door. However, opening pressure is only part of the story; the pressure decay from the door tests is significantly slower than for

the foil, indicating that venting is less efficient due to the inertia of the door. It is not cleared from the aperture, as the foil is, causing a considerable blockage after opening.

There also appear to be two distinct groupings of the door results, with the lowest pressure being around 17% of the highest, giving a significant deviation. Unlike the foil, there is no possibility of fitting the door in a manner that leaves it weaker from one test to the next. The probability of difference is likely down to the specific mechanism of how the pressure overcomes the three catches.

The foil is fragile, and the sealing method is not ideal; any issues with sealing, such as moisture or contamination affecting the bond or slight damage to the foil during fitting, are likely to affect the burst pressure. Videography made it possible to identify when the foil bursts as intended. Many tests were attempted, but the success rate was low. However, three tests with four rows of congestion were successful, allowing investigation into the effect of congestion with a vent that is considered 100% efficient by standards [188].
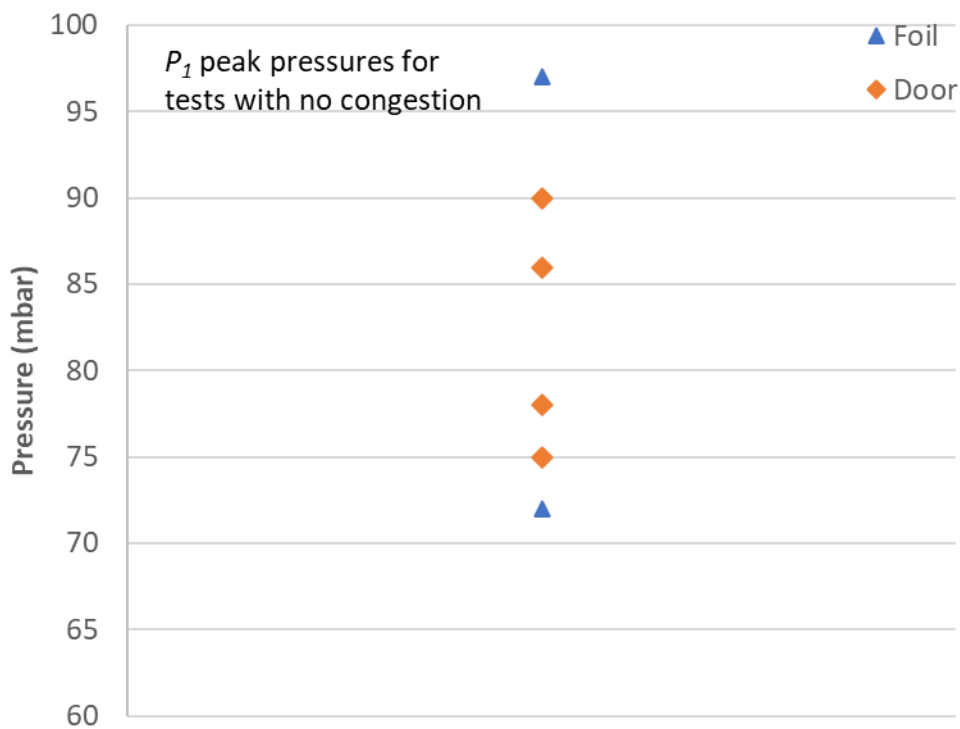
Figure 73 - Peak *P₁* pressures for Tests 10, 11, 12, 15, 16 and 17

5.5 Effects of Four Rows of Internal Congestion on Flame and Pressure Development

As expected, adding congestion increases the internal flame speed and, therefore, the speed of the event. With four rows of congestion and the foil as a vent covering, the pressure development (Figure 74) is much faster than Test 10 (Figure 63), leading to a higher opening pressure, P_1 and more pronounced P_2 and P_3.

With the door and four rows of congestion, there is also a significant increase in overpressure at P_1 (Figure 75). The door flex and partial venting still seem to affect the pressure rise in the earlier stages; however, it is much less effective in checking the rate of pressure rise than in tests when there is no congestion. This is because the increased flame acceleration that the congestion creates is too great to be significantly offset by venting at the seal. The high-speed video images (Figure 76) show that the door is still not clear of the vent when the flame exits. The door appears to be open to a similar degree when the flame exits for tests with and without congestion (Figure 68). The increased pressurisation rate in the congested test means that the inertia of the door is more significant in raising the final internal pressure. As with the uncongested tests, a pressure rise is recorded on the external pressure transducers that correlate to the peak of P_1, but there are no obvious P_2 and P_3 peaks. However, there is a brief reversal of the pressure decay that could result from some external combustion.

The foil stretches significantly again before bursting (Figure 77). This expansion in volume is likely to affect the pressure development, relieving the compression as it occurs up to the point of bursting. Even with this, the correlation between the increase in pressure for the door with and without congestion is less substantial with the foil; this is because the foil is easily removed once it bursts; this occurs almost instantly, within the 4.17 ms of the two consecutive video frames in Figure 78. Then, the pressure drops sharply, and due to the length-to-vent area ratio, venting is concluded very rapidly. On the other hand, the door is still causing a considerable blockage throughout the venting process.
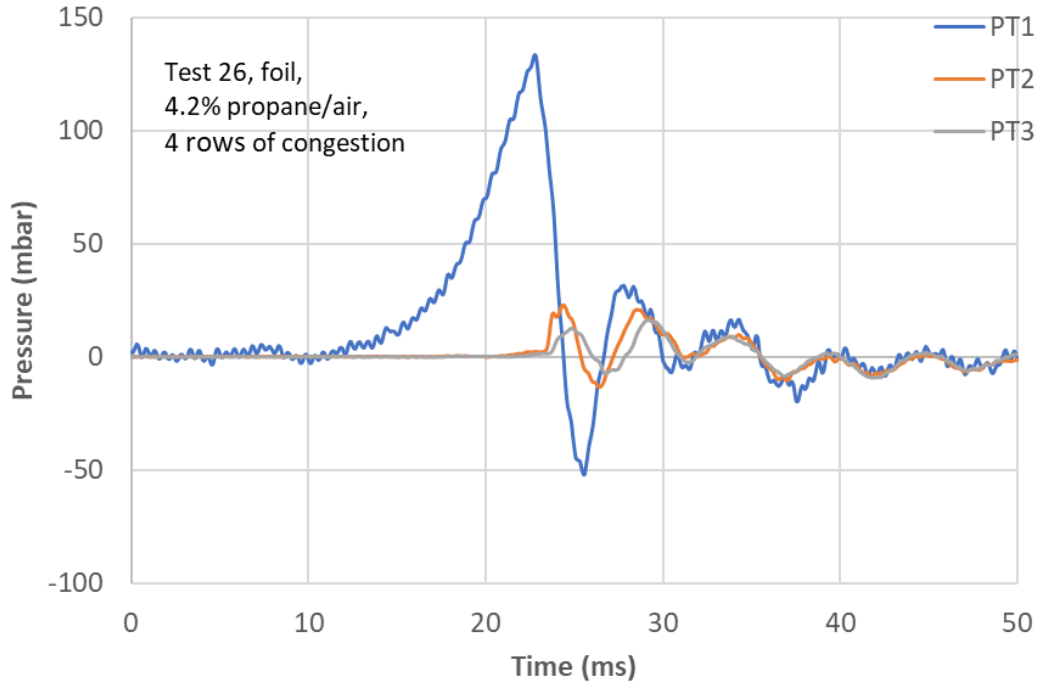
Figure 74 - Pressure trace for Test 26
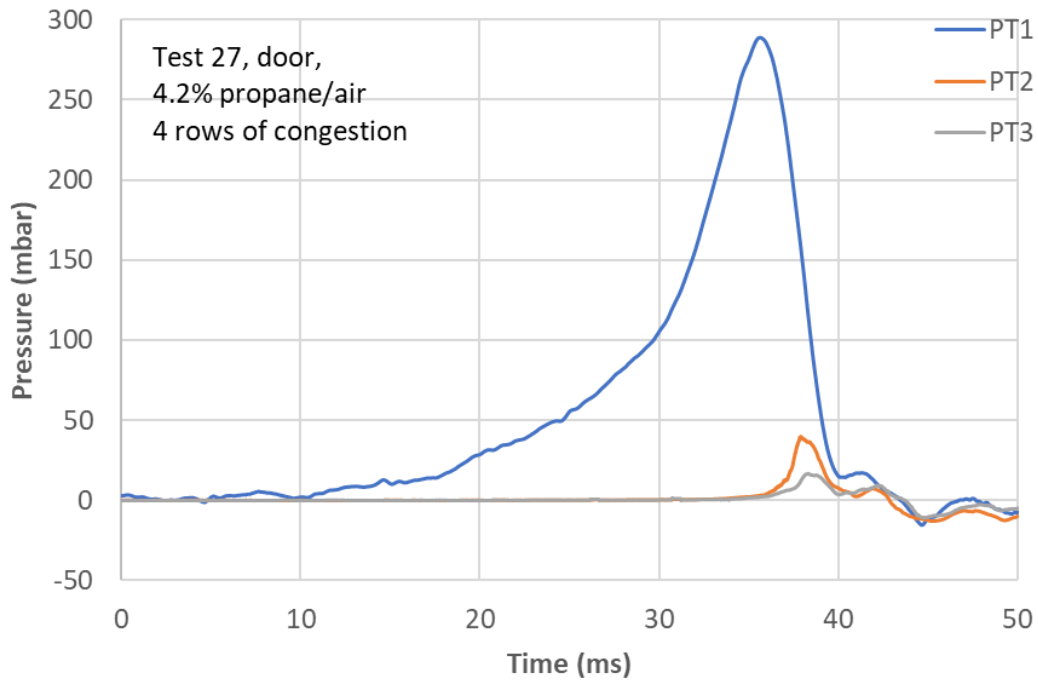
Figure 75 - Pressure trace for Test 27
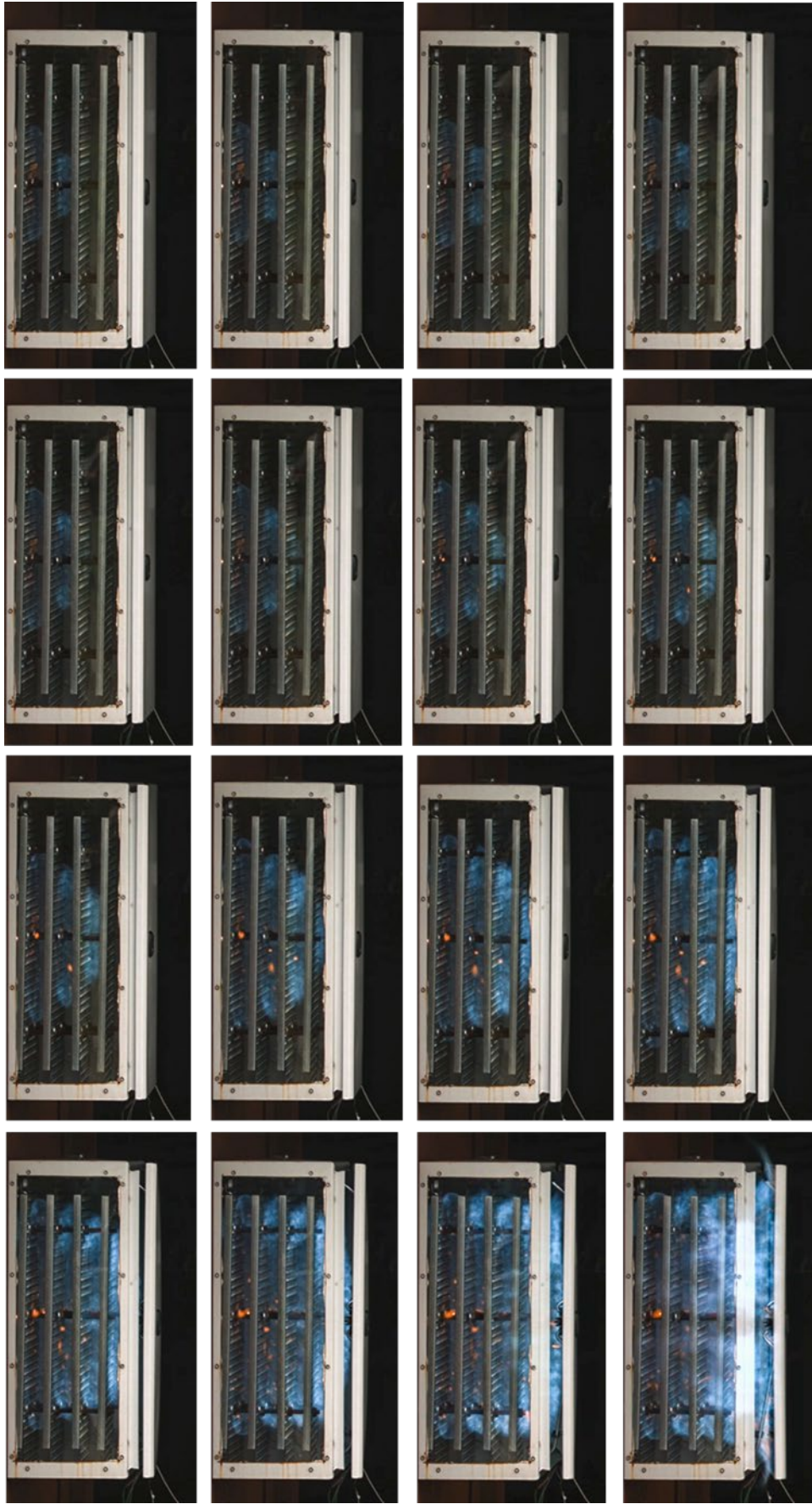
Figure 76 - Flame development in Test 27,1 ms frame interval 1

Figure 77 – Flame development in Test 26, 1 ms frame intervals
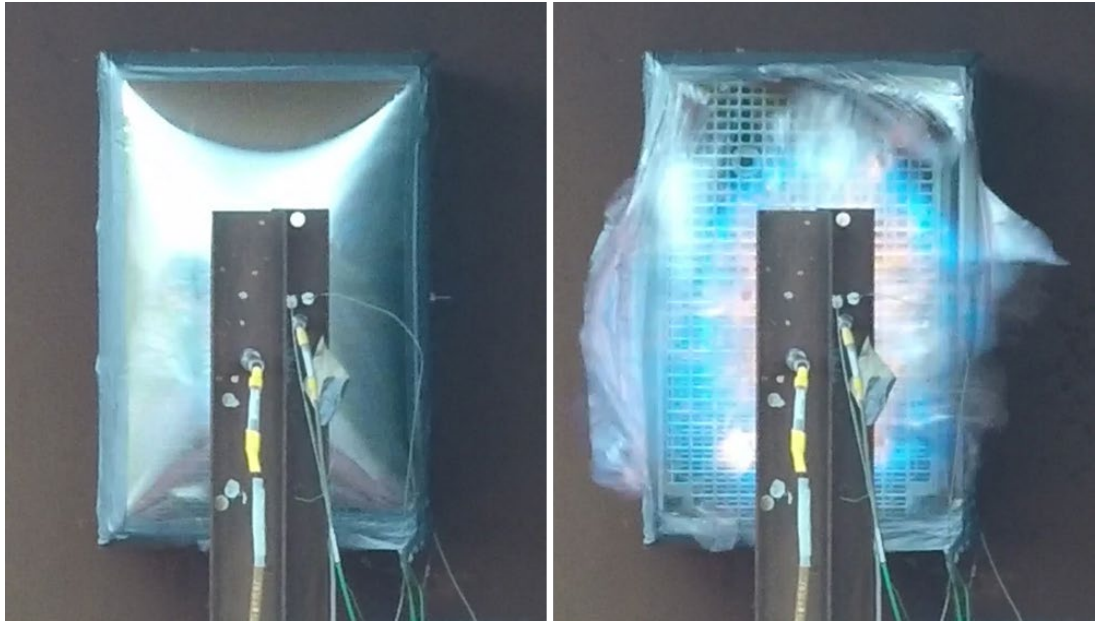
Figure 78 - Foil bursting, Test 26, frame interval 4.17 ms

5.6 Effects of Quantity and Positioning of Internal Congestion

The effect that congestion has on increasing explosion overpressures is well documented in many different explosion studies [51, 53, 54-57, 59, 80,1 32, 143 & 189-192]. Repeated obstacles consisting of grids can effectively increase the flame speed and severity of an explosion [94]. In a study by Yu et al., a square plate with square holes produced a more severe explosion than most other shapes except triangles [58]. The chassis plates used as congestion in these experiments had rectangular holes. The spacing between repeated grids is critical; if they are too close, acceleration may be limited, as the flame requires some distance downstream of an obstruction to accelerate to maximum value. If they are too far apart, continued acceleration will not occur, just episodic acceleration and deceleration without any overall increase [55, 56, 62 & 193].

The location of the obstacles in relation to the vent can also have an effect [194]. There is an optimal point where the flame size is large enough to be severely affected by the congestion, but there is not enough distance to the vent for the flame speed to decrease. In the limited space of the control boxes, the results (Figure 79) show that when two rows of congestion are

used, the explosion is more severe if the congestion is positioned in front of the vent aperture. However, when placed towards the back of the box, the overpressures are similar to tests without congestion, indicating that any effect the congestion has at increasing flame speed is diminished in the remaining uncongested volume.

The results show that four rows in the limited space are the optimum configuration tried, giving a significantly higher overpressure in most cases than three rows. However, two results show a considerably lower overpressure than the other four experiments. These two experiments, Tests 29 and 30, show a reduced rate of pressure rise compared to those with a higher overpressure (Figure 80). Analysis of the high-speed video shows that in Tests 29 and 30, the door begins to vent at the top and as the door opens, the door is twisted (Figure 81), exposing a significantly larger vent area; in the other tests, the door opens and remains relatively parallel to the box, restricting the vent area to a slot. The door has a three-point locking system of two steel bars and a plastic catch (Figure 31). The bars are push-fitted into the plastic catch to provide a pivot point to rotate the bars away from the lip of the box when the lock is opened (Figure 82). How these three locking points fail on application of pressure is variable. In the tests with the lower pressures, the top bar appears to fail first, early in the pressure rise. This type of failure mode could occur by chance in a real-world event. However, studying the worst cases that lead to higher pressure is beneficial.
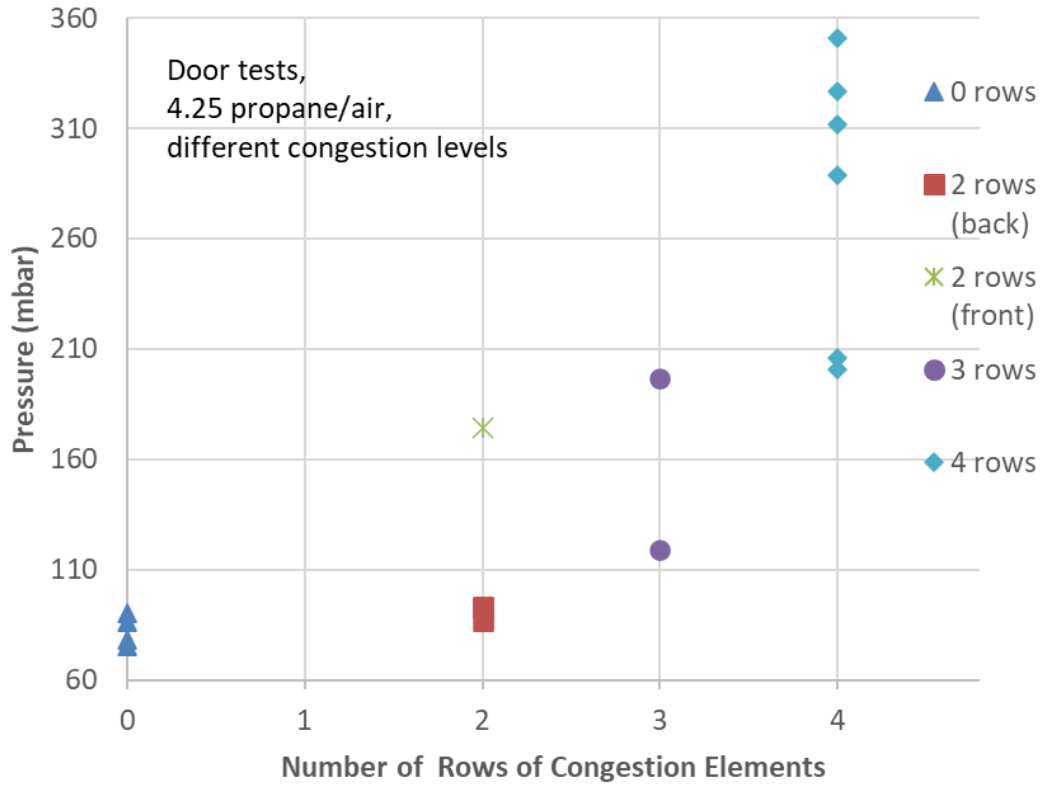
Figure 79 - Peak P_1 overpressures for door experiments with different rows of congestion
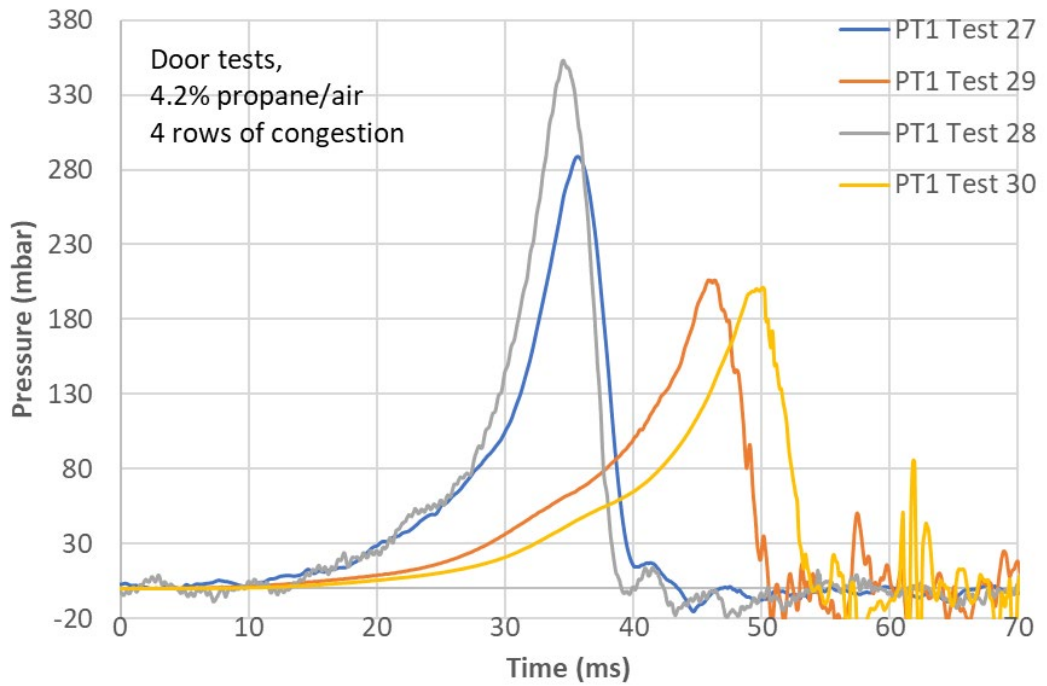
Figure 80 - PT 1 pressure traces for Tests 27-30
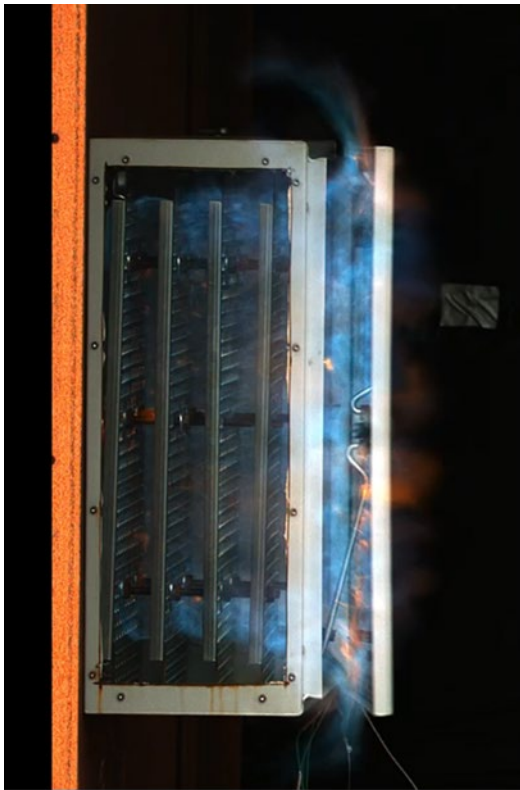
A   B

Figure 81 – High-speed video frames showing the door opening of Tests 27 (image A) and Test 29 (image B)

Figure 82 - Box door showing steel bar connection to central plastic catch

5.7 Static Pressure Behaviour of the Box

The analysis of the results suggested that investigations of the box's behaviour during quasi-static pressurisation could improve our understanding of gas outflow rates and volume increases.

5.7.1 Outflow Versus Pressure in Quasi-static Conditions

As the box was known to leak with the application of pressure, it was impossible to hydrostatically pressure test the box. Therefore, a quasi-static method using air with slow pressure increases and a maintained inlet flow was needed to understand the gas leakage rate during pressure rise.

A new box with a door was subjected to a pneumatic quasi-static pressure test. The pressure was increased slowly (<2 mbar/second) in small increments with an SMC low-pressure high-precision regulator. Once the pressure, measured with a GE Druck DPI800 differential pressure indicator, had stabilised, the flow rate into the box was measured with a Bronkhorst Mass-View flow meter.

The box held pressure up to 22 mbar and started to leak at 23 mbar with a flow rate of 0.4 ln/min; at 24 mbar, a noise was heard, and the flow rate increased significantly to 14.5 l_n/min (Figure 83). The pressure was increased in steps up to the point that the restrictions of the mass flow controller and the high precision allowed the flow, which was 234 mbar. This exceeded the pressure the door opened in the uncongested explosion tests. Additionally, the distance between the door lip and the main body of the box lip was measured with a micrometre to understand the door lock mechanism deflection as a function of pressure. With the flow meter removed, the pressure could be increased to a maximum of 500 mbar. At this pressure, the door remained closed.

Plotting the measured flow rate against the square root of pressure suggests that the vent area around the seal increases rapidly at a pressure between 20 and 30 mbar and then much more slowly for further pressure rises. The door measurements (Figure 84) show that the door is initially displaced by 0.69 mm in the centre at low pressure, then again by a further 0.42 mm at 200 mbar. The extent to which the door opens is limited by the lash in the

catch mechanism and its strength; note this extent was considerably higher in the experiments. The door lip is seated onto a foam rubber seal; the door compresses this when closed to form a seal against ingress protection. When the door is closed, there is a further 2.2 mm of compression possible of the foam if the door is pushed inwards. Distortion of the foam during pressurisation gives additional potential for the vent area to increase.
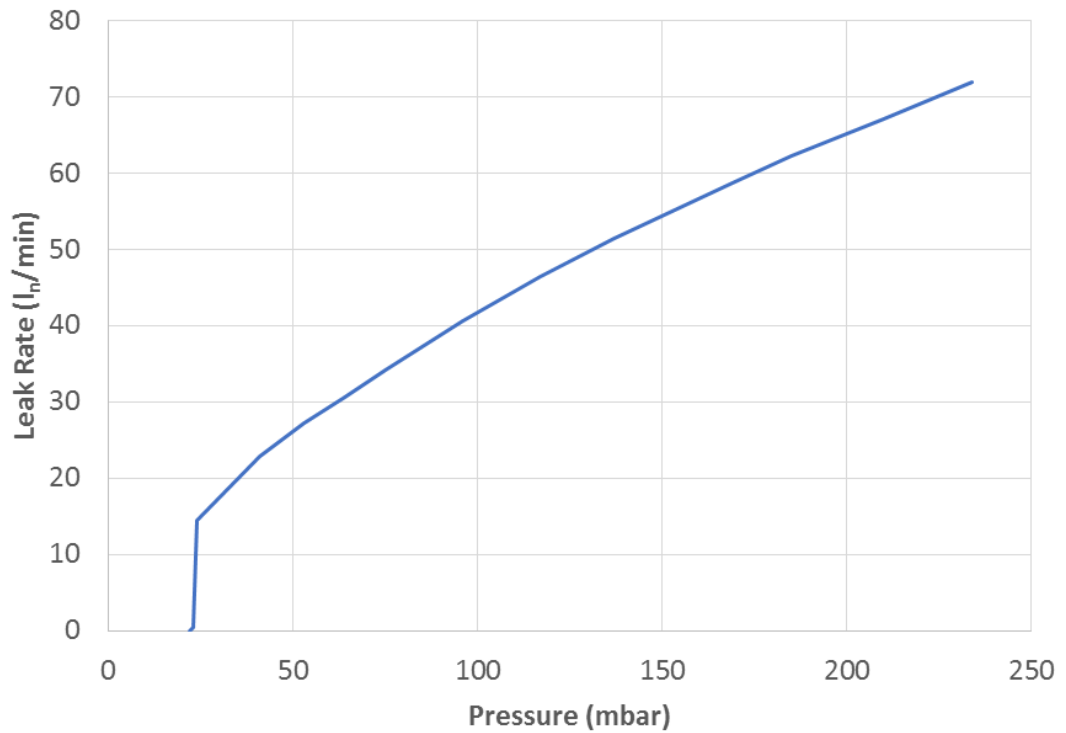
Figure 83 - Leak rate of the pseudo-static test result of a new box with a door.
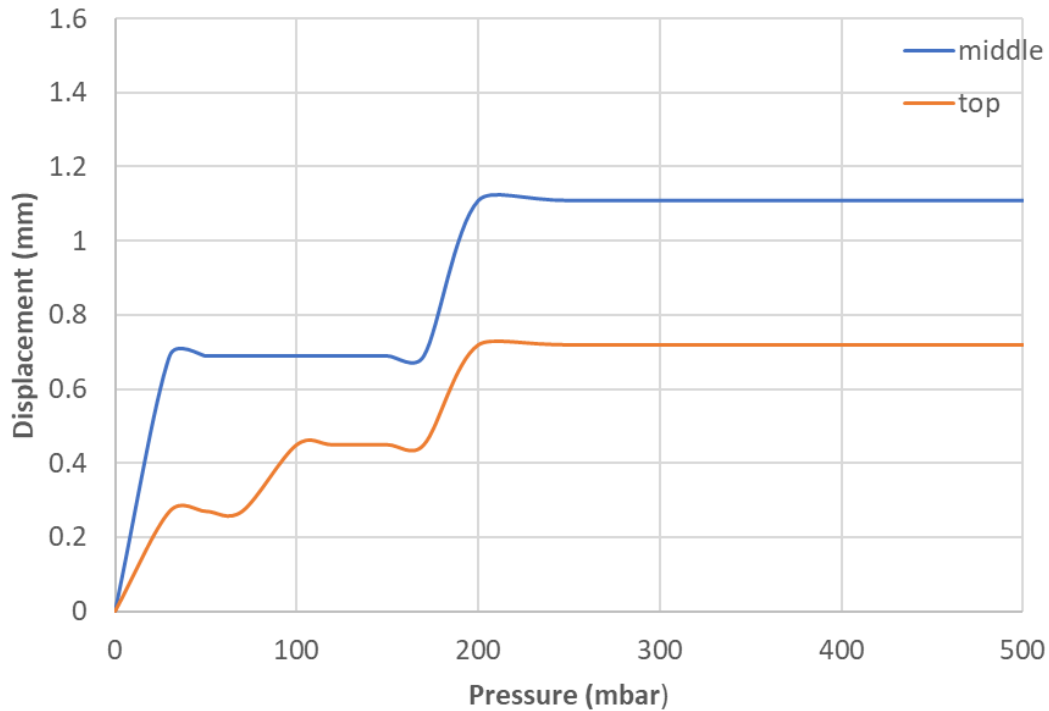
Figure 84 – Door displacement as a function of pressure, measured in the centre and top of the door

5.7.2 Quasi-Static Burst Pressure of Door and Foil

Due to the low-pressure leakage that occurs with the box, it is not possible to conduct a true static pressure test of the box. Therefore, a quasi-static pneumatic test was used instead. The box was subjected to a flow rate of 200 l_n/min with a maximum drive pressure increased from 0.5 bar to 7.5 bar over a period of 10 seconds. This was repeated with both the foil and the door, with the pressure measured per the explosion tests to determine if the static burst pressure was comparable to the explosion burst pressure.

The foil burst at 75 mbar, lower than the 97 mbar measured in the explosion experiment. The static burst pressure is expected to be lower than the explosion burst pressure [128]. There is a response time for the foil to burst and be displaced from the vent, relieving pressure. With a high rate of pressure rise from an explosion, the maximum burst pressure is reached and exceeded before the burst response is fully effective.

In the quasi-static test on the door, deformation of the frame allowed venting of substantial inflows and internal pressures without the catch failing. In the explosion experiments, the lowest pressure the door opened was 75 mbar. In the quasi-static outflow test, the door could withstand 500 mbar without the catches failing; note this was not tested any higher for that test. In both cases, gas venting started at much lower pressures. The explanation must be that the entire pressure rise event in the explosion experiment occurred in under 60 ms, with the final rise, after the pause caused by the onset of gas outflow, occurring in under 20 ms. Enough momentum is associated with the pressure rise and response of the door components to apply a dynamic strain on the door, overcoming the catches. The catches are strong, but they can flex as the two connection points to the door are made using plastic components, and there is a distance between the connection point on the door and where the connection is made with the lip of the box (Figure 31). The door can also flex if pressure is applied unevenly, although this is not expected to be the case in these tests.

Overall, the behaviour of these boxes was significantly different in quasi-static loading to that observed in explosion tests.

5.8 Numerical Modelling of Pressurisation

Video images after ignition (Figure 62) show a growing hemispherical flame shape, and the rate of pressure rise for a given flame speed can be predicted [195]. The flame speeds are so low that the pressure will rise uniformly throughout the box. The venting pressures are assumed to be low enough, and the box is sufficiently rigid that changes in its volume prior to venting are negligible.

The later pressurisation and venting can also be modelled. Assumptions have to be made about the pressure at which the rubber door seal is breached and the effective size of the resulting vent.A_{vent}. The pressure at which the door catches fail must also be taken from the experiment. Still, the door's opening can be calculated given the moment of inertia about the hinge and internal pressure.

The equation for the expanding radius of the flame R is

$$\frac{dR}{dt} = V_b E$$

Where V_b is the burning velocity and E is the expansion ratio

Generally, the burning rate was assumed to be constant, but in some cases, the effect of a small change in the burning velocity after venting was investigated.

The equation for the mass of unburned gas within the box is as follows.

$$\frac{dM}{dt} = -\rho V_b 2\pi R^2 - \rho A_{vent}\sqrt{\frac{2P}{\rho}} - \rho C_d A_{door}\sqrt{\frac{2P}{\rho}}$$

A$_{vent,}$ the effective area of the vent at the vena contracta, has to be taken from the experiment. The discharge coefficient, C_d, for the door is assumed to be 0.6.

The equation for the volume of unburned gas within the box is as follows

$$\frac{dV}{dt} = -EV_b 2\pi R^2 + \frac{HW^2}{2}\frac{d\theta}{dt}$$

The change in pressure of the unburned gas is calculated from the change in density, assuming compression of the unburned gas is isentropic.

$$P = P_0\left(\frac{M}{V\rho_0}\right)^\gamma$$

The area of the door vent is

$$A_{door} = HW\theta + W^2\theta$$

The equation of motion of the door is

$$\frac{d^2\theta}{dt^2} = \frac{PHW^2}{2I}$$

Figure 85 shows the predicted rates of early pressure rise for a range of burning velocities. In all cases, it is assumed that the expansion ratio is 7. The results show that the effective burning velocity is close to 0.40 m/s, and the flame speed (where the burned gas is stationary) is 0.4 x 7 = 2.8 m/s. If the displacement of the door against the catch were included, the derived flame speed would be slightly higher. These figures are only marginally

above the propane laminar flame speed, suggesting that flame instabilities have a modest effect on burning velocity at this stage. This is to be expected as the onset of flame instability of near stoichiometric propane flames is at a radius of about 300 mm if unobstructed. The effect of the wall and ignition device is likely to trigger instability sooner, leading to enhanced average burning velocities for smaller flames [47].

Results of modelling for the later stages of a typical uncongested test are shown in Figure 86. In this modelling, the assumed vent size increases linearly (from zero) to 0.0039 m^2 between a pressure of 28 and 40 mbar. Thereafter, the vent increases gradually and linearly to 0.0044 m^2 at 100 mbar. The onset pressure for significant venting is slightly higher than in the static test (around 24 mbar). The door was observed to move out several millimetres before the seal venting pressure was reached (see Frame D2 in Figure 68). Since the total perimeter of the door is 2 m, such a displacement corresponds to a vent area in the same order as that assumed.

The pressure for door failure is assumed to be 90 mbar. This is well below the high pressures that could be sustained if the pressure was applied in a quasi-static manner where the catch mechanism was not exposed to dynamic loads.

After seal failure, a slight increase in burning velocity (from 0.4 to 0.44 m/s) is assumed. This change in flame speed accounts for the observed increase in pressurisation and might be caused by flame distortion as the seal venting flow starts.

When there was congestion, the rate of pressurisation was higher. Again, the videos show that, until the door fails, the flame is roughly hemispherical, so a simple model of combustion rate is possible. In this case, the initial average burning velocity was around 0.8 m/s (flame speed 5.6 m/s). The results suggest an increase in the burning rate to about 1.1 m/s after seal venting and then further very substantial increases as the door started to open at around 80 mbar. The final phase of flame acceleration was presumably traceable to the onset of flow towards the vent, which drove unburned gas through the congestion array, increasing turbulence levels and, consequently, flame speeds. The final phase was not modelled as the

hemispherical symmetry of the flame would have broken down after this point, and a single value could not adequately represent the burning velocity.
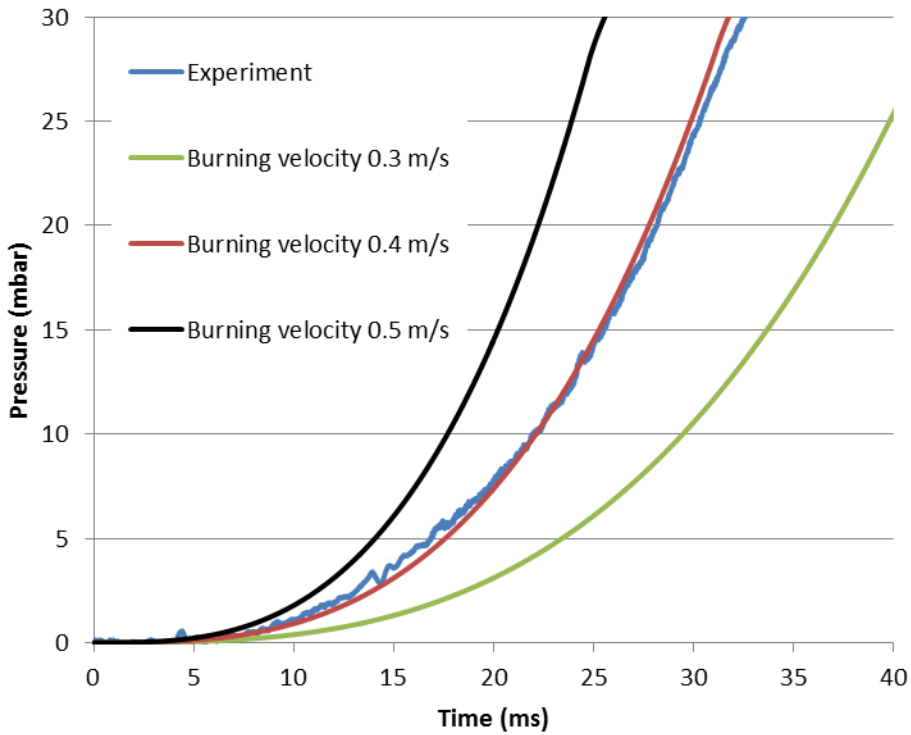
Figure 85 - Modelling of the early stages of pressurisation
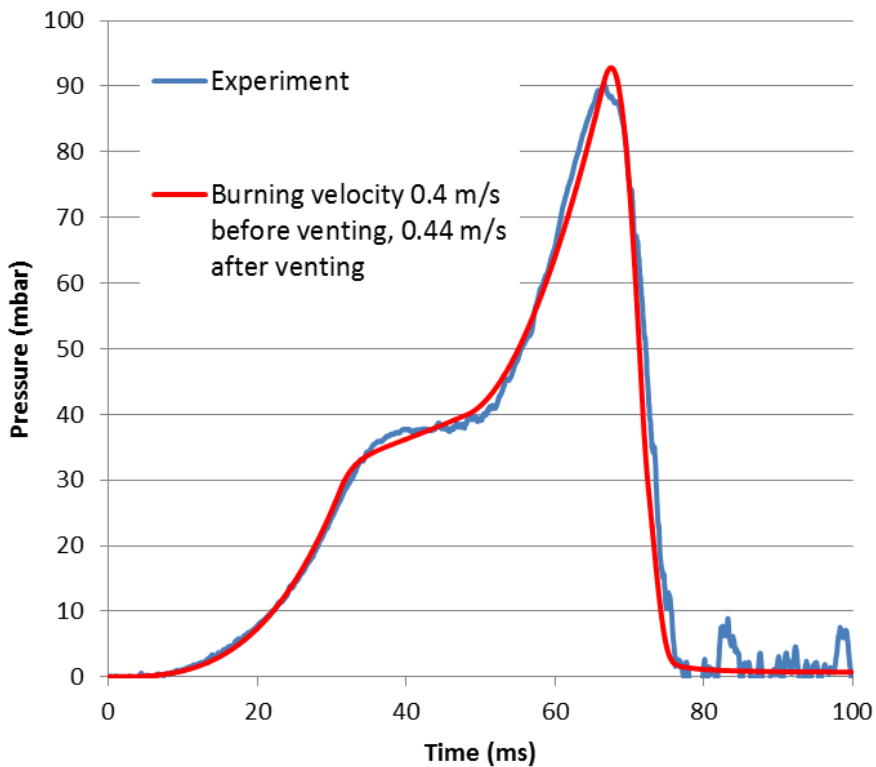
Figure 86 - Modelling of pressurisation and venting in Test 11
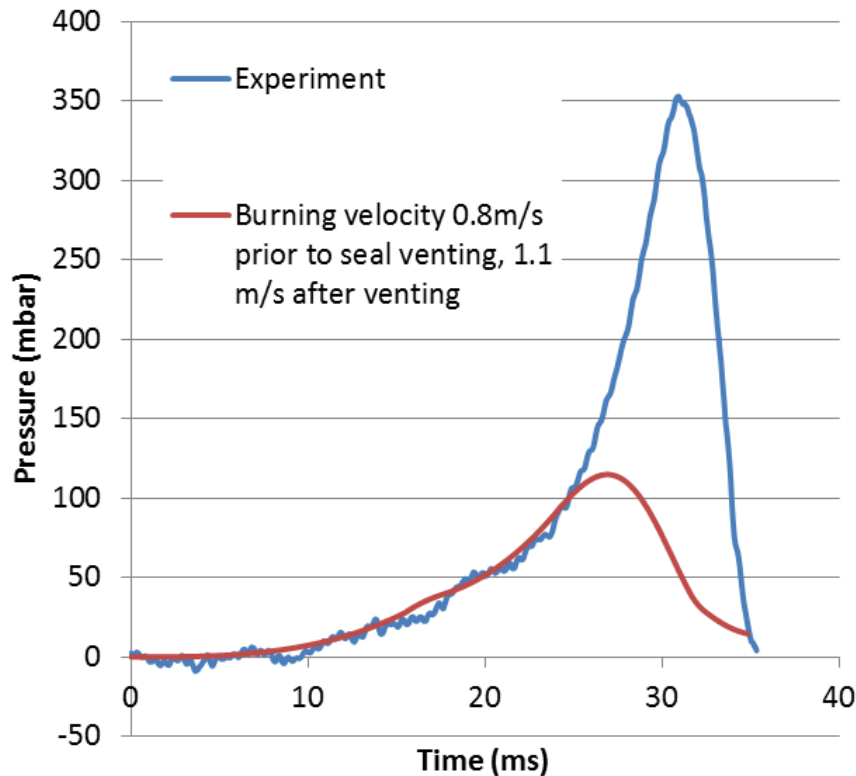
Figure 87 - Pressurisation in box with congestion

5.9 Effect of Door on Flame Exit and External Flame Speed

The considerable pressures and restricted vent area caused by the door impact the flame shape. The door is open by no more than 30 mm when the flame begins to exit, and combustion is complete before the door is completely open. The vent comprises a rectangular slot at the side of the box and a triangular opening at the top and bottom. The external flame does not develop into a mushroom shape but is initially a flat petal shape which expands sideways (in a direction perpendicular to the plane of the vent) for approximately 1 metre (Figure 88).

Due to the venting location with the door on, the flame does not reach the external thermocouples. The video records of tests with the door allow an alternative method of assessment of the rate of progress of the flame outside the box. The video was captured at 240 frames per second, giving an interval of 4.17 ms between frames. This is a much lower resolution than

the thermocouple measurements, but in the absence of that, this data provides some useful information. In the first frame in which the flame is seen external to the box, it has travelled 250 mm. Using the side view (Figure 76), with a higher frame rate to estimate the time of emergence before this image gives a flame speed of approximately 100 - 200 m/s. The measured pressure at the time of the emergence of the flame was around 290 mbar, corresponding to an expanded gas velocity of around 200 m/s. The flame travels a further 300 mm in the next 4.17 ms frame interval (an average of 72 m/s) and an additional 100 mm in the next frame (24 m/s), indicating a rapid decay in flame speed. Given the vent geometry and high venting velocities indicated by the flame speeds, it would be expected that the shear turbulence would be very high, causing dilution with the entrained air, which would result in a slowing of the gas flow and some dilution below the lower flammable limits (LFL) for a proportion of the volume.

Using the video to observe the external flame, in Test 26, the flame was a rough mushroom shape around 1000 mm in diameter (Figure 89). In Test 27, the flame is a rough petal shape, approximately 800 x 600 x 150 mm, at its extremes before the flame dilutes (Figure 76 and Figure 89). Although the shapes are very different, it is clear that the door produces a much smaller flame than the foil in terms of volume.

Suppose the flame shape for the foil test is simplified to a hemisphere, and the size is calculated using the expanded gas volume. In that case, the theoretical maximum diameter of the flame is around 1200 mm. This is very close to the observed flame size. This suggests that most of the gas has burned, and only a small proportion was diluted below the LFL. This shows that the resulting outflow of gas has a broad central core in which the flow is irrotational and largely unaffected by the vorticity in the shear layers at the edge. This type of flow has been described as a "rolling vortex bubble" [34 & 122]. As these layers roll up, the potential core of the resulting vortex is eroded slowly by relatively low levels of shear and, therefore, dilution.

Conversely, if the door flame shape is simplified to a disc of width 150 mm, the expected flame diameter would be around 1900 mm, which is much larger than the reach of the flame observed (800 mm): this suggests that a

high proportion of the ejected gas was diluted to the point where it did not burn. The ejected gas test forms a narrow, high-speed jet. Only a very small proportion of the gas remains in the jet's irrotational potential core. Most of the ejected gas is immediately entrained into the turbulent shear layer where high flame speeds could develop. In these experiments, the box is surrounded by air, so entrainment leads to rapid dilution of the unburnt gas below the initial (stoichiometric) concentration.
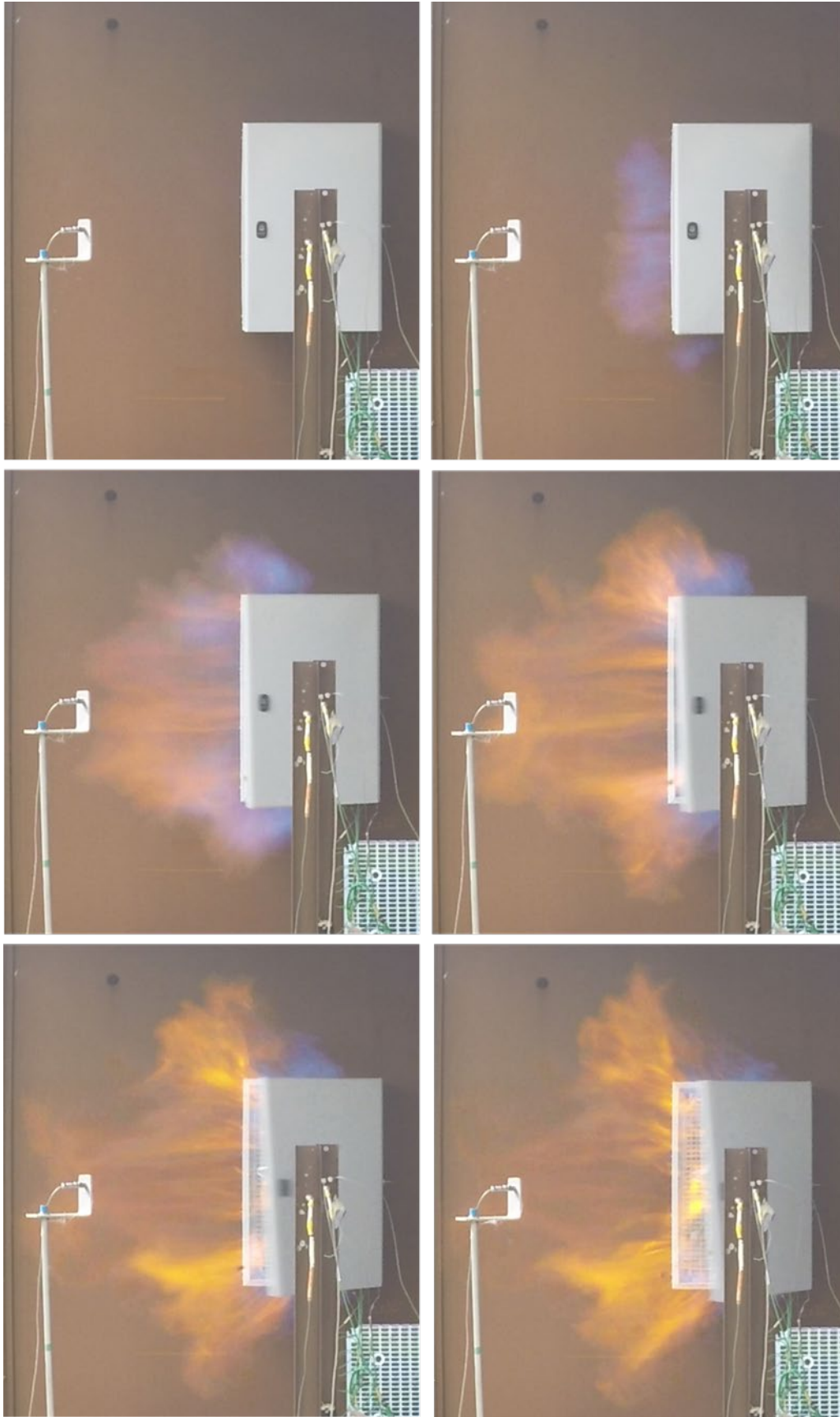
Figure 88 - Test 27 video images of flame exit, 4.17 ms frame interval
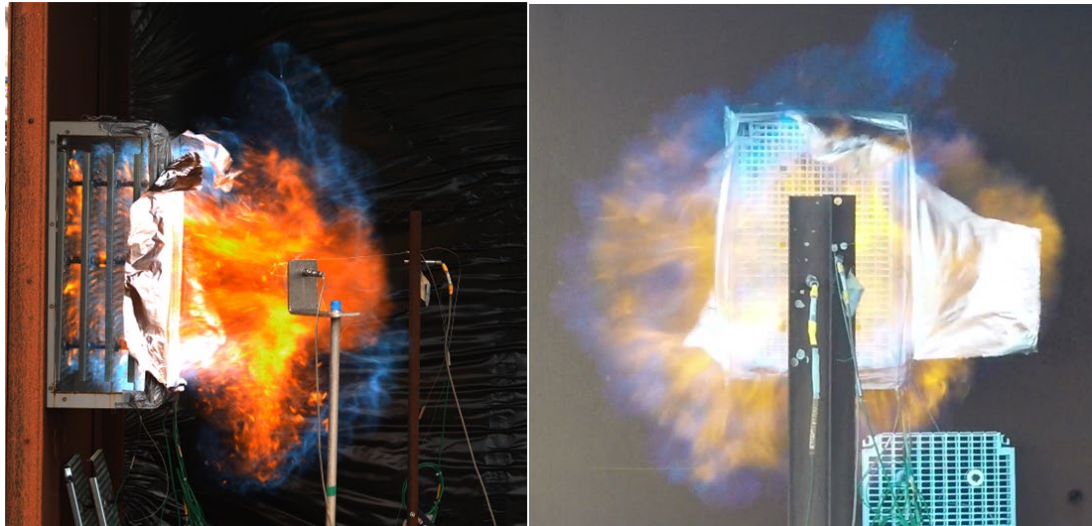
Figure 89 - Test 26 flame shape from side and front

5.9 Conclusions

The use of PVC cling film as a vent covering was abandoned due to it stretching considerably and not bursting. Foil was found to be a good representation of a bursting membrane. However, the shape of the box and the method of fixing meant that it was prone to tearing early during pressurisation. Many experiments were carried out, but only a small percentage led to a successful test. However, without congestion, there was some similarity between the peak pressure with the door and foil results, and the results were predictable using a simple phenomenological model. Once congestion was added, the difference was substantial; the foil was light and easily removed from the vent area, exposing the entire area. The heavy door took some time to open fully, causing a significant blockage to the vent area after the initial opening.

The boxes are designed to prevent ingress, not hold pressure. The door and its locking mechanisms are flexible, allowing the release of pressure at very low pressures, as can be seen in the pressure traces. Under static conditions, this flexibility prevents the door-locking mechanisms from failing. However, the momentum and forces involved in an internal explosion can overcome these and open the door at relatively low pressures.

The manner in which the door opens is not predictable; the door can open preferentially at the top or bottom, indicating that the failure occurs at one of

the top or bottom catches first, meaning the door will twist as it opens. The extent will depend on the time difference between the catches failing. However, it can also fail because of the pressure of overcoming all the catches nearly instantaneously, and this will result in the door appearing to open with the edge of the door parallel to the box. The way the locking mechanism fails significantly affects the P1 maximum pressure due to differing vent areas. The larger the vent area, caused by the door twisting, the lower the peak pressure.

The flame shape of the foil and door were considerably different, the venting mechanisms of a large rolling vortex out of a large vent area, for the foil caused a standard mushroom-shaped flame. Observations of the flame size indicated that in the foil experiments, most of the vented gas was consumed by the external explosion. In the door experiments, the venting was much faster out of a substantially smaller area comprising of a long, thin peripheral slot, and the flame formed a flat petal shape. The flame size suggested that not all of the gas burned, possibly due to the sheer forces between the vented gas mixture and the surrounding atmosphere, causing dilution below the lower flammable limit for a proportion of the vented gas, meaning it was not available for combustion.

Chapter 6
Explosions Propagating from Electrical Control Box into an External Flammable Atmosphere

6.1 Introduction

These experiments were designed to investigate the explosion propagation mechanisms from commercially available electrical control cabinets with a hinging door to an external flammable atmosphere, per objective 3 from Section 1.6.

Four rows of congestion were used for all the experiments with the box. Four experiments were carried out with the external cube rig covered with the plastic film but not filled with a flammable atmosphere to understand the effects of venting into the tent and the effect of the explosion venting from the box on the tent itself. In all four of these experiments, the tent was not breached by the explosion; there was enough flex in the tent to accommodate the increase in pressure, and heat was lost before excessive damage occurred to the plastic film.

Comparative experiments were carried out with both the box and tent filled with 4.2% propane/air and the ignition initiated in the box with the door on and with the ignition initiated in the tent alone. Additionally, experiments were conducted with the box without the door to understand the effects of the semi-confined and congested ignition source without a vent cover on the explosion severity of the volume in the tent.

Experiments were also conducted with a row of 50 mm diameter pipes, 50 mm apart, placed 500 mm from the door opening in the path of the vented gases and flames to assess the potential for further flame acceleration by means of obstacles once the flame speed had begun to slow.

Due to cost and resources, the number of experiments that could be conducted was limited.

6.2 Pressure Development

The pressure development with the box in an explosive atmosphere (Figure 90) follows a similar pattern to the box alone (Figure 76), with additional peaks associated with the combustion of the gas external to the box inside the tent rig. The dominant peak is P_1, the internal pressurisation of the box before the door is open enough to allow the pressure to decay. There is also a peak on PT2 associated with the door opening and accelerating gas outflow. Shortly afterwards, there is a second peak, P_2, likely due to the vented gas's external explosion and the cube's flammable atmosphere; this also registers slightly on PT3. A third peak on all three pressure transducers, P_3, is likely associated with the maximum flame area.
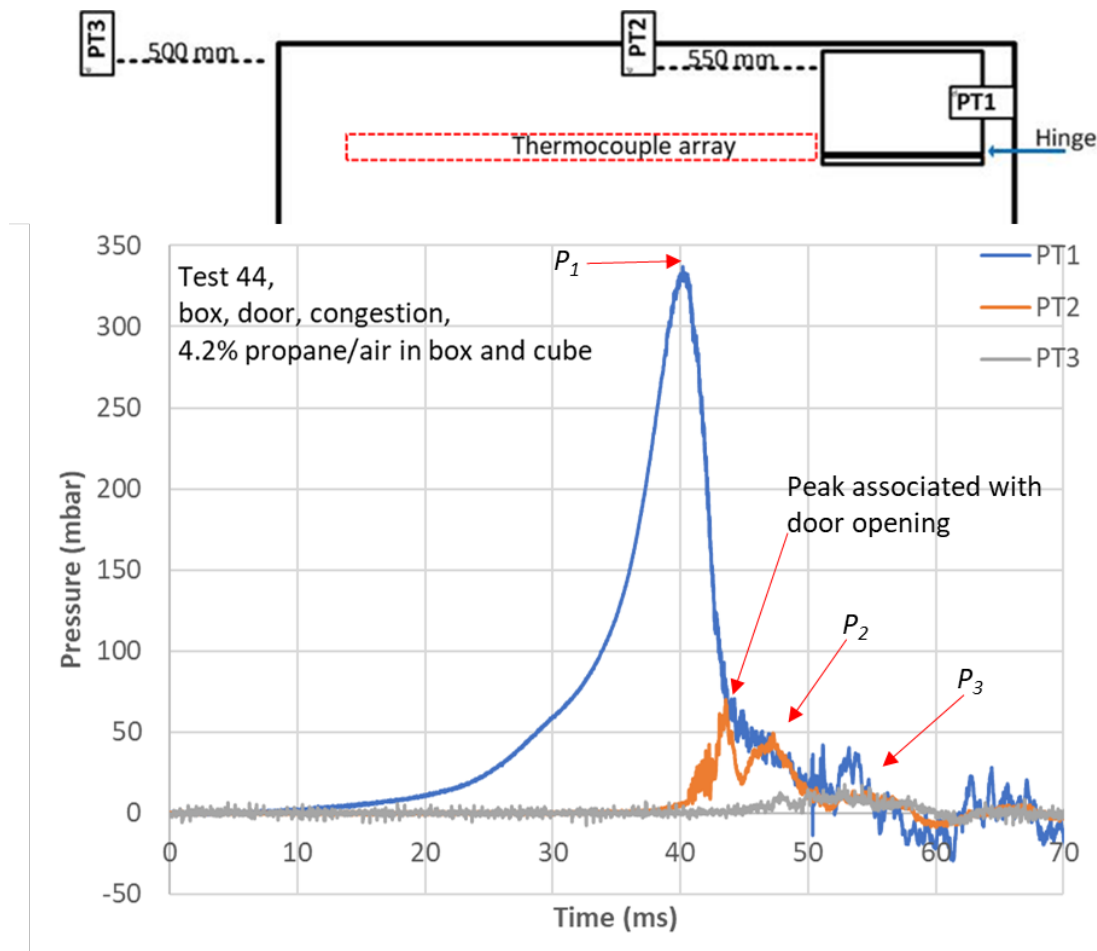
Figure 90 - Pressure trace for Test 44

6.3 Overview of Pressure Results

Table 7 provides an overview of the pressure measurements from Tests 33 to 44. For Tests 37 and 38, PT3 appeared to show a fault and recorded no data. For Test 41, the data acquisition system failed, and no data was captured; however, the high-speed videography did provide a record.

Table 7 - Overview of pressure measurements for Tests 33 to 44

Test	Condition	Tent atmosphere	P_1 at PT1 (mbar)	PT 2 door opening (mbar)	P_2 at PT2 (mbar)	P_3 at PT3 (mbar)
33	Box with door	air	327	57	13	0
34	Box with door	air	296	50	14	0
35	Box with door	air	328	58	18	0
36	Box with door	air	299	64	14	0
37	Box, no door	4.2% C_3H_8/air	23	3	7	No data
38	Box with door	4.2% C_3H_8/air	180	16	No data	5
39	Box with door	4.2% C_3H_8/air	212	54	37	10
40	Box with door, obstacles	4.2% C_3H_8/air	146	28	37	10
41	Box with door, obstacles	4.2% C_3H_8/air	No data	No data	No data	No data
42	Box, no door	4.2% C_3H_8/air	19	3	10	3
43	No box	4.2% C_3H_8/air	N/A	N/A	7	5
44	Box with door	4.2% C_3H_8/air	337	70	49	17

6.4 Evaluation of Flame Speed Measurement Methods

The results of flame speed measurements from Test 36 were assessed. For this experiment, the thermocouples were located at 50 mm spaces for the first 250 mm and then every 100 mm with the exposed tips in line with the door opening. They were sampled at 50 kHz, giving a sample interval of 20 µs. The experiment was filmed from the front at a rate of 5000 fps, giving a frame interval of 200 µs.

The point of increase in potential difference for the thermocouple data was taken as the time of flame arrival; only six of the seven thermocouples registered a change in potential difference that could be determined over the noise of the sample. The thermocouple at 250 mm registered excessive noise for the duration of the sample. When the signal measured was switched from voltage to temperature, the thermocouple did not produce excessive noise. However, with the equipment available, there was no method of measuring temperatures beyond 200 Hz.

For the video, a high-contrast scale with 50 mm block markings was placed in sight of the frame. The point at which the flame arrives visually at each marking was taken as the flame arrival time. The flame front was noted to be irregular in shape, with rolling wisps of flames at the leading edge (Figure 91). The furthest extent of any tip was taken as the flame leading edge for measurement.

The flame arrival time was used to calculate the average flame speed between the measured points (Figure 92). These show a common trend but have very different results. The issue with both methods is that there is an element of subjectivity in determining the flame arrival time. The potential difference of a thermocouple between the hot and cold junction when impinged with flame is around 2 mV, and the noise can have an amplitude of around 0.2 mV with up to 1 ms frequency. This makes determining the point of rapid increase difficult. There is also an issue with the thermocouple response time. As the flame is shown to have an irregular rolling edge, with wisps of flame extending up to 80 mm from the main core of the flame, there is a possibility that the thermocouples may be hit out of sequence by a flame. With the video, there is a reliance on visualisation of the flame, and

measurements are subject to errors due to viewing angles and any depth of plane differences between the scale and flame. There is also an issue with the resolution of data due to the frame rate and number of pixels allowing for the resolution of the scale. The frame rate was increased to 10000 fps for further tests, slightly improving the resolution.

The video has advantages over the thermocouple data as there is no response time issue, and measurement points are not limited by the number of thermocouples; they can be made across the entire frame. However, the data has enough uncertainty and subjectivity to only be useful as an indication. Due to this, the results are presented as the average speed between two points at 50 mm separation; the speed at 50 mm is derived from the time it takes the flame to travel from 0 mm to 50 mm, etc.
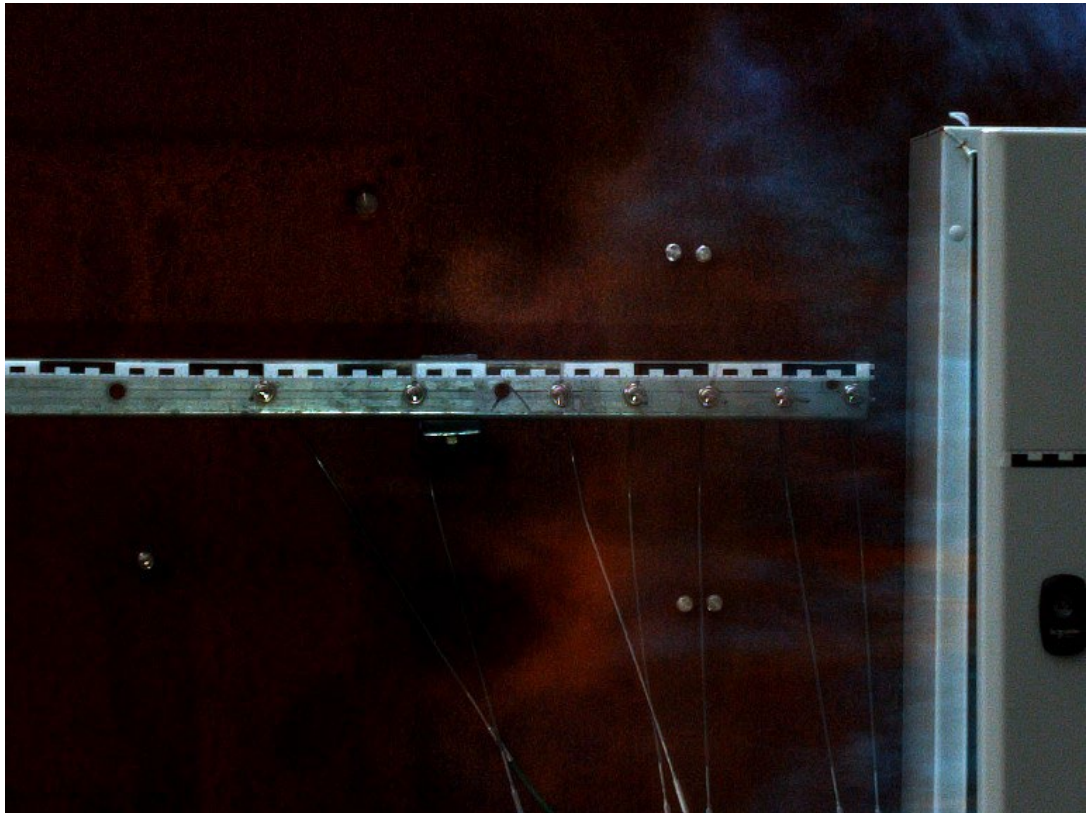
Figure 91 - Exited flame from Test 36 showing irregular leading edge.
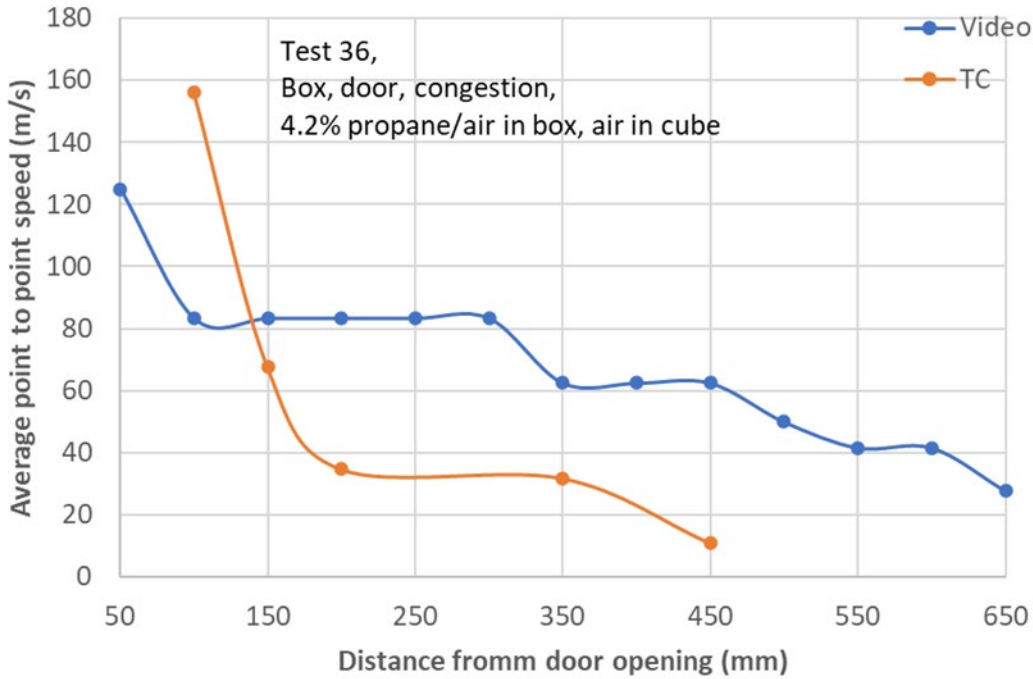
Figure 92 - Average point to point flame speed using thermocouple and high-speed video data; note the thermocouple at 50 mm was used as a zero point

6.6 Overview of Flame Speed Measurement Results

As discussed, the flame speed results derived from the high-speed videography, as an indication only, are detailed in Table 8.

Table 8 - Average point to point flame speeds between 50 mm intervals

Distance (mm)	Test 36 Box only (m/s)	Test 40 Ext. cong. (m/s)	Test 41 Ext. cong. (m/s)	Test 42 Box no door (m/s)	Test 43 Tent only (m/s)	Test 44 Box & Tent (m/s)
50	125.0	50.0	125.0	50.0	8.3	166.7
100	83.3	71.4	125.0	25.0	6.7	71.4
150	83.3	71.4	100.0	25.0	5.6	100.0
200	83.3	62.5	100.0	20.0	4.5	100.0
250	83.3	62.5	125.0	14.3	5.7	100.0
300	83.3	45.5	100.0	11.1	6.3	100.0
350	62.5	33.3	50.0	9.1	6.3	100.0

Distance (mm)	Test 36 Box only (m/s)	Test 40 Ext. cong. (m/s)	Test 41 Ext. cong. (m/s)	Test 42 Box no door (m/s)	Test 43 Tent only (m/s)	Test 44 Box & Tent (m/s)
400	62.5	38.5	55.6	7.7	8.3	83.3
450	62.5	26.3	71.4	6.7	8.9	55.6
500	50.0	21.7	50.0	6.7	8.9	41.7
550	41.7	-	-	7.1	8.8	41.7
600	41.7	10.9	40.0	10.0	8.2	45.5
650	27.8	-	-	11.6	7.9	38.5
700	-	13.2	43.5	14.3	7.8	31.3
750	-	33.3	41.7	13.5	9.1	29.4
800	-	22.7	41.7	14.7	8.3	29.4
850	-	26.3	62.5	14.7	8.3	29.4
900	-	26.3	55.6	18.5	10.0	27.8
950	-	25.0	50.0	17.9	14.3	23.8
1000	-	25.0	35.7	20.0	14.3	23.8
1050	-	31.3	27.8	20.0	16.7	21.7
1100	-	31.3	29.4	21.7	16.7	21.7
1150	-	25.0	23.8	21.7	16.7	20.8
1200	-	25.0	23.8	23.8	16.7	19.2
1250	-	25.0	25.0	23.8	16.7	20.0
1300	-	25.0	25.0	25.0	16.7	22.7
1350	-	25.0	25.0	25.0	21.7	26.3
1400	-	25.0	25.0	25.0	21.7	26.3
1450	-	25.0	26.3	25.0	23.8	25.0

6.7 Baseline Experiments

The experiments were designed to be comparative, with the baseline experiments being the box inside the cube frame tent in the new position

without an explosive atmosphere and the cube filled with a flammable atmosphere and ignited without the box.

6.7.1 Box in Cube Tent with No Explosive Atmosphere

The four experiments inside the frame rig show a reasonable amount of reproducibility. To some extent, the tent protects the experiment from the effects of the weather, reducing the diluting effects of the wind on the vented unburnt gases. As expected, the box's internal maximum pressure, P_1 peak, was comparable with previous experiments Figure 93. Tests 34 and 36 were towards the lower level of maximum pressure seen previously; video analysis shows a very slight preferential opening at the bottom of the door for these tests, which will affect the vent area to a small degree.

The external explosion, P_2, overpressures measured inside the cube were limited. The cube tent was not damaged beyond minor heat damage by the explosion, and no overpressures were registered on PT3, situated outside the cube.

The results show that the venting process generates turbulence. As the vented gases mix with the relatively quiescent atmosphere in the tent, they are diluted below the flammable limit.
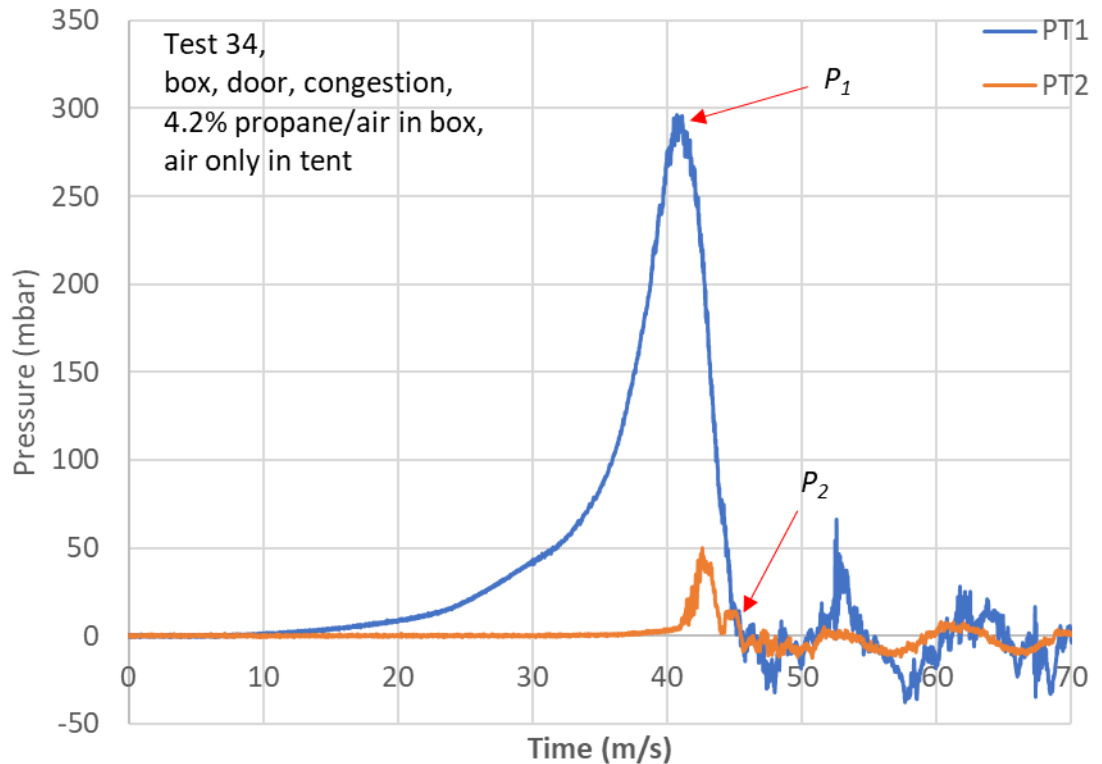
Figure 93 - Pressure trace for Test 34

6.7.2 Ignition of Flammable Atmosphere in the Tent Cube Only

Test 43 was conducted without a box. The ignition source was located in the same place within the tent as it would be in the box, on the back wall. As expected, the flame kernel grew hemispherically out from the back wall at a steady rate. The flame shows signs of instability early in the growth due to the back wall and the ignitor; the flame kernel splits at one point (Figure 94). There was some local flame acceleration along the thermocouple array (Figure 95); however, the flame speed gradually increased. The flame gradually becomes more cellular due to the Darrieus-Landau instability [196]. Once the tent plastic sheeting ruptures, the induced directional flows distort the flame.

As expected, very low overpressures were measured (Figure 96). However, the trace, along with the obvious flame channelling when the plastic ruptures, demonstrates that the weak plastic cover provides a very limited confinement element.
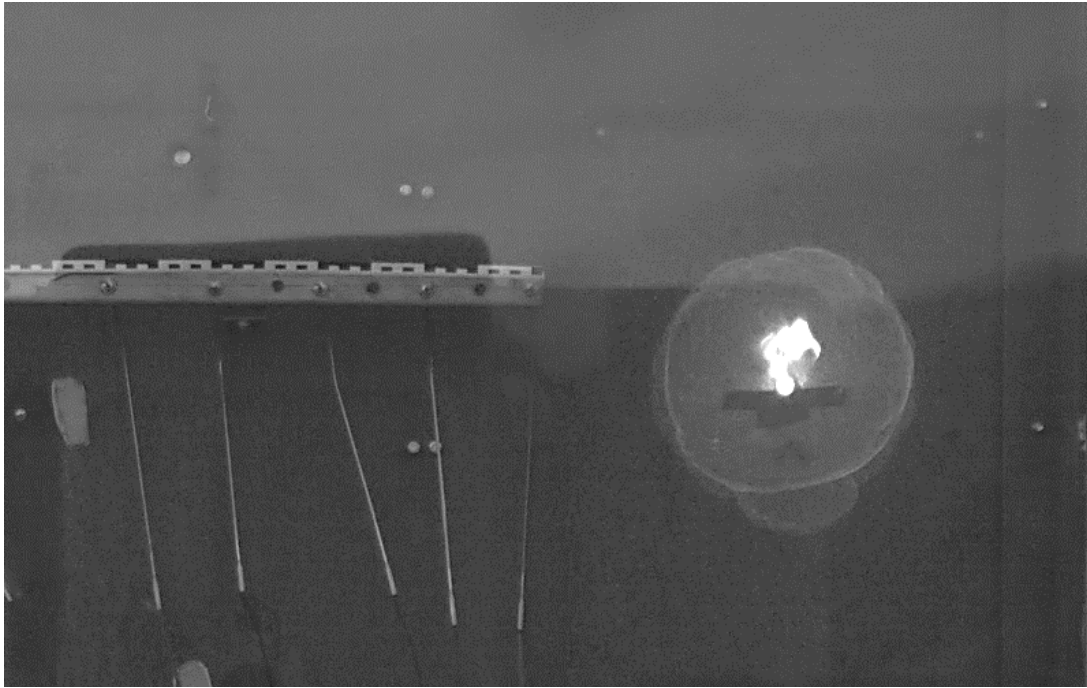
Figure 94 - Test 43 flame at 250 mm diameter and showing signs of instabilities
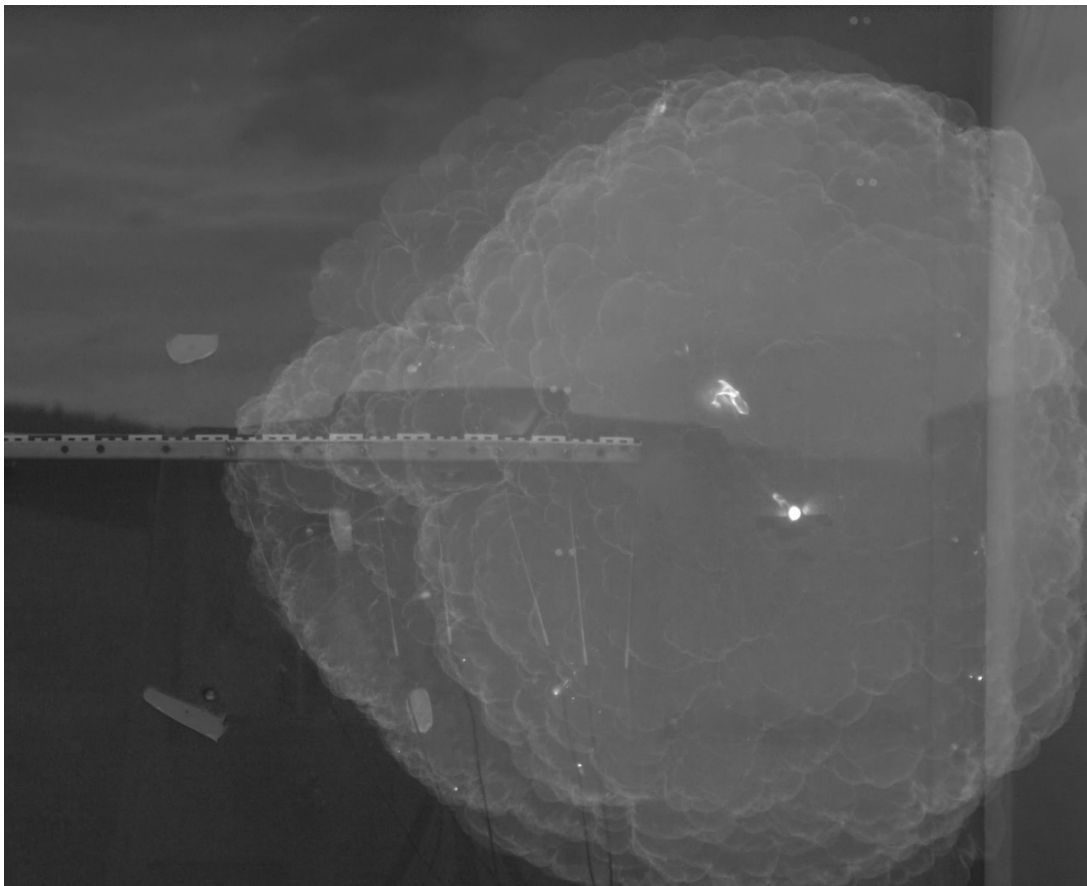
Figure 95 - Image from high-speed video of Test 43
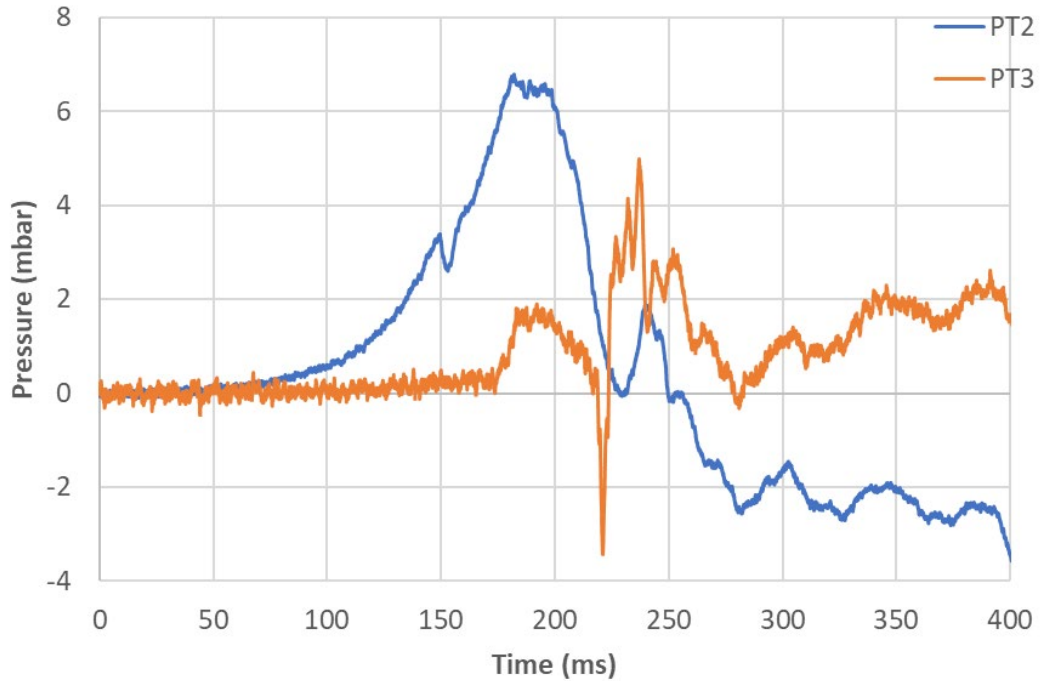
Figure 96 - Pressure trace for Test 43

6.8 Explosion Propagating from a Congested Box with No Door

Without the door, but with congestion, the flame still accelerates inside the box due to the congestion and partial confinement and exits with a mushroom head shape around the box aperture (Figure 97). Without the confinement, the mushroom shape has no 'stem', as seen in the foil tests (Figure 89). The flame grows hemispherically (Figure 98) until it hits the side of the tent closer to the box, which disrupts the hemisphere in that plane as the tent does not burst at this point. The flame speed gradually reduces until the side wall, furthest from the box, with the thinner plastic, ruptures (Figure 99), and then the flame starts to extend with the outflow. There is also some local acceleration along the thermocouple array.

The pressure trace shows that, as expected, with no door or vent covering the box, P_1 is significantly reduced (Figure 102); however, with the semi-confinement and congestion in the box, there is a distinct pressure rise and fall and a pressure rise associated with flame exit registering on PT2. The explosion of the gas in the cube registers a much higher peak pressure on

PT1 than PT2 because the explosion is centred in front of the open box, and PT 2 in the centre of the back wall of the cube is then offset. The time delay between the peaks for PT1 and PT2 also indicates this. The overpressure measured on PT3 is very low at 3 mbar, showing minimal external blast effects.

Figure 97 - Test 42 flame shape as it exits the box

Figure 98 - Test 42 hemispherical flame development
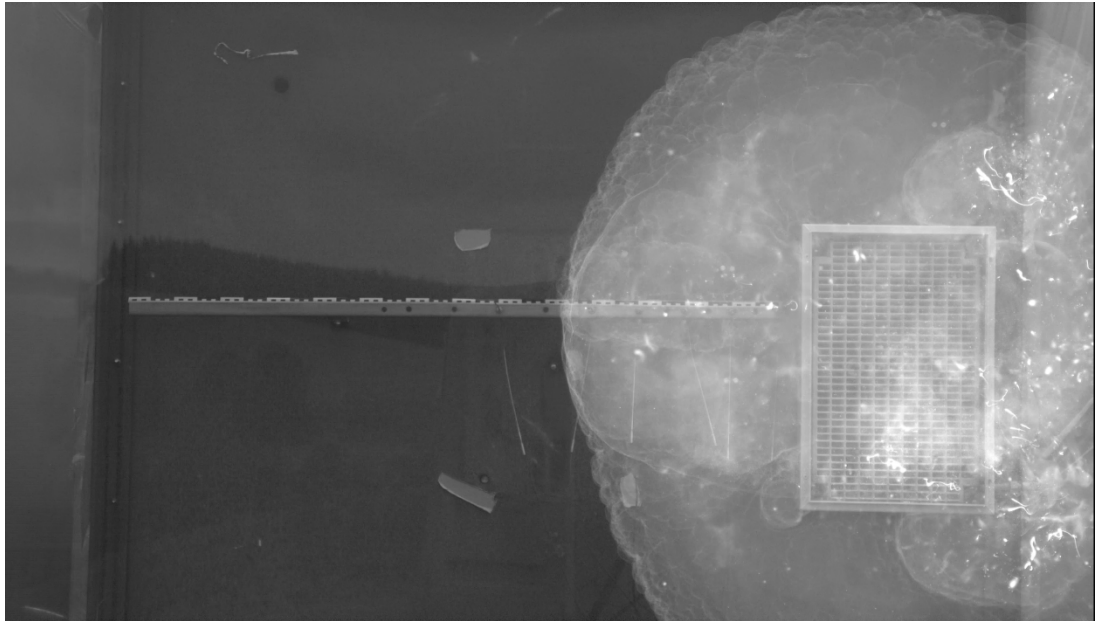
Figure 99 - Test 42 flame at the point of tent rupture
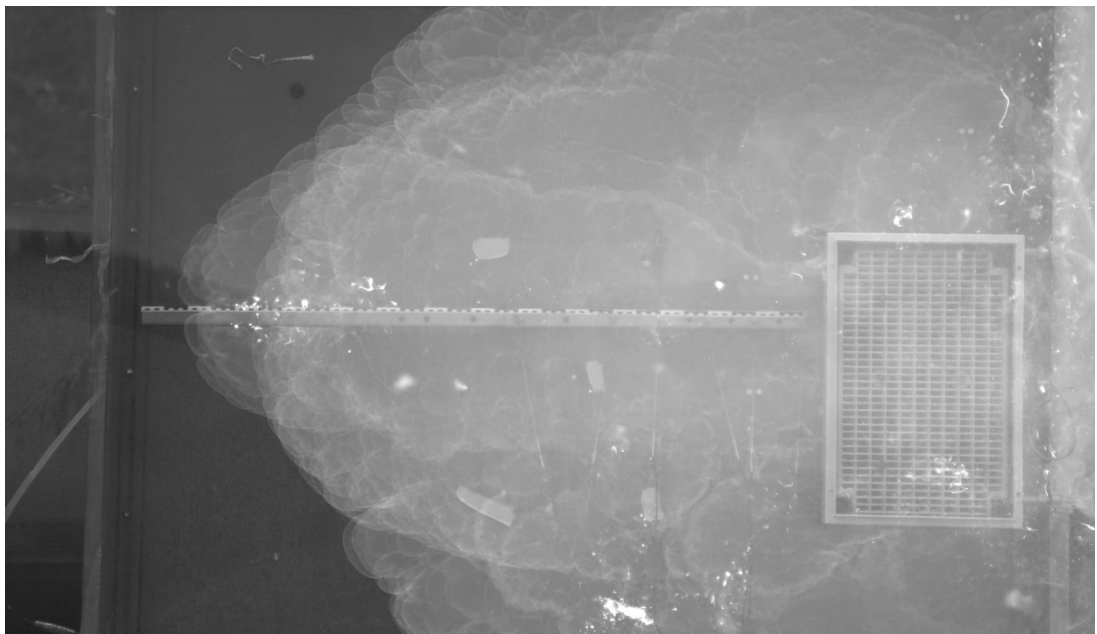
Figure 100 - Test 42 flame stretch once the side of the tent is fully open
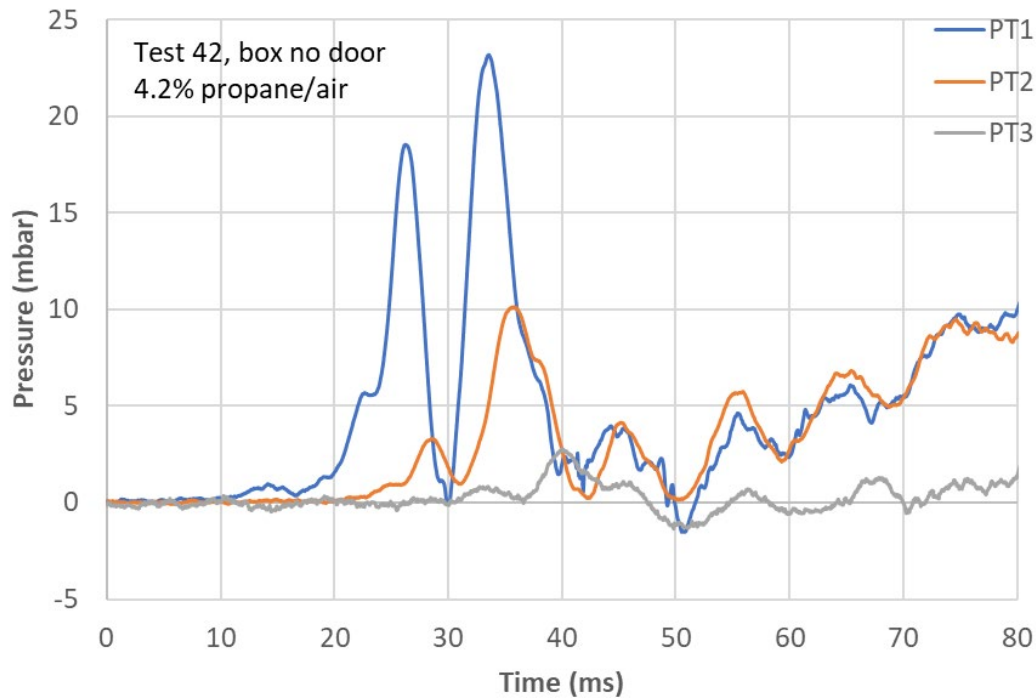
Figure 101 - Test 42 pressure trace

6.9 Explosions Propagating from a Congested Box with Door On

Of the three experiments conducted, Tests 38 and 39 show a reduced P_1 peak pressure compared to the experiments with the box alone (Tests 33-36) and Test 44. The video analysis shows that the door opening of these two tests is uneven, with the top of the door opening first in Test 38 and the bottom opening first in Test 39; this phenomenon was discussed in Chapter 5 and highlights again that the door failure mechanisms are variable. Tests 33-36 repeatability show that the likely outcome is the door failure mechanism that produces the highest overpressures. Still, many door/catch assemblies fail early at the top or bottom, leading to lower pressures.

Test 44 (box with door and gas in the tent) finally produced internal pressures comparable with the control experiments (Tests 33-36). The effects of reduced dilution of the outflow and enhanced external combustion could then be seen more clearly. The pressure associated with the initial external explosion (P_2) was increased by a factor of between 2.7 and 3.7. The pressure for a given explosion severity is expected to be related to the

cube root of the volume of gas consumed. This suggests that the significant phase of the external explosion when there is gas in the box and tent extends to a volume 20-50 times (2.7^2 to 3.73^2) that when there is only gas in the box.

By comparison, the ratio of total volumes in the box and the tent is well over 100 and only a proportion of the gas in the isolated box is involved in the external explosion. This indicates that only a small portion of the tent volume is involved in an explosion of significance in pressure generation. This aligns with the observation of flame speed and video evidence of the explosion.

Test 44 was conducted in low light and filmed at 10000 frames per second, giving frame intervals of 100 µs, and the frame exposure time was 74.77 µs. This gave an ideal opportunity to examine the flame behaviour at low luminescence (Figure 102). The appearance of the flames in frames A1-A3 of Figure 100 is due to the low luminance flame moving whilst the Phantom's complementary metal–oxide-semiconductor (CMOS) sensor is exposed. As the flame travels across the sensor's field of view, the light is recorded on the pixels; the flame front will effectively paint across the sensor, resulting in a smeared image [197 & 198]. Once the flame slows and the burning intensity increases, producing higher light levels, this effect is less significant, and the flame image is sharper.

The flame travels the first 50 mm in 300 µs, giving a point-to-point average flame speed of 166.67 m/s. However, in the first frame, the flame around the door catch travels 32 mm (A1 of Figure 103), suggesting a flame speed of 320 m/s. This speed could be higher as there is no way of determining at which point in the exposure window or interval between frames the flame emerged from the box and travelled that distance.

The flame then slows significantly to give the stated average over the 50 mm and continues to slow before recovering again to give an average speed of 100 m/s between 100 mm and 350 mm distance intervals. It begins to reduce in speed sharply over the next 100 mm before gradually slowing so that by the time the flame has travelled 1050 mm, the flame speed is comparable to Tests 42 and 43 (Figure 103).

At the point the pressure is highest in the box, and before the emergence of the flame, the door is open only by a small slot, typically up to 1 mm along the entire 600 mm height of the door. For an instance, the jet of vented gas will behave like a slot jet. However, the driving pressure constantly changes, and the vent area is increasing. Therefore, the dynamics of a slot jet do not apply to most of the venting event [199]. The initial high-speed venting through the nominally 600 mm x 1 mm slot will be subjected to a high degree of shear, and the turbulence will subside quickly on a length scale related to the slot width [154]. As the door opens and there is less restriction, the vented gas stream is wider and decays on a longer scale, and the driving pressure is continuously declining. Measured flame speeds are dominated by the convection of burning gases as they are forced out of the box. The enhanced propagation of the flame (that leads to increases in the intensity of external explosion) is consequently more significant in the transverse direction, i.e. broadening of the flame jet. [200].

Overall, the effects of the turbulence induced by venting through the door and flame exit are highly localised, and the initial flame speeds are not sustained within the combustion of the cube volume. The limited volume of the box and the vent size and shape do not allow the formation of a jet sufficient to induce shock and downstream vortices that can trigger high-order explosions in propane [151, 153, 185 & 201].

Analysing the initial average flame speed versus the maximum peak overpressure inside the box shows an approximately linear relationship (Figure 104). There is more difficulty measuring the higher flame speeds due to resolution, and the method is not perfect, meaning that the results are mostly indicative. However, the results show that it is possible to predict the average flame speeds over the first 50 mm based on the internal pressure measurements. Note that the observed average flame speeds are much less than the maximum velocity associated with the burned gas flow, as predicted by the energy equation (Bernoulli's equation). This is partly because the pressures have declined when the flame is ejected from the box and partly because the distance over which the velocities are measured (50mm) is quite long compared with the decay of velocity associated with entrainment along the jet.

The larger-scale flame spread is directional; the flame takes 262 ms to travel the 1.75 m from the front of the box to the front of the tent compared to the 42 ms to travel 1450 mm axially from the door opening to the side of the tent. The creation of a large vent in the direction of travel for the flame from the door will impact the directionality difference. However, the opposite side of the tent also vented during the explosion (Figure 105).
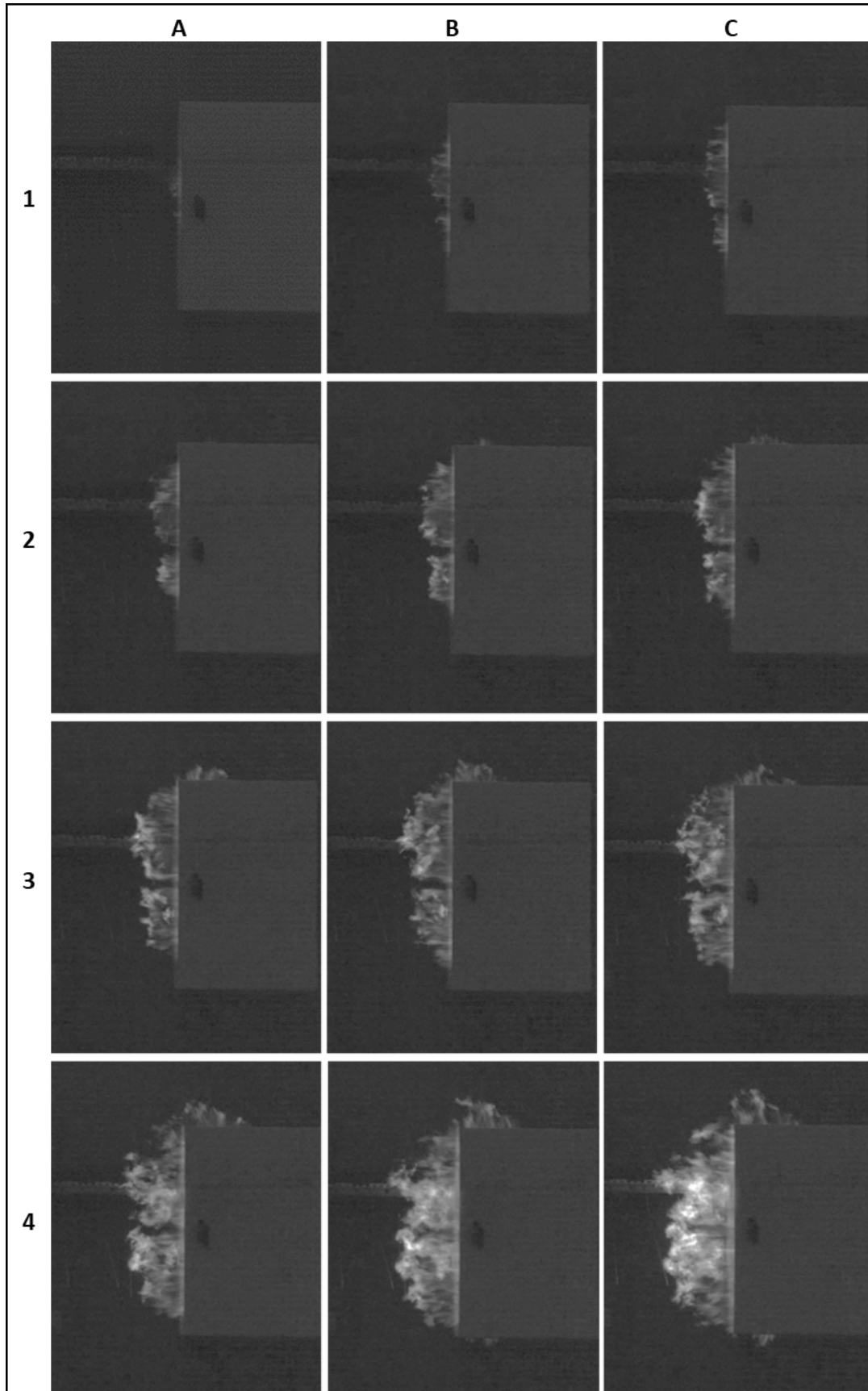
Figure 102 - Test 44 exiting flame and establishment of ignition of cube atmosphere, frame interval 200 μs
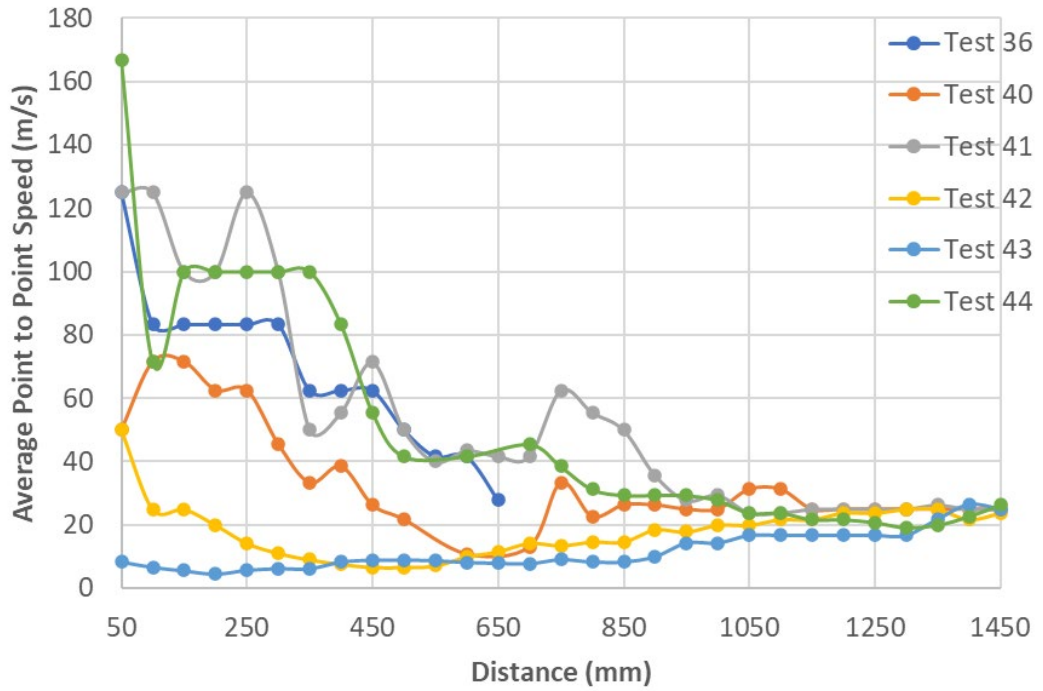
Figure 103 - Point-to-point average flame speeds for Tests 36 and 40-44.
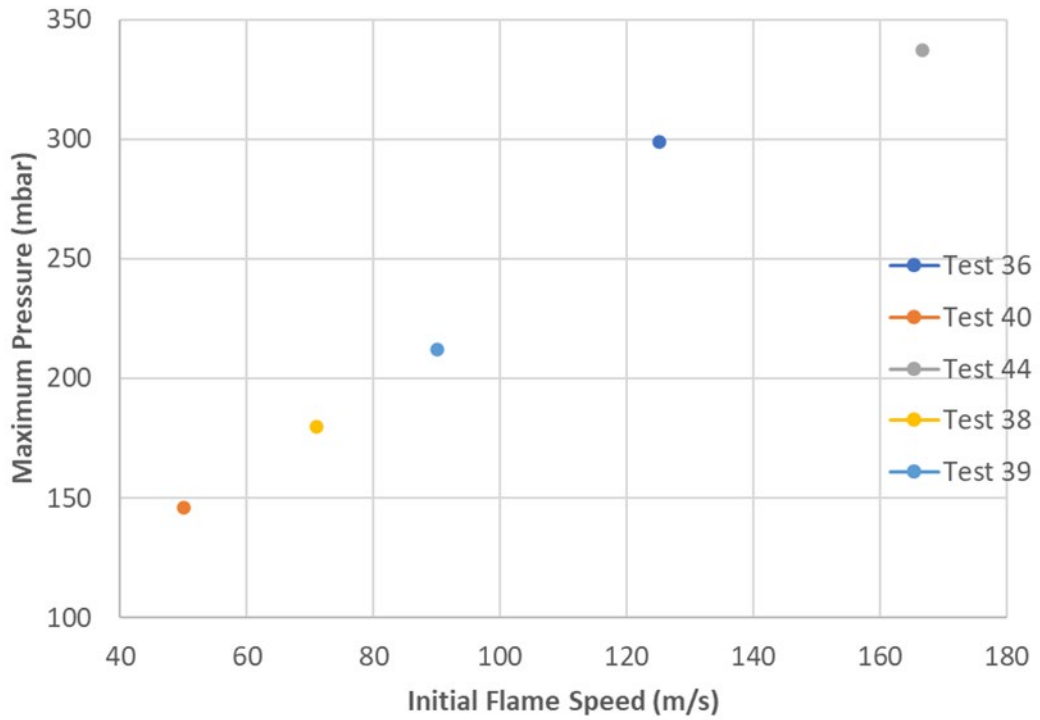
Figure 104 – Maximum *P₁* overpressure versus the average flame speed over the first 50 mm of travel for Tests 36, 38-40 and 44

Figure 105 - Test 44 - Flame venting from tent, note test was carried out in low light, resulting in an overexposed image of the flame

6.5 Effects of External Congestion on Explosion Propagating from Box

Turbulence-inducing elements, combined with fast flame speeds, can significantly increase overpressures. This study has demonstrated that the high flame speeds are highly localised to the area affected by the highest speed parts of the jet. Even with Test 44, which produced the highest flame speeds, the flame jet slowed significantly within 350 mm from the box opening. Much research could be conducted to understand what levels and spacing of congestion close to the box could increase the explosion severity. However, Tests 40 and 41 were performed to investigate if a row of obstacles replicating a pipe rack of five 50 mm diameter pipes with a blockage ratio had any impact on explosion severity when positioned 500 mm from the box opening facing the venting stream.

The data acquisition system failed for Test 41. However, video analysis shows some slight preferential opening to the bottom, in line with Test 36, which had a similar initial flame speed for the first 50 mm travelled. The P_1 overpressures in Tests 36 and 41 were likely similar.

Test 40 had significantly lower overpressures than previous experiments with the box with the door on (Figure 106). The video analysis shows that the door opened at the top of the door was significantly distorted, to the point that the effect was visible from the front, and flames also exited from the top and hinge side (Figure 108); this would have led to a significant increase in vent area compared to Test 44. Furthermore, the flame propagating out of the box at the top and sides resulted in a large flame surface area, causing intense burning above and in front of the box at a much earlier stage than in other experiments. This affected the pressure trace; the P_2 peak is merged with the peaks associated with the door opening. However, the P_1 peak pressure and the initial flame speed are still proportional and fit within the trend line for the other results (Figure 104).

The flame speed measurements for both Test 40 and 41 (Figure 108) show that the flame speed increased before the flame reached the congestion but slowed as the flame passed through the pipes and then increased again once past the congestion before slowing and then being dominated by the outflow from the cube 1150 mm from the vent. The slowing of the flame in the axial direction as it approaches the obstacle array is expected because of the blockage presented by the array. Overall enhancement of the explosion intensity is limited because the congestion array is in an open field with no confinement, so there is an unobstructed path for gas flow around the congestion elements, with only a proportion of the flow passing through the grid. However, the congestion will increase flame speed through several different mechanisms [78]. When the vented gas and the flow ahead of the flame hits the pipes, a proportion will be deflected [202]. This causes turbulence in the region before the congestion. The effect is visible in the video as the flame doesn't just travel axially from the vent; as it reaches the congestion, it also accelerates towards the front of the cube. As some of the gas flow goes around the obstruction and through the obstruction and the flame is distorted, turbulent vortices will be caused beyond the congestion. The faster the venting and flame speed, the further the vortices will occur beyond the blockage. This can be seen by the fact that the flame acceleration peaks at 750 mm for Test 40 and 850 mm for Test 41 with higher initial flame speeds.

Some slight increase in external combustion intensity does seem to be associated with the introduction of obstacles. For example, the P2 peak for Test 40 was the same as Test 39, which had a 31% higher P1 peak pressure. This increase is significant proportionally; however, the actual overpressure is still low at 37 mbar, as the volume is unconfined.
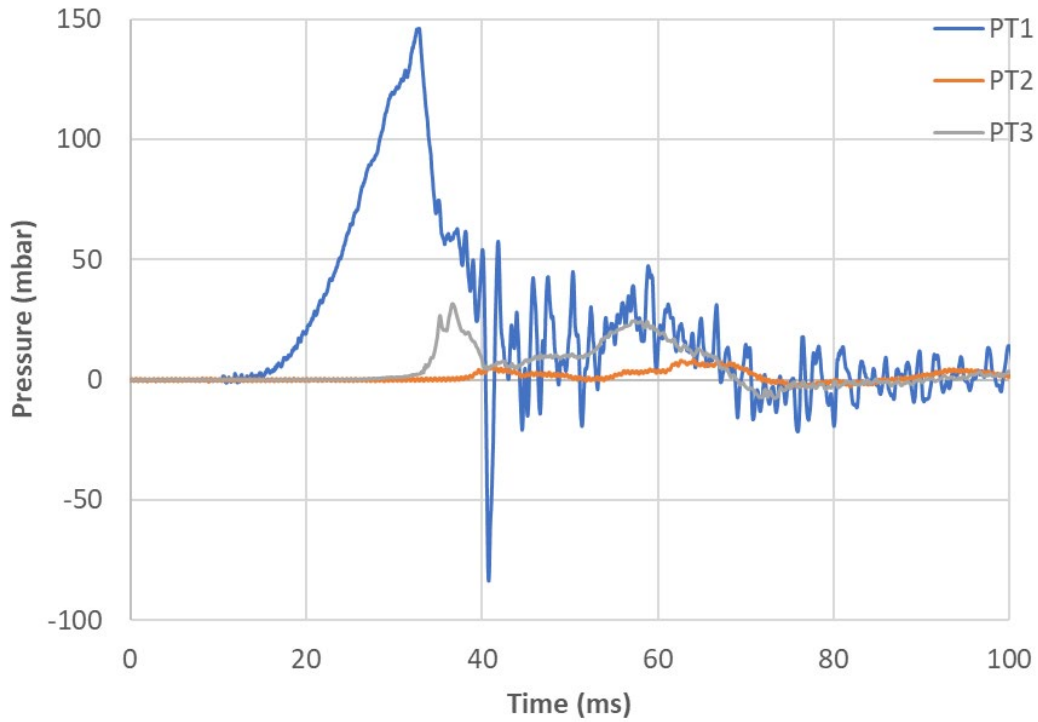
Figure 106 - Pressure trace for Test 40
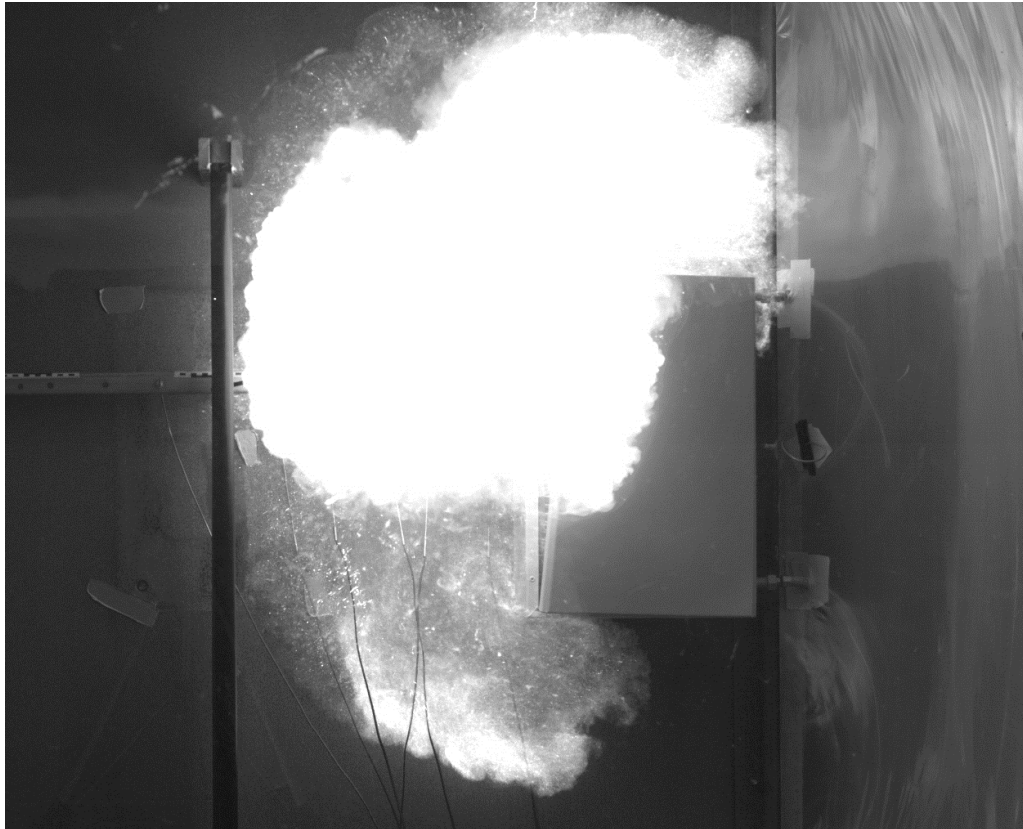
Figure 107 - Test 40 twisting of door and flame exiting from top and hinge side as well as opening
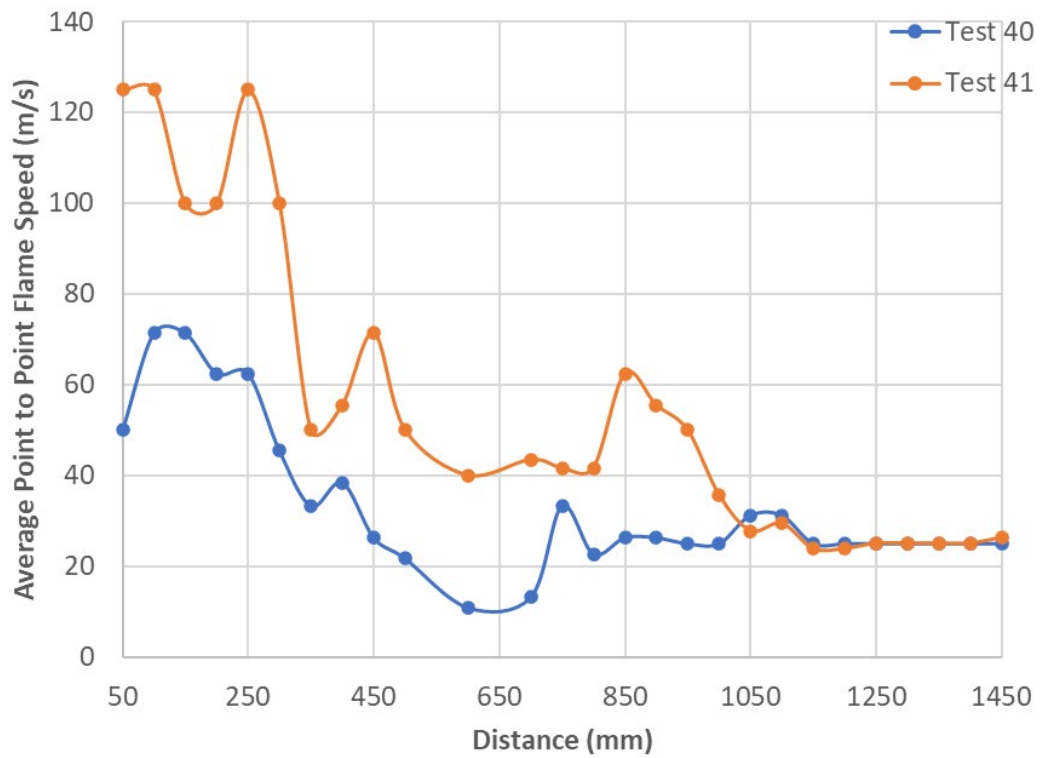
Figure 108 - Average point to point flame speeds for Tests 40 and 41

6.6 Conclusions

Using the control box with the door as a propagating ignition source for the volume in the tent significantly impacts the overpressures generated by the combustion of the tent volume. The P_2 maximum pressure recorded for Test 43, ignition in the tent volume only, was 7 mbar; however, for Test 44, with the box as a propagating ignition source, the peak pressure was 49 mbar. The way the locking mechanism failed had a significant effect on the P_1 maximum pressure as a result of differing vent areas. The larger the vent area, caused by the door twisting, the lower the peak pressure was. The results indicate that a lower P_1 pressure results in a lower P_2 pressure.

Flame speed measurement in the open field was difficult with thermocouples if the flame was not spherical and the front was wrinkled; this method was not pursued further. Using high-speed videography allowed flame speed measurements via observation if the flame and a scale were visible. However, the resolution was limited by the frame rate, and the camera view angle can impact how the flame is observed relative to the scale. In conclusion, the results are indicative and not definitive. However, the flame speed measurements in these experiments in the first 50 mm of travel show a linear relation between flame speed and maximum pressure. As expected, the higher the pressure, the higher the initial flame speed.

The flame travel in the first video frame of the door experiments indicated very high flame speed for tens of millimetres. This demonstrates that a gas slot-jet was vented at high speeds in the door's early opening stages. However, as the slot-jet size was long and narrow, the volume of highly turbulent gas ahead of it was limited because entrainment would cause the centreline velocity to decay very quickly. The flame speeds were reduced significantly within 350 mm of travel from the door opening. The flame speeds in all experiments dropped or rose to around 24-26 m/s once the tent was breached, as they became governed by the outflow of gas from the breached tent wall.

Placing a congestion array at 500 mm seemed to have a limited impact on the overall overpressures; the congestion did not lead to sustained high flame speeds. This indicates for gases with similar or less reactive properties to propane that, 500 mm is a sensible minimum distance from electrical control boxes to be kept free of congestion elements to minimise the escalation of a potential explosion event when it emerges from an electrical control box. However, if much larger boxes than the 600 mm x 400 mm x 250 mm ones used in these experiments or higher reactive gases are involved, this will need further investigation. Likewise, if the boxes are situated in confined spaces, this needs to be considered.

Chapter 7
Conclusions

7.1 Overall Conclusions

The outcomes of the steel cladding panel experiments demonstrated a probable failure mechanism whereby the lightweight steel cladding panels tended to hinge open during the early explosion stages. The panels were dislodged from their fixings, leaving the fixings often intact in the purlins. Where the panels overlapped, the escalating force was sufficient to pull the top panel over the fixing; yet, as this occurred, the displaced panel facilitated pressure relief while the lower sheet remained attached to its fixing, serving as a hinge point. The panel, hinging on the row of fixings, moved as the pressure drove an outflow of unburnt gas, acting as a moving congestion element. This movement induced turbulence into the outflow, significantly amplifying the external explosion's severity. The panels were only dislodged as the pressure peaked shortly before the flame exited the vessel.

In these experiments, the external atmosphere was air. With two panels hinging open, the resulting outflowing jets would partially dilute the stoichiometric mixture and weaken the external explosion. In a scenario where a building submerged in a vapour cloud possesses numerous panels, opening even a portion of these panels can induce significant turbulence without dilution. Such buildings, often encasing high-hazard processes, are favoured due to their low-pressure failure point, ostensibly posing minimal escalation hazard during explosions. However, the findings challenge the presumption that the strength of the building construction primarily governs the overpressures generated by an explosion in such a structure. This presumption is debunked as the panels interfere with gas outflow instead of being cleanly dislodged by rising pressure.

The present results suggest that the severity of the external explosion could be mitigated by introducing a weakness in the steel panel system. Even with a single panel among the three. fully and speedily opening, the external explosion severity remained comparable to scenarios where all three panels opened without vent aperture restriction, and internal pressures didn't

augment as they did when all panels were robustly fixed. This indicates that the exacerbated severity of the external explosion, observed when the panels hinged open, is attributed more to the obstacle effect rather than the reduced vent area.

For tests propagating from a commercial electrical box with a hinged door but without congestion, the development and relaxation of pressure could be predicted reasonably well from laminar flame speeds and the inertial properties of the door. When congestion was added, the flame speeds significantly increased in a way that could not be determined from the more fundamental properties of the mixture. The inertia of the door led to substantially increased pressures compared with those that would be observed with a foil that failed instantaneously across the whole area of the box.

The opening of the electrical control box door was not predictable. The door opened preferentially at the top or bottom, indicating that the failure occurred at one of the top or bottom catches first, resulting in a twisting door as it opened. The extent of deformation depended on the time difference between the catches failing. However, it also failed by the pressure overcoming all the catches nearly instantaneously, resulting in the door opening without twisting. The way the locking mechanism failed significantly affected the P_1 maximum pressure due to differing vent areas; the larger the vent area caused by the door twisting, the lower the peak pressure.

Employing the control box as a propagating ignition source for the 8 m³ volume within the tent significantly influenced the overpressures produced by the combustion of the tent volume. The results suggest that a lower internal pressure in the box reduces pressure from the explosion within the tent volume. Therefore, the discussed effect the door locking mechanism failure had on the P_1 internal pressures translated to the pressures as a result of the explosion in the tent volume.

The initial flame travel in the door experiments showed high flame speed over a few tens of millimetres, illustrating that gas is expelled at high velocities with the door slightly open. However, given the slot's long and narrow dimensions, the generated turbulence ahead will be minimal, and

entrainment will prompt a swift decay. Flame speeds significantly diminished within 350 mm of travel from the door opening. In all experiments, flame speeds decreased or stabilised around 24-26 m/s upon tent breach, now governed by the gas outflow from the breached tent wall.

Introducing a congestion array at 500 mm moderately elevated the overall overpressures yet did not sustain high flame speeds. This suggests that for gases with similar or lower reactivity than propane, a 500 mm separation distance is prudent between electrical control boxes and potential congestion elements outside the boxes, given the potential for vapour cloud envelopment. However, further investigation is warranted if larger control boxes than the 600 mm x 400 mm x 250 mm utilised in these experiments or if higher reactive gases are involved. Similarly, this factor requires consideration if the boxes are placed in confined spaces.

The findings demonstrate that the failure mechanisms of both the steel-panel-clad building and the control boxes strongly influence the severity of an explosion emanating from within, with the severity of the internal explosion augmenting the effects of the external explosion. Constraints on the testing scale precluded full confirmation that these effects were significant during the early stages of the Buncefield explosion.

Overall, this investigation markedly enhances understanding of explosion propagation dynamics within industrially relevant and common settings, thus facilitating the advancement of more robust safety measures and structural designs to attenuate the severity of potential Vapour Cloud Explosions.

Much of this project's work has been published as an HSE Research Report by the UK Health and Safety Executive (HSE), freely accessible to duty holders on the HSE website. The findings have also been shared with His Majesty's Specialist Inspectors at the HSE and are being utilised to inform and assess industry safety cases for major hazard sites.

7.2 Recommendations for Future Research

Because of the pandemic, it was not possible to combine both sets of experiments and investigate the effects of an explosion propagating from the control box into a congested steel-cladded building submerged into a gas cloud. Therefore, understanding this nesting effect in future work would be advantageous. This would also have allowed for a study into the impact of environmental dust on the severity of the more significant explosions that would have resulted from this work; this could also form part of any future work.

The steel cladding vessel incorporated merely three panels in this work; the turbulent venting interaction between two hinged-open panels significantly intensified the explosion's severity. In practical scenarios, even small buildings will incorporate many more panels. Future research with explosion chambers constructed entirely out of lightweight steel panels could investigate how panel failure at a larger scale could affect explosion severity. Enveloping such a chamber in a larger, unconfined flammable cloud could further explore the nesting effect on explosion mechanism and severity.

The congestion positioned 500 mm from the electrical control box did not lead to a sustained increase in flame speed in the open field. Further research to understand the effects of congestion much closer to a control box and the effects of confinement, for instance, when the control box is in a small room or corridor, would be industrially beneficial. All experiments were conducted using propane as a fuel. Investigating the effects of these scenarios with more reactive fuels, such as hydrogen, will be crucial for the transition to Net Zero.

References

1.   Skjold, T., C. Souprayen, and S. Dorofeev, (2018), Fires and explosions. *Progress in Energy and Combustion Science*. **64**: p. 2-3.

2.   Allianz (2022), Global Claims Review. *https://www.agcs.allianz.com/news-and-insights/reports/claims-in-focus.html*.

3.   Parker, R.J., (1975), The Flixborough Disaster. Report of the Court of Inquiry. *Department of Employment. Her Majesty's Stationary Office, London*.

4.   CSB (2020), Fires and Explosions at TPC Group Port Neches Operations Facility.

5.   Steel Construction Institute, (2009), Buncefield Explosion Mechanism Phase 1 (Volumes 1 and 2). *HSE Research Report RR718*

6.   Atkinson, G., E. Cowpe, J. Halliday, and D. Painter, (2017), A review of very large vapour cloud explosions: Cloud formation and explosion severity. *Journal of Loss Prevention in the Process Industries*. **48**: p. 367-375.

7.   Major Incident Investigation Board, (2007), The Buncefield Incident – 11th December 2005 – The Final Report of the Major Incident Investigation Board, Vol 1.

8.   Atkinson, G., S. Coldrick, S. Gant, and L. Cusco, (2015), Flammable vapor cloud generation from overfilling tanks: Learning the lessons from Buncefield. *Journal of Loss Prevention in the Process Industries*. **35**: p. 329-338.

9.   Atkinson, G. and S. Gant, (2012), Buncefield investigation Liquid flow and vapour production. *HSE Research Report RR936*. **http://www.hse.gov.uk/research/rrhtm/rr908.htm**.

10.   Devenish, B.J., G.G. Rooney, H.N. Webster, and D.J. Thomson, (2010), The Entrainment Rate for Buoyant Plumes in a Crossflow. *Boundary-Layer Meteorology*. **134**(3): p. 411-439.

11.   Gant, S.E. and G.T. Atkinson, (2011), Dispersion of the vapour cloud in the Buncefield Incident. *Process Safety and Environmental Protection*. **89**(6): p. 391-403.

12. Atkinson, G., J. Hall, and A. McGillivray, (2017), Review of Vapor Cloud Explosion Incidents. *HSE Research Report RR1113*.

13. MoPNG Committee (2010), Independent Inquiry Committee Report on Indian Oil Terminal Fire at Jaipur on 29th October 2009; completed 29th January 2010.

14. CSB (2015), Caribbean Petroleum Tank Terminal Explosion and Multiple Tank Fires (October 23rd 2009)(Final Investigation Report).

15. Mishra, K.B., K.D. Wehrstedt, and H. Krebs, (2014), Amuay refinery disaster: The aftermaths and challenges ahead. *Fuel Processing Technology*. **119**: p. 198-203.

16. Carrara, M., (1921), LOCARD, E.-L'enquête criminelle et les méthódes scientifiques.

17. Inman, K. and N. Rudin, (2002), The origin of evidence. *Forensic Science International*. **126**(1): p. 11-16.

18. Mercx, W.P.M. and A.C. vandenBerg, (1997), The explosion blast prediction model in the revised CPR 14E (Yellow Book). *Process Safety Progress*. **16**(3): p. 152-159.

19. Bakke, J.R., K. van Wingerden, P. Hoorelbeke, and B. Brewerton, (2010), A study on the effect of trees on gas explosions. *Journal of Loss Prevention in the Process Industries*. **23**(6): p. 878-884.

20. Abdolhamidzadeh, B., T. Abbasi, D. Rashtchian, and S.A. Abbasi, (2011), Domino effect in process-industry accidents – An inventory of past events and identification of some patterns. *Journal of Loss Prevention in the Process Industries*. **24**(5): p. 575-593.

21. Salzano, E. and V. Cozzani, (2005), The analysis of domino accidents triggered by vapor cloud explosions. *Reliability Engineering & System Safety*. **90**(2-3): p. 271-284.

22. Pettitt, G.N., R.R. Schumacher, and L.A. Seeley, (1993), Evaluating the probability of major hazardous incidents as a result of escalation events. *Journal of Loss Prevention in the Process Industries*. **6**(1): p. 37-46.

23. (2002), The Dangerous Substances and Explosive Atmospheres Regulations, in 2776. *United Kingdom*.

24. Directive 99/92/EC on the minimum requirements for improving the safety and health protection of workers potentially at risk from explosive atmospheres (15th individual Directive within the meaning of Article 16(1) of Directive 89/391/EEC, in ATEX 137. *EU*.

25. Directive 2014/34/EU - equipment and protective systems intended for use in potentially explosive atmospheres (recast), in ATEX 114. *EU*.

26. Kumaresh, G.R., I. Fossan, M.M. Venkatraman, K.E. Giljarhus, O. Spangelo, and S. Jensen, (2016), CFD-Based Transient Ignition Probability Modeling of Gas Leaks in Enclosures. *International Journal of Computational Methods*. **13**(2): p. 16.

27. Mansfield, D., D. Aberdeen, S. Connolly, and M. Scanlon. (2006) Plant specific ignition probability model and correlations for use in onshore and offshore QRA. in *Institution of Chemical Engineers Symposium Series.* Institution of Chemical Engineers; 1999.

28. Rew, P., H. Spencer, and A. Franks. (1997) A framework for ignition probability of flammable gas clouds. in *Institution of Chemical Engineers Symposium Series.* Hemsphere Publishing Corporation.

29. Rew, P.J., H. Spencer, and J. Daycock, (2000), Off-site ignition probability of flammable gases. *Journal of Hazardous Materials*. **71**(1): p. 409-422.

30. UKOOA, *IP Research Report: Ignition probability review, model development and look-up correlations*. 1st ed. 2006, London: Energy Institute.

31. Zhu, C., J. Jiang, and X. Yuan, (2012), Study on ignition probability of flammable materials after leakage accidents. *Procedia Engineering*. **45**: p. 435-441.

32. Pula, R., F.I. Khan, B. Veitch, and P.R. Amyotte, (2006), A grid based approach for fire and explosion consequence analysis. *Process Safety and Environmental Protection*. **84**(B2): p. 79-91.

33. Bradley, D., G.A. Chamberlain, and D.D. Drysdale, (2012), Large vapour cloud explosions, with particular reference to that at Buncefield. *Philosophical Transactions of the Royal Society a-*

Mathematical Physical and Engineering Sciences. **370**(1960): p. 544-566.

34. Daubech, J., C. Proust, and G. Lecocq, (2017), Propagation of a confined explosion to an external cloud. *Journal of Loss Prevention in the Process Industries*. **49**: p. 805-813.

35. National Fire Protection Association, *NFPA 68: Standard on explosion protection by deflagration venting*. 2013: National Fire Protection Association.

36. Lou, H.H., D. Chen, C.B. Martin, X. Li, K. Li, H. Vaid, K.D. Singh, and P. Gangadharan, (2012), Optimal Reduction of the C1–C3 Combustion Mechanism for the Simulation of Flaring. *Industrial & Engineering Chemistry Research*. **51**(39): p. 12697-12705.

37. Metghalchi, M. and J.C. Keck, (1980), Laminar burning velocity of propane-air mixtures at high temperature and pressure. *Combustion and flame*. **38**: p. 143-154.

38. Shinde, V., A. Fulzele, and S. Kumar, (2024), Experimental measurements of laminar burning velocity of premixed propane-air flames at higher pressure and temperature conditions. *Fuel*. **356**: p. 129561.

39. Lind, C., (1975), What causes unconfined vapor cloud explosions. *Loss Prevention*. **9**: p. 101-105.

40. Aldredge, R.C. and B. Zuo, (2001), Flame acceleration associated with the Darrieus-Landau instability. *Combustion and Flame*. **127**(3): p. 2091-2101.

41. Clanet, C. and G. Searby, (1998), First experimental study of the Darrieus-Landau instability. *Physical review letters*. **80**(17): p. 3867.

42. Creta, F., N. Fogla, and M. Matalon, (2011), Turbulent propagation of premixed flames in the presence of Darrieus–Landau instability. *Combustion Theory and Modelling*. **15**(2): p. 267-298.

43. Matalon, M., (2018), The Darrieus–Landau instability of premixed flames. *Fluid Dynamics Research*. **50**(5): p. 051412.

44. Troiani, G., F. Creta, and M. Matalon, (2015), Experimental investigation of Darrieus–Landau instability effects on turbulent

premixed flames. *Proceedings of the Combustion Institute*. **35**(2): p. 1451-1459.

45. Yang, S., A. Saha, Z. Liu, and C.K. Law, (2018), Role of Darrieus–Landau instability in propagation of expanding turbulent flames. *Journal of Fluid Mechanics*. **850**: p. 784-802.

46. Bychkov, V.V. and M.A. Liberman, (2000), Dynamics and stability of premixed flames. *Physics Reports*. **325**(4): p. 115-237.

47. Bauwens, C.R.L., J.M. Bergthorson, and S.B. Dorofeev, (2019), Modeling the formation and growth of instabilities during spherical flame propagation. *Proceedings of the Combustion Institute*. **37**(3): p. 3669-3676.

48. Bradley, D., M. Lawes, and M.S. Mansour, (2011), The Problems of the Turbulent Burning Velocity. *Flow, Turbulence and Combustion*. **87**(2): p. 191-204.

49. Bradley, D., A. Lau, M. Lawes, and F. Smith, (1992), Flame stretch rate as a determinant of turbulent burning velocity. *Phil. Trans. R. Soc. Lond. A*. **338**(1650): p. 359-387.

50. Gardner, C., H. Phylaktou, and G. Andrews. (1998) Turbulent Reynolds number and turbulent-flame-quenching influences on explosion severity with implications for explosion scaling. in *Institution of Chemical Engineers Symposium Series No 144*.

51. Gubba, S.R., S.S. Ibrahim, W. Malalasekera, and A.R. Masri, (2011), Measurements and LES calculations of turbulent premixed flame propagation past repeated obstacles. *Combustion and Flame*. **158**(12): p. 2465-2481.

52. Li, D., Q. Zhang, Q.J. Ma, S.L. Shen, J.C. Chen, and S.Y. Ren, (2016), Influence of built-in obstacles on unconfined vapor cloud explosion. *Journal of Loss Prevention in the Process Industries*. **43**: p. 449-456.

53. Alharbi, A., A.R. Masri, and S.S. Ibrahim, (2014), Turbulent premixed flames of CNG, LPG, and H-2 propagating past repeated obstacles. *Experimental Thermal and Fluid Science*. **56**: p. 2-8.

54. Di Sarli, V., A. Di Benedetto, and G. Russo, (2009), Using Large Eddy Simulation for understanding vented gas explosions in the presence of obstacles. *Journal of Hazardous Materials*. **169**(1-3): p. 435-442.

55. Na'inna, A.M., H.N. Phylaktou, and G.E. Andrews, (2021), Prediction of distance to maximum intensity of turbulence generated by grid plate obstacles in explosion-induced flows. *Journal of Loss Prevention in the Process Industries*. **69**: p. 104318.

56. Li, G., Y. Du, J. Liang, S. Wang, B. Wang, and S. Qi, (2018), Characteristics of gasoline–air mixture explosions with different obstacle configurations. *Journal of the Energy Institute*. **91**(2): p. 194-202.

57. Ogawa, T., V.N. Gamezo, and E.S. Oran, (2013), Flame acceleration and transition to detonation in an array of square obstacles. *Journal of Loss Prevention in the Process Industries*. **26**(2): p. 355-362.

58. Yu, M., K. Zheng, and T. Chu, (2016), Gas explosion flame propagation over various hollow-square obstacles. *Journal of Natural Gas Science and Engineering*. **30**: p. 221-227.

59. Bychkov, V., V. Akkerman, D. Valiev, and C.K. Law, (2010), Influence of gas compression on flame acceleration in channels with obstacles. *Combustion and Flame*. **157**(10): p. 2008-2011.

60. Chan, C., I.O. Moen, and J.H.S. Lee, (1983), Influence of confinement on flame acceleration due to repeated obstacles. *Combustion and Flame*. **49**(1-3): p. 27-39.

61. Lohrer, C., C. Drame, B. Schalau, and R. Gratz, (2008), Propane/air deflagrations and CTA measurements of turbulence inducing elements in closed pipes. *Journal of Loss Prevention in the Process Industries*. **21**(1): p. 1-10.

62. Na'inna, A.M., H.N. Phylaktou, and G.E. Andrews, (2013), The acceleration of flames in tube explosions with two obstacles as a function of the obstacle separation distance. *Journal of Loss Prevention in the Process Industries*. **26**(6): p. 1597-1603.

63. Park, D.J., Y.S. Lee, and A.R. Green, (2008), Experiments on the effects of multiple obstacles in vented explosion chambers. *Journal of Hazardous Materials*. **153**(1-2): p. 340-350.

64.   Zhao, S., Y. Fan, H. Lv, and B. Jia, (2017), Effects of a jet turbulator upon flame acceleration in a detonation tube. *Applied Thermal Engineering*. **115**: p. 33-40.

65.   Atkinson, G. (2012), Effects of constraints on gas flow on the severity of vapour cloud explosions, in *Icheme Symposium Series No. 158*. Southport Convention Centre, Southport, UK.

66.   Atkinson, G., E. Cowpe, D. Painter, and J. Patel (2015), Explosion risks at small LNG sites, in *ICheme Symposium Series No 160*. Edinburgh UK.

67.   Oran, E.S., V.N. Gamezo, and R.K. Zipf, (2015), Large-Scale Experiments and Absolute Detonability of Methane/Air Mixtures. *Combustion Science and Technology*. **187**(1-2): p. 324-341.

68.   Liberman, M.A., M.F. Ivanov, and A.D. Kiverin, (2015), Radiation heat transfer in particle-laden gaseous flame: Flame acceleration and triggering detonation. *Acta Astronautica*. **115**: p. 82-93.

69.   Beyrau, F., M.A. Hadjipanayis, and R.P. Lindstedt, (2013), Ignition of fuel/air mixtures by radiatively heated particles. *Proceedings of the Combustion Institute*. **34**: p. 2065-2072.

70.   Finigan, D.J., B.D. Dohm, J.A. Mockelman, and M.A. Oehlschlaeger, (2012), Deflagration-to-detonation transition via the distributed photo ignition of carbon nanotubes suspended in fuel/oxidizer mixtures. *Combustion and Flame*. **159**(3): p. 1314-1320.

71.   Ivanov, M.F., A.D. Kiverin, and M.A. Liberman, (2015), Ignition of deflagration and detonation ahead of the flame due to radiative preheating of suspended micro particles. *Combustion and Flame*. **162**(10): p. 3612-3621.

72.   Liberman, M.A., M.F. Ivanov, and A.D. Kiverin, (2015), Effects of thermal radiation heat transfer on flame acceleration and transition to detonation in particle-cloud hydrogen flames. *Journal of Loss Prevention in the Process Industries*. **38**: p. 176-186.

73.   Zhu, C.J., B.Q. Lin, B.Y. Jiang, Q. Liu, and Y.D. Hong, (2012), Simulation of dust lifting process induced by gas explosion disaster in underground coal mine. *Disaster Advances*. **5**(4): p. 1407-1413.

74. Hong, S., Z. Liu, E. Zhao, S. Lin, L. Qiu, J. Qian, H. Liu, and S. Xia, (2017), Comparison of behavior and microscopic characteristics of first and secondary explosions of coal dust. *Journal of Loss Prevention in the Process Industries*. **49**: p. 382-394.

75. Zeeuwen, J., C. Van Wingerden, and R. Dauwe (1983), Experimental investigation into the blast effect produced by unconfined vapour cloud explosions, in Proceedings of 4th International Symposium on Loss Prevention and Safety Promotion in the Process Industries. *Harrogate, UK*.

76. Hirst, W. and J. Eyre, (1980), Maplin Sands experiments 1980: Combustion of large LNG and refrigerated liquid propane spills on the sea, in Heavy Gas and Risk Assessment—II. 1983, Springer. p. 211-224.

77. Neff, D., R. Meroney, and S.J. Wiergma (1981), The behavior of LNG vapor cloud, in Report, Contr. p. 0203.

78. Harrison, A.J. and J.A. Eyre, (1987), The Effect of Obstacle Arrays on the Combustion of Large Premixed Gas/Air Clouds. *Combustion Science and Technology*. **52**(1-3): p. 121-137.

79. Van den Berg, A., (1985), The multi-energy method: a framework for vapour cloud explosion blast prediction. *Journal of Hazardous Materials*. **12**(1): p. 1-10.

80. Baker, Q.A., M.J. Tang, E.A. Scheler, and G.J. Silva, (1996), Vapor cloud explosion analysis. *Process Safety Progress*. **15**(2): p. 106-109.

81. Atkinson, G., (2017), Development of heavy vapour clouds in very low wind speeds. *Journal of Loss Prevention in the Process Industries*. **48**: p. 162-172.

82. Atkinson, G. and S. Coldrick, (2012), Vapour cloud formation Experiments and modelling. *HSE Research Report RR908*.

83. Briggs, G.A., R.S. Thompson, and W.H. Snyder, (1990), Dense gas removal from a valley by crosswinds. *Journal of Hazardous Materials*. **24**(1): p. 1-38.

84. Atkinson, G., (2006), Buncefield Investigation: Forensic examination of an emergency pumphouse. *HSL Report FS/06/11.*

85. Chen, A., (2013), Structural response to vapour cloud explosions.

86. Gill, J., G. Atkinson, E. Cowpe, and D. Painter, (2016), Vapour cloud explosions in steel clad structures. *Symposium Series No 161,* Hazards 26 Conference, Edinburg, UK.

87. Chamberlain, G., E. Oran, and A. Pekalski, (2019), Detonations in industrial vapour cloud explosions. *Journal of Loss Prevention in the Process Industries*. **62**: p. 103918.

88. Johnson, D.M. and V.H.Y. Tam, (2017), Why DDT is the only way to explain some vapor cloud explosions. *Process Safety Progress*. **36**(3): p. 292-300.

89. Johnson, D.M., G.B. Tomlin, and D.G. Walker, (2015), Detonations and vapor cloud explosions: Why it matters. *Journal of Loss Prevention in the Process Industries*. **36**: p. 360-366.

90. Oran, E.S., G. Chamberlain, and A. Pekalski, (2020), Mechanisms and occurrence of detonations in vapor cloud explosions. *Progress in Energy and Combustion Science*. **77**: p. 100804.

91. Atkinson, G. and L. Cusco, (2011), Buncefield: A violent, episodic vapour cloud explosion. *Process Safety and Environmental Protection*. **89**(6): p. 360-370.

92. Atkinson, G., L. Cusco, D. Painter, and V. Tam (2009), Overpressure and directional indicators in large vapour cloud explosions, in IChemE Symposium Series No. 155.

93. Pekalski, A., J. Puttock, and S. Chynoweth, (2015), Deflagration to detonation transition in a vapour cloud explosion in open but congested space: Large scale test. *Journal of Loss Prevention in the Process Industries*. **36**: p. 365-370.

94. Davis, S., E. Merilo, D. Engel, A. Ziemba, M. Pinto, and K. van Wingerden, (2017), Large scale detonation testing: New findings in the prediction of DDTs at large scales. *Journal of Loss Prevention in the Process Industries*. **48**: p. 345-357.

95. Atkinson, G., E. Cowpe, and D. Painter. (2016) Application of detonation diagnostics to the Flixborough Explosion. in *Symposium Series No 161, Hazards 26 Conference, Poster 12.* IChemE Edinburgh.

96. Glasstone, S. and P. Dolan, (1977), The effects of nuclear weapons, 3rd. *Edition. The United States Department of Energy, Washington, DC*.

97. Baker, W.E., P. Cox, J. Kulesz, R. Strehlow, and P. Westine, *Explosion hazards and evaluation*. Vol. 5. 2012: Elsevier.

98. Vandenberg, A.C. and A. Lannoy, (1993), methods for vapor cloud explosion blast modeling. *Journal of Hazardous Materials*. **34**(2): p. 151-171.

99. Fluid Gravity (2009), Further pancake cloud detonation results, in *Fluid gravity Client Report CR106/09*.

100. Gugan, K., (1979), Unconfined vapour cloud explosions. *Inst. Chem. Eng.*

101. Sadee, C., D. Samuels, and T. O'Brien, (1977), The characteristics of the explosion of cyclohexane at the Nypro (UK) Flixborough plant on 1st June 1974. *Journal of occupational accidents*. **1**(3): p. 203-235.

102. Johnson, D.M., (2010), The potential for vapour cloud explosions - Lessons from the Buncefield accident. *Journal of Loss Prevention in the Process Industries*. **23**(6): p. 921-927.

103. Tam, V.H., (2011), The Buncefield accident—why was the explosion so severe? *Loss Prevention Bulletin*,(222).

104. Johnson, D., A. Pekalski, V. Tam, and B. Burgan. (2018) The importance of deflagration to detonation transition in explaining major vapour cloud explosion incidents. in *12th International Symposium on Hazards, Prevention, and Mitigation of Industrial Explosions, Kansas City, MO*.

105. Davis, S., Pagliaro, J., Botwinick, D., DeBold, T., van Wingerden, K., Allason, D. and Johnson, D.M. (2019), Do not believe the hype: Using case studies and experimental evidence to show why the HSE is wrong about excluding deflagration-to-detonation transitions. *Process Safety Progress*, **38:** p. 1-12.

106. Baker, Q.A.T., J. K. Malik, D. R. Edel, M. T (2019), Caribbean Petroleum VCE case hstory, in Hazards 29. *Birmingham UK*.

107. Brunoro Ahumada, C., F.-I. Papadakis-Wood, P. Krishnan, S. Yuan, N. Quddus, M.S. Mannan, and Q. Wang, (2020), Comparison of

explosion models for detonation onset estimation in large-scale unconfined vapor clouds. *Journal of Loss Prevention in the Process Industries*. **66**: p. 104165.

108. Taveau, J., (2012), The Buncefield explosion: Were the resulting overpressures really unforeseeable? *Process Safety Progress*. **31**(1): p. 55-71.

109. Horn, B.J., Martin L. Goodrich, and J. Kelly Thomas (2015), Deflagration Load Generator Repeatability and Application to Test Article Blast Loading, in American Institute of Chemical Engineers 11th Global Congress on Process Safety. *Austin, Texas*.

110. Harris, R. and M. Wickens, (1989), Understanding vapour cloud explosions-an experimental study. *Publ./Institution of gas eng.*

111. Davis, S., D. Engel, K.v. Wingerden, and E. Merilo, (2017), Can gases behave like explosives: Large-scale deflagration to detonation testing. *Journal of Fire Sciences*. **35**(5): p. 434-454.

112. Davis, S., M. Groethe, D. Engel, and K. van Wingerden. (2016) Large Scale Testing-Development of Advanced CFD Tools for the Enhanced Prediction of Explosion Pressure Development and Deflagration Risk on Drilling and Production Facilities. in *Offshore Technology Conference.* Offshore Technology Conference.

113. Liberman, M., N. Kleeorin, I. Rogachevskii, and N.E.L. Haugen, (2017), Mechanism of unconfined dust explosions: Turbulent clustering and radiation-induced ignition. *Physical Review E*. **95**(5): p. 5.

114. Liberman, M.A., M. Kuznetsov, A. Ivanov, and I. Matsukov, (2009), Formation of the preheated zone ahead of a propagating flame and the mechanism underlying the deflagration-to-detonation transition. *Physics Letters A*. **373**(5): p. 501-510.

115. Li, T. and R.P. Lindstedt, (2017), Thermal radiation induced ignition of multipoint turbulent explosions. *Process Safety and Environmental Protection*. **107**: p. 108-121.

116. Hadjipanayis, M.A., F. Beyrau, R.P. Lindstedt, G. Atkinson, and L. Cusco, (2015), Thermal radiation from vapour cloud explosions. *Process Safety and Environmental Protection*. **94**: p. 517-527.

117. Moore, S.R. and F.J. Weinberg, (1983), A study of the role of radiative ignition in the propagation of large explosions. *Proc. R. Soc. Lond. A*. **385**(1789): p. 373-387.

118. Moore, S.R. and F.J. Weinberg, (1987), Further studies of the role of radiative ignition in the propagation of large explosions. *Proc. R. Soc. Lond. A*. **409**(1836): p. 1-20.

119. Mitu, M., V.Brinzea, A.M. Musuc, D. Razus, and D. Oancea, (2011), Deflagration parameters of propane–air mixtures in a closed cylindrical vessel. *UPB Scientific Bulletin, Series B: Chemistry and Materials Science*. **73**: p. 17-26.

120. Fan, Y. and D.A. Crowl, (2000), Predicting the maximum gas deflagration pressure over the entire flammable range. *Journal of Loss Prevention in the Process Industries*. **13**(3): p. 361-368.

121. Crowl, D.A., (1992), Calculating the energy of explosion using thermodynamic availability. *Journal of Loss Prevention in the Process Industries*. **5**(2): p. 109-118.

122. Maxworthy, T., (1972), The structure and stability of vortex rings. *Journal of Fluid Mechanics*. **51**(1): p. 15-32.

123. Li, J. and H. Hao, (2017), Internal and external pressure prediction of vented gas explosion in large rooms by using analytical and CFD methods. *Journal of Loss Prevention in the Process Industries*. **49**: p. 367-381.

124. Pedersen, H.H., G. Tomlin, P. Middha, H.N. Phylaktou, and G.E. Andrews, (2013), Modelling large-scale vented gas explosions in a twin-compartment enclosure. *Journal of Loss Prevention in the Process Industries*. **26**(6): p. 1604-1615.

125. Fakandu, B., G. Andrews, and H. Phylaktou, (2014), Gas Explosion Venting: Comparison of Square and Circular Vents. *Chemical Engineering Transactions*. **36**: p. 163-168.

126. Fakandu, B., G. Andrews, and R. Phylaktou, *Gas explosion venting: comparison of experiments with design standards and laminar flame venting theory*. 2016.

127. Fakandu, B., C. Mbam, G. Andrews, and H. Phylaktou, (2016), Gas Explosion Venting: External Explosion Turbulent Flame Speeds that

Control the Overpressure. *Chemical Engineering Transactions*. **53**: p. 1-6.

128. Fakandu, B.M., G.E. Andrews, and H.N. Phylaktou, (2015), Vent burst pressure effects on vented gas explosion reduced pressure. *Journal of Loss Prevention in the Process Industries*. **36**: p. 429-438.

129. Qi, S., Y. Du, S.M. Wang, Y. Zhou, and G.Q. Li, (2016), The effect of vent size and concentration in vented gasoline-air explosions. *Journal of Loss Prevention in the Process Industries*. **44**: p. 88-94.

130. Tomlin, G., D.M. Johnson, P. Cronin, H.N. Phylaktou, and G.E. Andrews, (2015), The effect of vent size and congestion in large-scale vented natural gas/air explosions. *Journal of Loss Prevention in the Process Industries*. **35**: p. 169-181.

131. Bimson, S., D. Bull, T. Cresswell, P. Marks, A. Masters, A. Prothero, J. Puttock, J. Rowon, and B. Samuels. (1993) An experimental study of the physics of gaseous deflagration in a very large vented enclosure. in *Proceedings of the 14 th International Colloquium on the Dynamics of Explosions and Reactive Systems, Coimbra, Portugal, August.*

132. Bauwens, C.R., J. Chaffee, and S. Dorofeev, (2010), Effect of Ignition Location, Vent Size, and Obstacles on Vented Explosion Overpressures in Propane-Air Mixtures. *Combustion Science and Technology*. **182**(11-12): p. 1915-1932.

133. Alexiou, A., G.E. Andrews, and H. Phylaktou, (1997), A comparison between end-vented and side-vented gas explosions in large L/D vessels. *Process Safety and Environmental Protection*. **75**(B1): p. 9-13.

134. Alexiou, A., G.E. Andrews, and H. Phylaktou, (1996), Side-vented gas explosions in a long vessel: The effect of vent position. *Journal of Loss Prevention in the Process Industries*. **9**(5): p. 351-356.

135. Alexiou, A., H. Phylaktou, and G.E. Andrews, (1996), The Effect of Vent Size on Pressure Generation in Explosions in Large L/D Vessels. *Combustion Science and Technology*. **113**(1): p. 645-652.

136. Association, N.F.P. (2007), Guide for venting of deflagrations.

137. Ferrara, G., S.K. Willacy, H.N. Phylaktou, G.E. Andrews, A. Di Benedetto, E. Salzano, and G. Russo, (2008), Venting of gas explosion through relief ducts: Interaction between internal and external explosions. *Journal of Hazardous Materials*. **155**(1-2): p. 358-368.

138. Forcier, T. and R. Zalosh, (2000), External pressures generated by vented gas and dust explosions. *Journal of Loss Prevention in the Process Industries*. **13**(3-5): p. 411-417.

139. Harrison, A.J. and J.A. Eyre, (1987), External Explosions" as a Result of Explosion Venting. *Combustion Science and Technology*. **52**(1-3): p. 91-106.

140. Hooker, P., J.R. Hoyes, J. Hall, and D. Willoughby, (2017), Experimental studies on vented deflagrations in a low strength enclosure. *International Journal of Hydrogen Energy*. **42**(11): p. 7565-7576.

141. Proust, C. and E. Leprette, (2010), The Dynamics of Vented Gas Explosions. *Process Safety Progress*. **29**(3): p. 231-235.

142. Zhang, C., H. Dong, S. Shang, K. Zhang, Y. Zhou, and W. Gao, (2023), Experimental investigation of the vented propane-air explosion characteristics at elevated static activation pressures in a large L/D duct. *Process Safety and Environmental Protection*. **176**: p. 945-955.

143. Zhang, Q., Y.X. Wang, and Z. Lian, (2017), Explosion hazards of LPG-air mixtures in vented enclosure with obstacles. *Journal of Hazardous Materials*. **334**: p. 59-67.

144. Cooper, M.G., M. Fairweather, and J.P. Tite, (1986), On the mechanisms of pressure generation in vented explosions. *Combustion and Flame*. **65**(1): p. 1-14.

145. Steel Construction Institute, (1992), Explosions in highly congested volumes. HSE: *London*.

146. Ugarte, O.J., V. Akkerman, and A.S. Rangwala, (2016), A computational platform for gas explosion venting. *Process Safety and Environmental Protection*. **99**: p. 167-174.

147. BS EN 14994, (2007), Gas explosion venting protective systems.

148. Fakandu, B.M., G.E. Andrews, and H.N. Phylaktou, (2015), Vent burst pressure effects on vented gas explosion reduced pressure. *Journal of Loss Prevention in the Process Industries*. **36**: p. 431-440.

149. Middha, P., R. Samaraweera, C. Coffey, and D. Price, (2016), The influence of explosion relief vent layouts on explosion overpressures in large biomass storage vessels,. *Chemical Engineering Transactions,*. **48**: p. 205-210.

150. Puttock, J. (1995) Fuel gas explosion guidelines—the congestion assessment method. in *Second European Conference on major Hazards Onshore and Offshore, IchemE.*

151. Carnasciali, F., J.H.S. Lee, R. Knystautas, and F. Fineschi, (1991), Turbulent jet initiation of detonation. *Combustion and Flame*. **84**(1–2): p. 170-180.

152. Chambers, J. and K. Ahmed, (2017), Turbulent flame augmentation using a fluidic jet for Deflagration-to-Detonation. *Fuel*. **199**: p. 616-626.

153. Mackay, D.J., S.B. Murray, I.O. Moen, and P.A. Thibault, (1989), Flame-jet ignition of large fuel-air clouds. *Symposium (International) on Combustion*. **22**(1): p. 1339-1353.

154. Angelino, M., I. Di Venuta, A. Boghi, I. Petracci, and F. Gori, (2023), Further results on the mean mass transfer and fluid flow in a turbulent round jet. *International Communications in Heat and Mass Transfer*. **141**: p. 106568.

155. Thomas, G.O. and A. Jones, (2000), Some observations of the jet initiation of detonation. *Combustion and Flame*. **120**(3): p. 392-398.

156. Moen, I.O., A. Sulmistras, B.H. Hjertager, and J.R. Bakke, (1988), Turbulent flame propagation and transition to detonation in large fuel-air clouds. *Symposium (International) on Combustion*. **21**(1): p. 1617-1627.

157. *Appendix 39 - Tank Farm Incidents A2 - Mannan, Sam*, in *Lees' Loss Prevention in the Process Industries (Fourth Edition)*. 2012, Butterworth-Heinemann: Oxford. p. 3098-3110.

158. Pan, C., X. Wang, G. Li, Y. Liu, and Y. Jiang, (2021), Influences of a square and circular vent on gasoline vapor explosions and its

propagation: Comparative experimental study. *Case Studies in Thermal Engineering*. **27**: p. 101225.

159. Zhang, C., H. Dong, Y. Zhou, S. Shang, and W. Gao, (2023), Flame behavior and pressure characteristics of vented propane-air explosions. *Journal of Loss Prevention in the Process Industries*. **85**: p. 105168.

160. Accord (2015), 32/1000 Box Profile CAD Drawing, in https://media.steelroofsheets.co.uk/uploads/files/2022/03/03/32_1000_Box_Profile.pdf.

161. Kistler (2013), Piezoresistive Absolute Pressure Sensors *https://www.kistler.com/files/document/000-003e.pdf?callee=frontend*.

162. Instruments, N. (2022), NI cDAQ-9188 Specifications. *https://www.ni.com/docs/en-US/bundle/cdaq-9188-specs/page/specs.html*.

163. Instruments, N. (2021), NI 9223 Specifications. *https://www.ni.com/docs/en-US/bundle/ni-9223-specs/page/specifications.html*.

164. Search, I.Q. *Centrifugal Blowers*. 2023 [cited 2023 01/08/2023]; Available from: https://www.iqsdirectory.com/articles/blower/centrifugal-blowers.html.

165. ADC (2007), MGA3000 Multi-Gas Analyser. *https://data2.manualslib.com/pdf6/134/13344/1334349-adc/mga3000_series.pdf?84ed27d056e32aafd6798e93cd6e108b*.

166. (2005), The Control of Noise at Work Regulations 2005.

167. Schneider (2017), Product Datasheet NSYS3DEX6425. *https://www.se.com/ww/en/product/NSYS3DEX6425/spacial-s3dex-atex-certified-h600xw400xd250-ip66-ik10-ral7035-/*.

168. *Explosion Venting*. null. Vol. null. 1988. null.

169. Phylaktou, H.N., G.E. Andrews, and P. Herath, (1990), Fast flame speeds and rates of pressure rise in the initial period of gas explosions in large L/D cylindrical enclosures. *Journal of Loss Prevention in the Process Industries*. **3**(4): p. 355-364.

170. Kodakoglu, F., H.F. Farahani, A.S. Rangwala, and V.y. Akkerman, (2020), Dynamics of explosion venting in a compartment with

methane-air mixtures. *Journal of Loss Prevention in the Process Industries*. **67**: p. 104230.

171. Jia, H., B. Cui, Y. Duan, and K. Zheng, (2022), Study on the Influence of Vent Shape and Blockage Ratio on the Premixed Gas Explosion in the Chamber with a Small Aspect Ratio. *ACS Omega*. **7**(26): p. 22787-22796.

172. Bradley, D. and A. Mitcheson, (1978), The venting of gaseous explosions in spherical vessels. I—Theory. *Combustion and Flame*. **32**: p. 221-236.

173. Carcassi, M., M. Schiavetti, and T. Pini, (2018), Non-homogeneous hydrogen deflagrations in small scale enclosure. Experimental results. *International Journal of Hydrogen Energy*. **43**(41): p. 19293-19304.

174. Schiavetti, M. and M. Carcassi, (2017), Analysis of acoustic pressure oscillation during vented deflagration and proposed model for the interaction with the flame front. *International Journal of Hydrogen Energy*. **42**(11): p. 7707-7715.

175. Schiavetti, M. and M. Carcassi, (2017), Maximum overpressure vs. H2 concentration non-monotonic behavior in vented deflagration. Experimental results. *International Journal of Hydrogen Energy*. **42**(11): p. 7494-7503.

176. Van Wingerden, C.J.M. and J.P. Zeeuwen, (1983), On the role of acoustically driven flame instabilities in vented gas explosions and their elimination. *Combustion and Flame*. **51**: p. 109-111.

177. McCann, D.P.J., G. Thomas, and D.H. Edwards, (1985), Gasdynamics of vented explosions Part I: Experimental studies. *Combustion and Flame*. **59**: p. 233-250.

178. Chow, S.K., R.P. Cleaver, M. Fairweather, and D.G. Walker, (2000), An experimental study of vented explosions in a 3 : 1 aspect ratio cylindrical vessel. *Process Safety and Environmental Protection*. **78**(B6): p. 425-433.

179. Guo, J., X.X. Sun, S.C. Rui, Y. Cao, K.L. Hu, and C.J. Wang, (2015), Effect of ignition position on vented hydrogen-air explosions. *International Journal of Hydrogen Energy*. **40**(45): p. 15780-15788.

180. Solberg, D., J. Pappas, and E. Skramstad. (1981) Observations of flame instabilities in large scale vented gas explosions. in *Symposium (International) on Combustion.* Elsevier.

181. Daubech, J., C. Proust, O. Gentilhomme, D. Jamois, and M. Ichard, (2013), Hydrogen-air Vented Explosions-New Experimental Data*.

182. Cao, Y., B. Li, and K. Gao, (2018), Pressure characteristics during vented explosion of ethylene-air mixtures in a square vessel*. Energy*. **151**: p. 26-32.

183. Xing, H., Y. Qiu, S. Sun, M. Wang, B. Li, and L. Xie, (2020), Visualization of explosion characteristics of methane-air mixtures with different ignition positions and vent areas in a large-scale venting chamber*. Fuel*. **279**: p. 118380.

184. Skjold, T., H. Hisken, S. Lakshmipathy, G. Atanga, L. Bernard, M. van Wingerden, K.L. Olsen, M.N. Holme, N.M. Turøy, M. Mykleby, and K. van Wingerden, (2019), Vented hydrogen deflagrations in containers: Effect of congestion for homogeneous and inhomogeneous mixtures*. International Journal of Hydrogen Energy*. **44**(17): p. 8819-8832.

185. Chang, X., B. Zhang, H.D. Ng, and C. Bai, (2020), The effects of pre-ignition turbulence by gas jets on the explosion behavior of methane-oxygen mixtures*. Fuel*. **277**: p. 118190.

186. Bai, C., X. Chang, and B. Zhang, (2020), Impacts of turbulence on explosion characteristics of methane-air mixtures with different fuel concentration*. Fuel*. **271**: p. 117610.

187. Sun, S., M. Wang, Y. Qiu, and K. Gao, (2019), Effect of a hinged rotating vent cover on a vented explosion*. Journal of Loss Prevention in the Process Industries*. **57**: p. 186-193.

188. BS EN 14797:2006 Explosion venting devices.

189. Ciccarelli, G., J.L. Boccio, T. Ginsberg, and H. Tagawa, (1996), The influence of initial temperature on flame acceleration and deflagration-to-detonation transition*. Symposium (International) on Combustion*. **26**(2): p. 2973-2979.

190. Di Sarli, V., A. Di Benedetto, G. Russo, S. Jarvis, E.J. Long, and G.K. Hargrave, (2009), Large Eddy Simulation and PIV Measurements of

Unsteady Premixed Flames Accelerated by Obstacles. *Flow Turbulence and Combustion*. **83**(2): p. 227-250.

191. Gamezo, V.N., T. Ogawa, and E.S. Oran, (2008), Flame acceleration and DDT in channels with obstacles: Effect of obstacle spacing. *Combustion and Flame*. **155**(1-2): p. 302-315.

192. Ibrahim, S.S. and A.R. Masri, (2001), The effects of obstructions on overpressure resulting from premixed flame deflagration. *Journal of Loss Prevention in the Process Industries*. **14**(3): p. 213-221.

193. Na'inna, A.M., H.N. Phylaktou, and G.E. Andrews, (2017), Explosion flame acceleration over obstacles: Effects of separation distance for a range of scales. *Process Safety and Environmental Protection*. **107**: p. 309-316.

194. Li, H., J. Guo, Z. Tang, J. Li, P. Huang, and S. Zhang, (2019), Effects of ignition, obstacle, and side vent locations on vented hydrogen–air explosions in an obstructed duct. *International Journal of Hydrogen Energy*. **44**(36): p. 20598-20605.

195. Gill, J., G. Atkinson, E. Cowpe, H. Phylaktou, and G. Andrews, (2020), Experimental investigation of potential confined ignition sources for vapour cloud explosions. *Process Safety and Environmental Protection*. **135**: p. 187-206.

196. Bradley, D., T.M. Cresswell, and J.S. Puttock, (2001), Flame acceleration due to flame-induced instabilities in large-scale explosions. *Combustion and Flame*. **124**(4): p. 551-559.

197. Lim, S.-J., D.-S. Leem, K.-B. Park, K.-S. Kim, S. Sul, K. Na, G.H. Lee, C.-J. Heo, K.-H. Lee, X. Bulliard, R.-I. Satoh, T. Yagi, T. Ro, D. Im, J. Jung, M. Lee, T.-Y. Lee, M.G. Han, Y.W. Jin, and S. Lee, (2015), Organic-on-silicon complementary metal–oxide–semiconductor colour image sensors. *Scientific Reports*. **5**(1): p. 7708.

198. Acar, H.M. and T. Kavuran. (2016) Photo art creativity in the education: Light drawing. in *SHS Web of Conferences.* EDP Sciences.

199. Gori, F. and E. Nino. (2003) Fluid Dynamics Measurements and Flow Visualizations of a Free Slot Jet of Air. in *ASME 2003 International Mechanical Engineering Congress and Exposition.*

200. Trueba-Monje, I. and J.A. Sutton, (2023), Flame structure and broadening in turbulent premixed jet flames. *Combustion and Flame*. **251**: p. 112676.

201. Jiang, X.H., B.C. Fan, and J.F. Ye, (2004), Turbulence, vortex and external explosion induced by venting. *Applied Mathematics and Mechanics-English Edition*. **25**(12): p. 1390-1397.

202. Gori, F. and I. Petracci. (2003) Fluid Dynamics Measurements and Numerical Simulations Around a Circular Cylinder Impinged by a Submerged Slot Jet of Air. in *ASME 2003 International Mechanical Engineering Congress and Exposition.*

Appendix A

Below, Table 9, is the experimental protocol for experiments with just the control box such as those in Chapter 5.

Table 9 - Experimental protocol for experiments with the control box

Step	Action
A	*Conduct visual inspection of plastic pipe work for damage*
B	*Establish communication with actuated valves and ensure all manual valves are closed, perform a visual valve action test of all valves*
C	*Ensure cylinder valves are closed and install regulators to air and propane lines*
D	*With multi meter check continuity of firing cables*
1	Finalise positioning of all instrumentation
2	Clear test area of all tools and non-essential equipment
3	Establish communication with control and data acquisition systems
4	Turn on gas analyser and pump
5	Check that area around the rig is clear
6	Enforce exclusion zone
7	Inform all staff on site (Dalehead) that test procedure is to begin and clear test site of all staff
8	Ensure firing box is set to safe and remove key and hand to whom will install the igniter
9	In short circuit install igniter into box through the back wall and tape the hole
10	Break short circuit and connect igniter to firing cable
11	Open manual valves to small propane and air MFCs (V9 and V4)
12	open air cylinder valve
13	Open the air regulator to correct setting

14	Open propane cylinder valve
15	Retire to control room
16	Install door lock-out, use key to open valve circuit and turn on power to valve circuits
17	Radio that filling will commence
18	Open box fill valve (V11)
19	Set the air flow rate on air MFC (I-2)
20	Open propane line valve (V2)
21	Set propane flow rate on propane MFC (I-4)
22	Once gas analyser is showing correct concentration wait for 2 minutes and then cut the flow of both MFCs to zero
23	Close propane line valve (V2)
24	Close the fill valve (V11)
25	Close the vent valve (V13)
26	Obtain final all clear from lookouts and warn test imminent
27	Start data acquisition
28	Install key to firing box and press fire
29	Check through window that all is safe
30	Open propane vent valve (V3) for 1 minute then close
31	Inform look out that test is complete but remain in place
32	Turn off power to valve circuits and remove lookout
33	Close air and propane cylinder valves and dial regulators to zero return to control room
34	Lock door lock and turn on power to valve circuits
35	Open box fill valve (V11)
36	Open air MFC until the flow shows as zero
37	Close box fill valve (V11)
38	Cycle propane line and vent valves (V2 and V3)
39	Power down valve control circuits and remove lockout

40	Call back all lookouts
E	*Bring in all sensitive control and instrumentation equipment*
F	*Remove regulators and store indoors*

Appendix B

Below, Table 10, is the experimental protocol for experiments with the box and tent rig for the experiments in Chapter 6, adapted for the different conditions as necessary.

Table 10 - Experimental Protocol for experiments with the control box inside the tent rig

Step	Action
A	*Conduct visual inspection of plastic pipe work for damage*
B	*Establish communication with actuated valves and ensure all manual valves are closed, perform a visual valve action test of all valves*
C	*Ensure cylinder valves are closed and install regulators to air and propane lines*
D	*With multi meter check continuity of firing cables*
1	Finalise positioning of all instrumentation
2	Clear test area of all tools and non-essential equipment
3	Establish communication with control and data acquisition systems
4	Turn on gas analyser and pump
5	Deploy lookouts, confirm communication is functioning and that area is clear
6	Enforce exclusion zone
7	Inform all staff on site that test procedure is to begin and clear test site of all staff
8	Ensure firing box is set to safe and remove key and hand to whom will install the igniter
9	In short circuit install both igniters into box through the back wall and tape the hole
10	Break short circuit and connect igniters to firing cables
11	Open manual valves to propane and air MFCs (V8, 9, 4, 5)
12	Set air PRV (V7) and open air valve

13	Open the air regulator to correct setting ensuring that the PRV is not set below this setting, if so, balance the two
14	Open propane cylinder valve
15	Retire to control room
16	Lock door, use key to open valve circuit and turn on power to valve circuits
17	Radio that filling will commence
18	Open box fill valve (V11)
19	Set the air flow rate on air MFC (I-2)
20	Open propane line valve (V2)
21	Set propane flow rate on propane MFC (I-4)
22	Once gas analyser is showing correct concentration wait for 2 minutes and then cut the flow of both MFCs to zero
23	Close propane line valve (V2)
24	Close the fill valve (V11)
25	Close the vent valve (V13)
26	Radio that filling will commence
27	Open box fill valve (V11)
28	Set the air flow rate on air MFC (I-1)
29	Open propane line valve (V2)
30	Set propane flow rate on propane MFC (I-3)
31	Once gas analyser is showing correct concentration wait for 2 minutes and then cut the flow of both MFCs to zero
32	Obtain final all clear from lookouts and warn test imminent
33	Start data acquisition
34	Install key to firing box and press fire
35	Check through window that all is safe
36	Open propane vent valve (V3) for 1 minute then close
37	Inform look out that test is complete but remain in place
38	Turn off power to valve circuits and remove lookout

39	Close air and propane cylinder valves and dial regulators to zero return to control room
40	Install door lock out and turn on power to valve circuits
41	Open box fill valve (V11)
42	Open air MFC until the flow shows as zero
43	Close box fill valve (V11)
44	Cycle propane line and vent valves (V2 and V3)
45	Power down valve control circuits and remove lockout
46	Call back all lookouts
E	*Bring in all sensitive control and instrumentation equipment*
F	*Remove regulators and store indoors*